INFORMATION TO USERS

This dissertation was produced from a microfilm copy of the original document. While the most advanced technological means to photograph and reproduce this document have been used, the quality is heavily dependent upon the quality of the original submitted.

The following explanation of techniques is provided to help you understand markings or patterns which may appear on this reproduction.

1. The sign or "target" for pages apparently lacking from the document photographed is "Missing Page(s)". If it was possible to obtain the missing page(s) or section, they are spliced into the film along with adjacent pages. This may have necessitated cutting thru an image and duplicating adjacent pages to insure you complete continuity.

2. When an image on the film is obliterated with a large round black mark, it is an indication that the photographer suspected that the copy may have moved during exposure and thus cause a blurred image. You will find a good image of the page in the adjacent frame.

3. When a map, drawing or chart, etc., was part of the material being photographed the photographer followed a definite method in "sectioning" the material. It is customary to begin photoing at the upper left hand corner of a large sheet and to continue photoing from left to right in equal sections with a small overlap. If necessary, sectioning is continued again — beginning below the first row and continuing on until complete.

4. The majority of users indicate that the textual content is of greatest value, however, a somewhat higher quality reproduction could be made from "photographs" if essential to the understanding of the dissertation. Silver prints of "photographs" may be ordered at additional charge by writing the Order Department, giving the catalog number, title, author and specific pages you wish reproduced.

University Microfilms

300 North Zeeb Road
Ann Arbor, Michigan 48106

A Xerox Education Company

RICE UNIVERSITY

THE EFFECT OF SURFACE ROUGHNESS ON THE REFLECTED AND EMITTED ENERGY FROM A ROUGH SURFACE OF INFINITE EXTENT SUBJECTED TO SOLAR IRRADIATION

by

David M. McStravick

A THESIS SUBMITTED
IN PARTIAL FULFILLMENT OF THE
REQUIREMENTS FOR THE DEGREE OF

DOCTOR OF PHILOSOPHY

Thesis Director's signature:

Houston, Texas

May, 1972

ACKNOWLEDGEMENT

The author wishes to express his appreciation to those people who have helped make this work possible. First of all he wishes to thank his advisor, Dr. A. J. Chapman, for his guidance and encouragement throughout his stay at Rice University. Also the author wishes to thank Dr. F. A. Wierum and Dr. W. W. Akers for their time and advice concerning his thesis. In particular, credit is due to his wife Kathie whose patience and support were invaluable during his graduate studies.

Finally the author would like to thank Rice University for the opportunity of an education. Also appreciation is extended to the following institutions for their financial aid: The Department of Health, Education and Welfare (National Defense Education Act), the Shell Company Foundation and the National Aeronautics and Space Administration (Sustaining Grant NGL 44-006-013).

TABLE OF CONTENTS

NOMENCLATURE

a	- ξ dimension of the center of a test area
a_o	- maximum χ dimension of the area treated by grid system analysis (A_g)
A_e	- effective area of a grid element after correction for sun shadowing and view blockage
A_g	- area in the mean surface level where the rough surface energy flux is calculated by grid system analysis
A_p	- a rectangular area in the mean surface level used in flat surface energy flux calculations
A_s	- area of a square grid element
A_{vb}	- area blocked from view by an inclined element
b_o	- maximum ξ dimension of the area treated by grid system analysis (A_g)
c_o	- χ intercept of the line which represents the limit of vision for a particular orientation of the receiving differential area
C	- correction factor to account for sun shadowing and view blockage
d	- distance between planes of projection for apparent area calculations of grid elements
d_{i_s}	- length of the shadowed region in the mean surface level
d_{i_v}	- length of the occulted region in the mean surface level

d_{vb} - length defined in Figure D-2

$f_{dA_j \rightarrow dA}$ - flat surface differential shape factor for the fraction of flux from dA_p received at dA

f - energy flux

f_{dA} - flat surface energy flux received at dA

F_{dA} - rough surface energy flux received at the differential area dA

F_{dA_ℓ} - rough surface energy flux received at the differential area dA from the region of the infinite surface not treated by grid system analysis

$\mathcal{F}$ - ratio of the rough surface energy flux to the flat surface energy flux received at dA

$\mathcal{F}_N$ - the ratio of the rough surface energy flux to the flat surface energy flux with view blockage neglected

$\mathcal{F}_{NN}$ - ratio of the rough surface energy flux to the flat surface energy flux received at dA with view blockage and sun shadowing neglected

G - irradiation of a surface

G_s - solar irradiation at the mean earth orbit

H - perpendicular height of the receiving differential area from the mean surface level

h - height deviation of a roughness element from the mean surface level

h_a - height of grid element measured in the plane of projection

h_{a_s} - height of the shadowed portion of an element as measured in the plane of projection

h_{a_v} - height of the occulted portion of an element as measured in the plane of projection

I - radiation intensity

J - radiosity of a surface

L - length of A_g

R - polar coordinate describing the distance of a point in the mean surface level from the origin of the coordinate system

R_c - distance to the center of a grid element from the origin of the coordinate system

R_{c_t} - distance to the center of a test area from the origin of the coordinate system

r - distance between the receiving differential area and a differential area in the mean surface level or in a grid element

r_c - distance between the receiving differential area and the center of a grid roughness element

S_{ij} - fraction of the area of the element (i,j) shadowed in sun shadowing

S_1, S_2, S_3, S_4 - integrals in the flat surface energy flux calculation of Appendices A and F

t - χ dimension of the center of a test area

V_{ij} - fraction of the area of the element (i,j) occulted in view blockage

u, v - variables used in solution of integrals in Appendix A

z - ratio of width to length of area A_g

α - square grid element dimension in units of H

α_s - sun orientation angle measured from the normal to the mean surface level (see Figure 2 for positive and negative cases)

β - angle between the normal to a differential area in the mean surface level or in a grid roughness element and the line joining this differential area with the receiving differential area

β' - angle between the normal to the receiving differential area and the line joining this differential area and a differential area in the mean surface level or in a grid roughness element

γ - orientation angle of the receiving differential area (positive and negative values indicated in Figure 2)

ε - angle between the vertical direction and the line joining the center of a grid element and the receiving differential area

ζ - angle between the projection of the grid element normal in the mean surface level and the line in the mean surface level connecting the grid element center and the origin of the coordinate system

η - angle between the normal to a surface and the incident solar energy G_s

θ - polar orientation angle of the grid element normal

λ - angle between a line joining the receiving differential area and any point in the mean surface level and the projection of this line in the mean surface level

λ_w - wavelength of incident radiation

ξ - one of coordinates of non-dimensionalized rectangular coordinate system in the mean surface level

π - 3.1415926

φ - azimuthal angle of grid element normal measured with respect to the direction of the sun for positive sun angles

χ - one of the coordinates in the non-dimensionalized rectangular coordinate system in the mean surface level

ω - angular coordinate of the polar coordinate system in the mean surface level

Subscripts

c - evaluated at the center of a grid element

ct - evaluated at the center of a test area

i - row number in grid system

j - column number in grid system

LIST OF FIGURES

Page

Page

I. INTRODUCTION

The moon's unusual environment as compared to an earth environment gives rise to some basic differences in the relative importance of the three modes of heat transfer. Due to the lack of an atmosphere convective heat transfer is absent in the lunar environment. The lunar material is of low thermal conductivity so that conductive heat transfer is typically small. Since the role of these two modes of heat transfer is reduced with respect to a corresponding earth configuration, radiative heat transfer takes on added significance in the lunar environment. The predominance of radiative heat transfer makes the radiative properties and directional character of these properties very important to the resulting heat transfer. In this analysis the effects of surface roughness of the lunar terrain are investigated using a geometric approach to treat the roughness. The directional character of the emissions and reflections of the surface is assumed to be diffuse. With this model the roughness has two basic effects on the amount of radiation received at a differential area located above the surface:

1) the radiosity of the surface is not uniform (variations in the orientation of the surface with respect to the incident solar energy causes variations in the radiosity of the surface).
2) The variations in the surface cause only certain portions of the surface to be "seen" at the receiving differential area.

The result of these two effects is that the energy flux received at a differential area for this type of surface will deviate considerably from the flat, diffuse surface case. To begin this analysis it is of interest to consider some of the basic aspects of surface roughness as applied to radiative heat transfer.

Generally problems in radiation heat transfer involve the interaction of radiant energy and a solid interface. The nature of the interface can have considerable effect on the resulting interaction and thus influence the heat transfer. Therefore, the effect of the surface condition is of interest in the study of heat transfer. For opaque substances the material near the surface plays the predominant role in determining the radiative characteristics of the substance.[1] For this reason the surface condition such as the geometric aspects and surface films can have significant effect on the radiative heat transfer between bodies. To account for these conditions

empirically the radiative properties of a material are often specified for certain test conditions or particular methods of preparation of the specimen. In accounting for surface roughness the method of surface finish is frequently used as the criteria for the condition of the surface. This method of surface description is qualitative, but it does give some indication of general surface geometry present. A look at almost any table of radiative properties shows that surface finish has a significant effect on properties of many engineering materials.[2][3]

Criteria for Surface Roughness

In order to discuss surface roughness it is of interest first to establish a criterion for roughness in a surface. In order to do this consideration is given to the definition of an optically smooth surface as described by the Rayleigh criteria. If the reflection of electromagnetic waves from a surface containing height variations h is considered, then the condition that must be satisfied for the surface to be optically smooth is that

$$\frac{h}{\lambda_w} \cos(\alpha_s) \rightarrow 0 \qquad \text{(see Chapter 2, Ref. 4)}$$

where

λ_w is the wave length of the incident energy

and

α_s is the angle the incident energy makes with the normal to the surface.

For this quantity to go to zero h/λ_w must tend to zero (the case of α_s tending to 90° is a limiting case and not of great interest here). The important point to note is that this ratio indicates the degree of roughness in a surface is dependent on the wavelength of the radiation under consideration. Since this analysis is concerned with heat transfer the radiation of interest is that of the visible and thermal spectral bands. As the range of the wavelength for these bands is from 10^{-1} to 10^{2} microns, very small height variations in the surface are sufficient to cause the surface to be considered as rough. In this analysis no attempt is made to account for, in detail, the effects of height variations on the order of magnitude of the wavelengths of interest, and only the major height variations in the surface (which due to approximations made in the calculations are restricted to a maximum value of about 10^{5} times the largest wavelength of interest) are considered. It is assumed that diffuse emissions and reflections result from these microscopic height variations (variations on the order of the radiation wavelengths).

Theoretical Analysis of Surface Roughness

Theoretical analysis and prediction of surface roughness effects is a very difficult problem and a considerable amount of work has been done in this area. As a first step, the idealized case of an optically smooth surface (i.e., the Rayleigh criteria is zero for all portions of the surface) has been studied by a number of investigators. Using electromagnetic wave theory and the assumption of an optically smooth surface the radiative properties of a material can be derived in terms of electrical and optical properties of the material.[5] This serves as a guide to radiative properties, but many engineering materials show striking deviation from these calculated values.[5] There are several reasons for the deviations, but one important reason is the geometrical roughness in the surface. As mentioned above the roughness is related to radiation wavelength so that materials can fit the idealized predictions in some regions of the spectrum but deviate in others.[5] The predicted values from analysis of the optically smooth case serve a useful purpose as a basis of comparison for empirical values and also give an indication of the anticipated trends of the empirical values.

To introduce roughness into a surface a reasonable first step is to consider a periodic, one-dimensionally rough surface. A typical periodic, one-dimensional surface consists of an infinite surface which has a system of parallel ridges and valleys which in cross section appear as a "saw tooth" profile. Many different periodic configurations have been used for the profile and among these are sine waves, uniform "V" shaped grooves, and uniform square shaped grooves. An extensive survey of the analysis of reflection from a one-dimensionally rough surface can be found in Chapter 4 of Reference (4). Several papers have been written on the resulting heat transfer for surfaces with one-dimensional roughness. An example is given in Reference (6). An example of experimental work done on this type of surface is given in Reference (7).

Since the surface roughness in most manufactured and natural surfaces is neither periodic nor explicitly given, the surface can only be described in terms of statistical properties. Numerous methods of describing a rough surface in a statistical manner are summarized in Chapter 5 and 6 of Reference (4). In the analysis described in Chapter 5 of this reference the basic assumption involved is that the radius of curvature of all portions of the surface is large with respect to the

wavelength of the incident energy. Also shadowing of portions of the surface by adjacent roughness anomalies is neglected, and the height variations are near the order of magnitude of the wavelength of the incident radiation. These approaches are not oriented toward heat transfer analysis but mainly to the reflection of radio waves from rough surfaces. The description of the models of surface roughness are of interest, and some results apply directly to reflection of thermal radiation. It is interesting to note that for height variations near the size of the wavelength the reflections become similar to the diffuse case. Also in this chapter consideration is given to a two-dimensionally rough surface. Another example of an analysis which considers the statistical aspect of roughness is given in Reference (8). In this paper the surface is represented as one-dimensionally rough and the irregularities are "V" shaped with the slopes of the sides of the "V" determined by a random distribution. The sides are assumed to be large with respect to the wavelength, and the sides are assumed to reflect in a specular fashion. Shadowing and multiple reflections are included in the analysis of reflection from this model. The results generally indicate a peak value at the specular reflection angle with lesser off-specular reflections depending on the slope distribution of the model.

Experimental Observation of Lunar Surface

Since the present analysis is oriented toward the moon's radiative characteristics it is of interest to consider experimental results for energy fluxes from the moon's surface. Early earth-bound measurements of the moon's thermal emissions by Petit and Nicholson[9] indicated that the moon does not follow Lambert's law for diffuse emission. This is to say that if the region observed is assumed to be a flat, diffuse surface and the incident solar irradiation is constant then the measured flux at a fixed distance from the surface should vary as the cosine of the angle of observation with respect to the normal to the surface. More recent measurements by Saari and Shorthill[10] indicate a maximum energy flux in the general direction of the incident radiation. Also measurements of reflected energy from the lunar surface by Orlova[11] indicate a peak value of the reflections in the direction of the incident solar radiation. The cause of this back scattering of energy is not known, but a possible explanation originally put forward by Petit and Nicholson is the surface roughness of the lunar terrain. For lunar emissions it should be mentioned that low conductivity of the lunar material and the lack of an atmosphere are important aspects of this explanation. In the current analysis a rough surface

is considered with the simplifying assumption that on a microscopic scale (on the order of magnitude of the wavelength of the radiation involved) the surface is diffuse and the results are compared with the experimental data for the lunar surface.

II. ASSUMPTIONS

In this analysis several assumptions are made concerning the nature of the rough surface. First the material composing the surface is assumed to have a very low value of thermal conductivity such that heat conduction in the surface can be neglected. In addition the surface is assumed to be in a vacuum so that convective heat transfer is eliminated. The only thermal radiation incident on the surface is assumed to be a flux of solar energy. Mutual irradiation between surface irregularities is assumed to be negligible. In this analysis the surface is assumed to be macroscopically rough, i.e., the major height variations are assumed to be several orders of magnitude larger than the longest wavelength of radiation involved. The elements forming the rough surface model are assumed to be both diffuse emitters and diffuse reflectors, and the absorbtivity of the elements is assumed to be independent of the direction of the incident energy. The assumption of diffuseness is clearly a simplification of the complex problem of the detailed interaction of radiation with matter and precludes

any representation of the height variations on a microscopic basis, i.e., height variations on the order of the radiation wavelengths under consideration. An additional assumption required by the method used to calculate the flux is that the height of the receiving differential area above the mean surface level is approximately two orders of magnitude greater than the height variations in the rough surface.

III. MODEL DESCRIPTION

The model used to describe the rough surface considers the surface as rough in two directions with the roughness having a statistical nature. The simplifying assumption of diffuse radiation is retained in the model. To establish a basis for measurements a mean surface level is defined. The mean surface level corresponds to the plane in the rough surface which has a volume of material above the plane equal to the void space below the plane. This mean plane serves as a reference for all roughness height variations and for dimensions to the surface. The energy flux is calculated for a differential area located at a height H above the mean surface level. A coordinate system is established in the mean surface level with the origin at the point of intersection of the mean surface level with a line from the differential area perpendicular to the mean surface level. The axes are labeled ξ and χ and are in units of H. The orientation of the normal to the differential area determines the portion of the

infinite surface which is "visible" and therefore determines the portion of the surface which can contribute to the energy flux at the differential area. The normal to the differential area and a line from the differential area perpendicular to the mean surface level define a plane which is a plane of symmetry for the geometry of the configuration. Solar radiation is assumed to be incident on the infinite surface and the center of the sun is assumed to lie in the plane of symmetry. This geometry is indicated in Figures 1 and 2.

At this point it is appropriate to consider an ideal case which will be used as a reference for all work done with the rough surface model. The ideal case consists of considering the mean surface level as an infinite, flat surface which is a diffuse emitter and reflector. The ratio of the energy flux from the model of a rough surface to the energy flux from the ideal surface will give the effect of surface roughness on the radiative properties of the surface.

Grid Elements

To model the rough surface a square grid system is established in the mean surface level by constructing grid lines parallel and perpendicular to the line of symmetry. The dimension of the square grid area elements

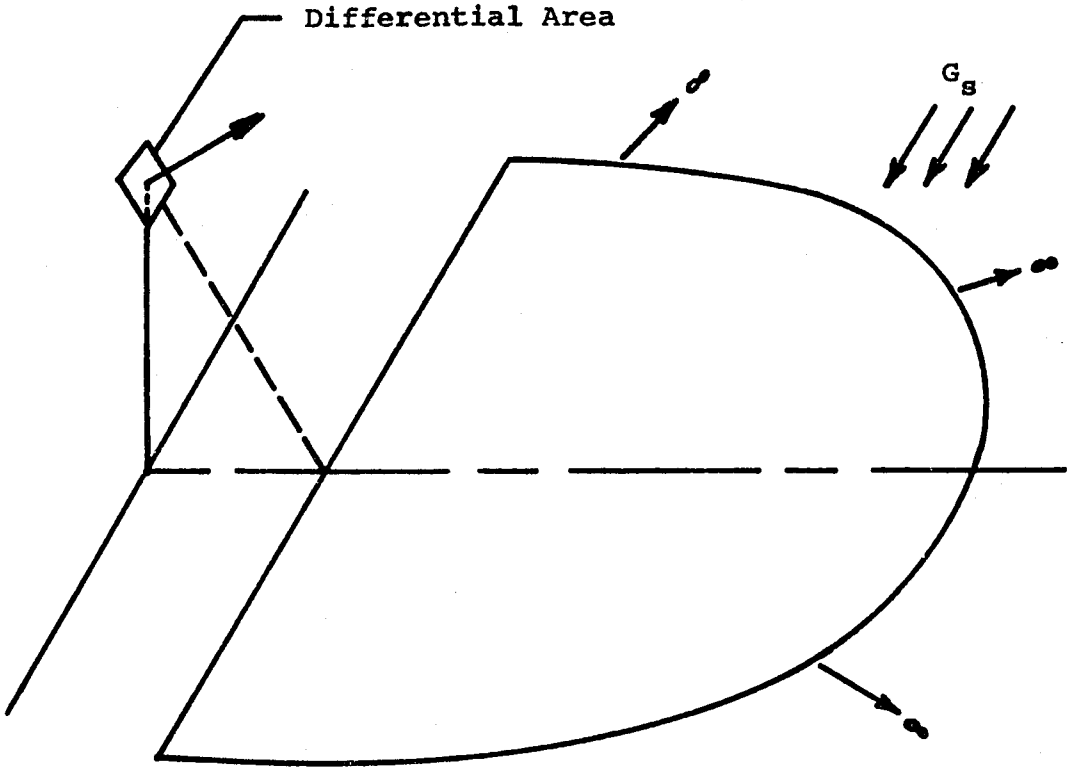

Figure 1: Differential area located above mean surface level

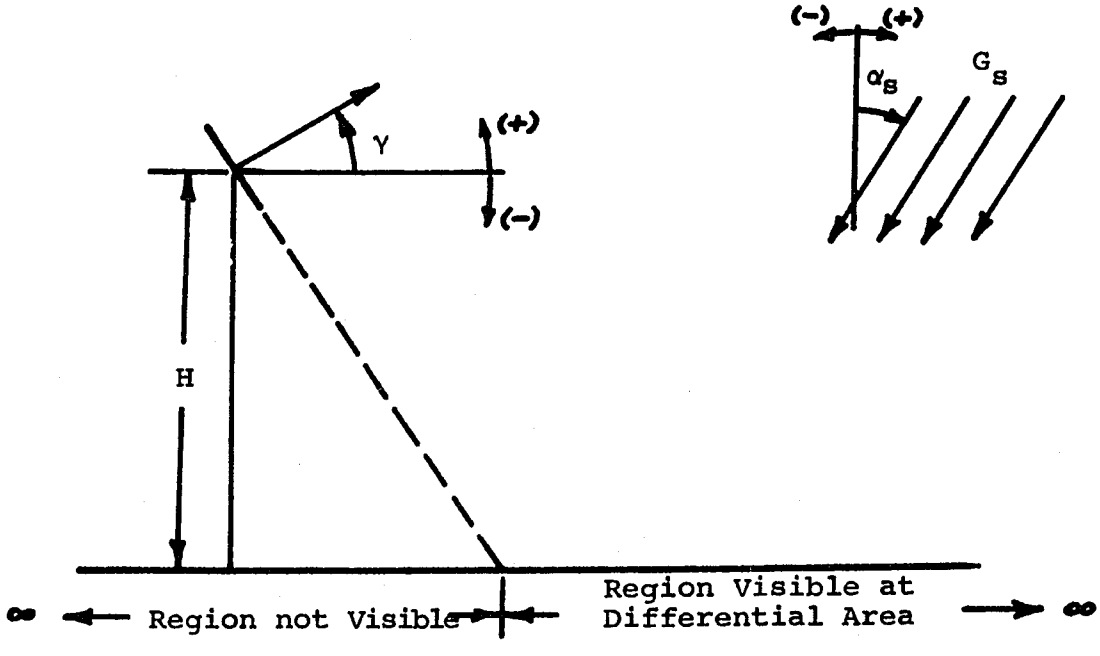

Figure 2: Cross section in plane of symmetry

is left unspecified for the moment, but it will always be small with respect to the height dimension H (less than 1/50 H). Each square grid element is assumed to be a diffuse emitter and reflector. To account for height variations in the surface the center of the element is fixed at the center of the grid square, and different orientations are assigned to each element. A normal to the grid area element is established at the center of the square, and the orientation of the element is specified by the polar and azimuthal angle of the normal. The polar angle θ is measured from the vertical direction (i.e., perpendicular to the mean surface level) and the azimuthal angle φ is the angle between the projection of the normal in the mean surface level and the direction of the sun for positive sun angles. A typical grid element with the associated angles is given in Figure 3. The sine of the polar angle determines the maximum deviation from the mean surface level for each element. To simulate the height variations in a rough surface a distribution of values is assigned to the sine of the polar angle. Two height distributions were investigated -- normal and random. A description of the method used to generate these distributions is given in Appendix E. To allow for azimuthal orientation variations the value

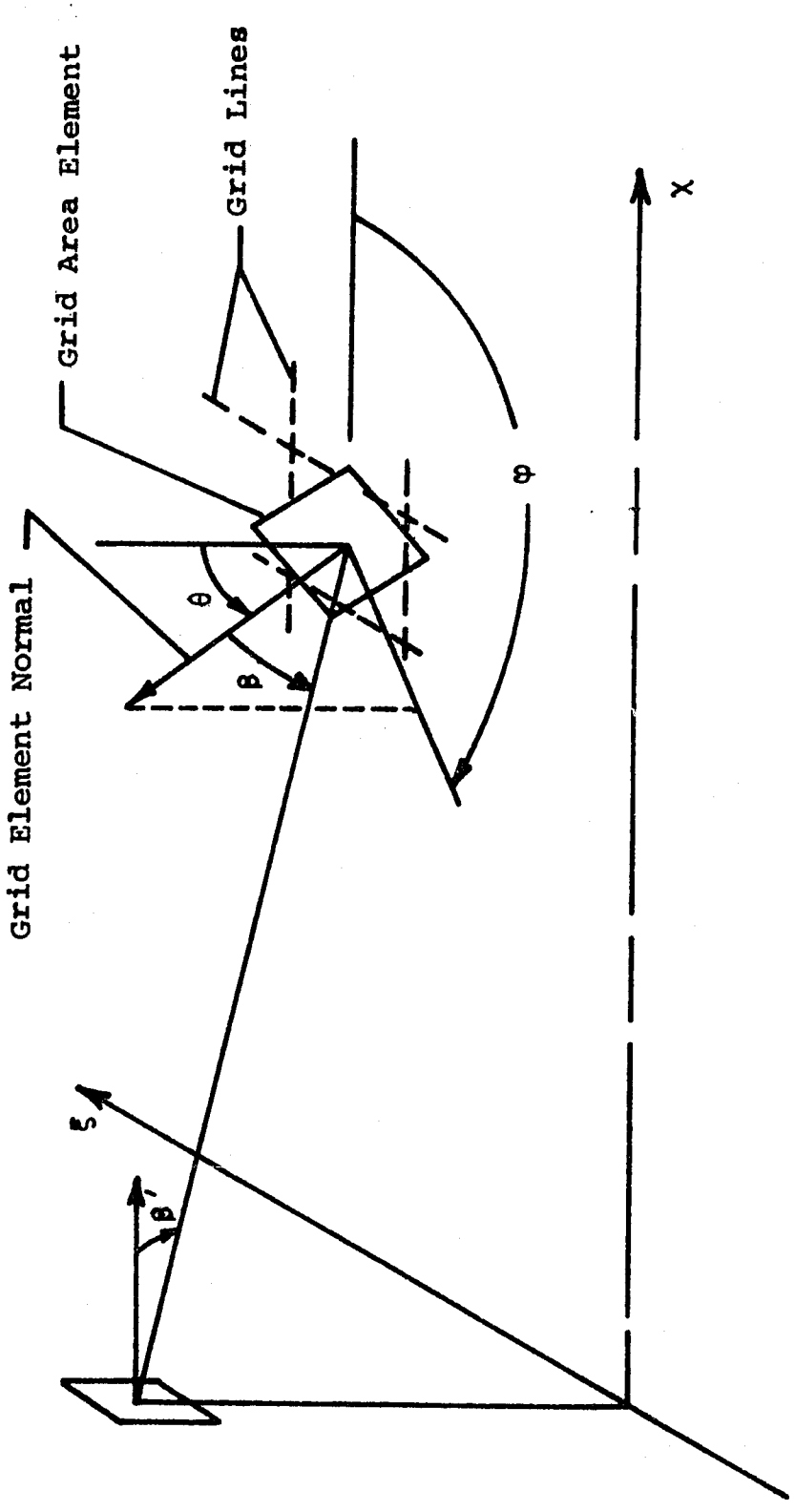

Figure 3: Detail of grid area element

of the azimuthal angle φ is specified by a random distribution for both cases of height distribution. This random distribution in direction is consistent with an isotropic surface (i.e., there is no preferential direction or grain in the surface). The range of the azimuthal angle is restricted such that the element can always be "seen" at the receiving differential area. This is accomplished by restricting φ between values of $\frac{\pi}{2} - \omega_c$ and $\frac{3\pi}{2} - \omega_c$ where ω_c is the angle measured in the mean surface level between the line of symmetry and the line joining the center of the element with the origin of the coordinate system. This restriction on φ insures that the normal to the element will always have a positive component in the direction of the receiving differential area. This can be seen by considering the restrictions on φ in Equations B-2 and B-3 of Appendix B. The general philosophy followed in constructing the rough surface is that only the portions of the surface which are irradiated and can be "seen" at a viewing point can contribute to the energy flux at that point. Clearly only a portion of the surface has been constructed using the inclined grid elements, and the incident energy striking the portions of the surface which have not been represented in the model is neglected with the assumption being that this radiation

energy cannot reach the viewing point. Likewise, portions of the surface which are visible but receive little or no irradiation are of negligible significance to the energy flux at the receiving differential area.

Sun Shadowing and View Blockage

To complete this model of a rough surface two additional geometric aspects are considered. The first is sun shadowing or the blockage of solar irradiation from a grid element by an adjacent element. Due to the assumption of the sun being in a plane containing the line of symmetry, the only elements that contribute to the shadowing of an element are in a column parallel to the line of symmetry which contain the element of interest and are in the direction of the sun. In this analysis only the first adjacent element of this column is considered in shadowing, and for this reason has been termed "first order shadowing". A similar aspect of the analysis considered is termed "view blockage". By view blockage is meant the occulting, or blocking from view at the differential area, a fraction of the element by a neighboring element. Numerous elements can be effective in view blockage depending on the location of the element of interest. Again in this analysis only first order effects are considered: only the first adjacent and

diagonally adjacent elements are considered. These elements are pictured in Figure 4 for various locations of the element of interest. The effect of each of the three elements is added together to give the total view blockage. It is typical that both sun shadowing and view blockage are present on an element, and in this case the one causing the larger decrease in area is used to calculate the effective area of the element.

One additional aspect of the range allowed for the azimuthal angle should be mentioned at this point. As stated earlier only a portion of the surface is constructed with the assumption that the neglected portions of the surface do not contribute to the energy flux at the observation point. For positive sun angles and in the region of the surface where view blockage is small ($0 \leq \xi \leq 1$ and $0 \leq \chi \leq 1$) this approach can lead to neglection of portions of the surface with large radiosities. To compensate for this in the region of $0 \leq \xi \leq 1$ and $0 \leq \chi \leq 1$ the azimuthal angle is allowed to have a range of 2π with positive sun angles. This allows more of the portions of the surface with large radiosity to be considered in the flux calculation and therefore gives a more realistic representation of the surface.

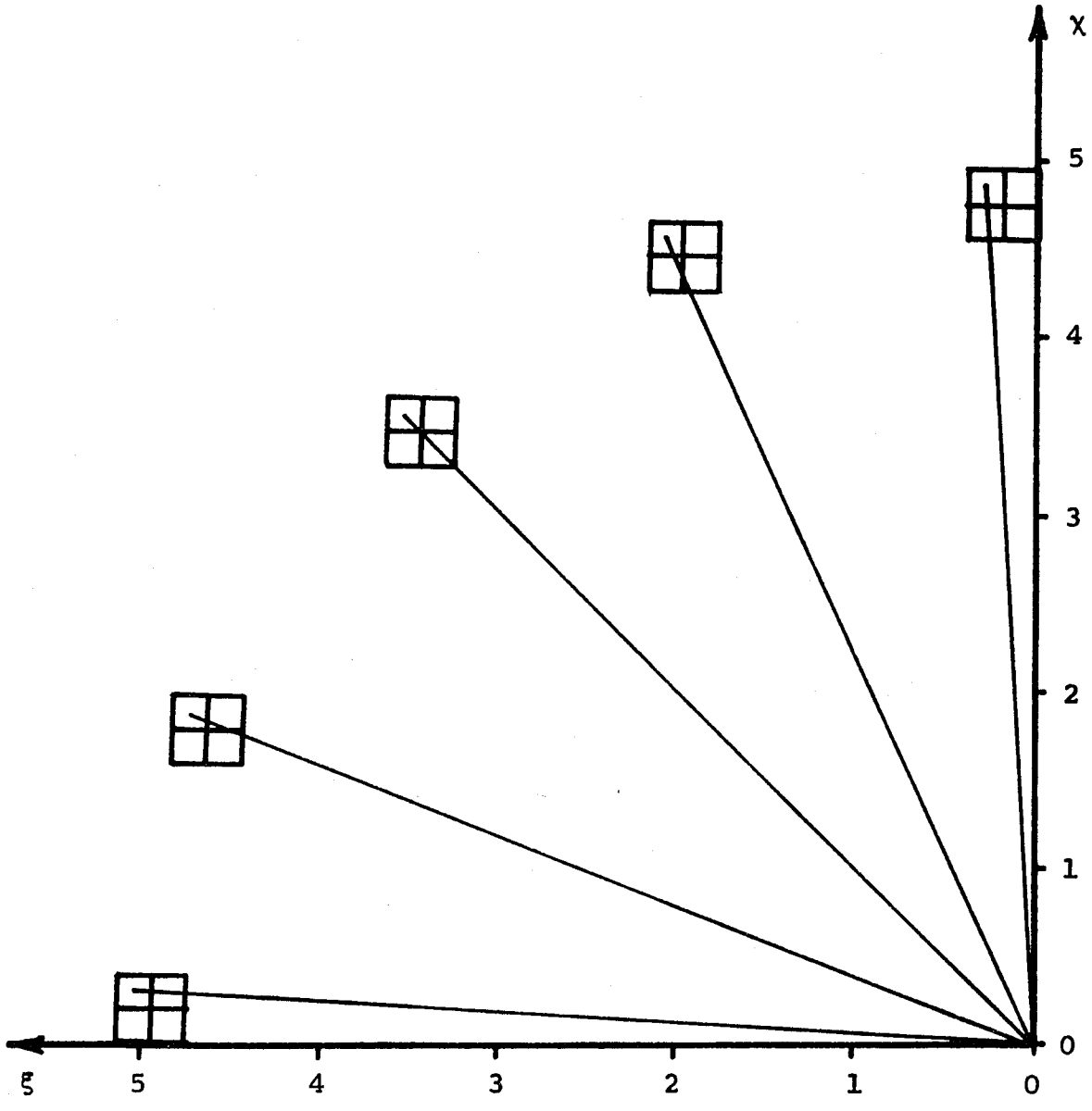

Figure 4: Elements involved in first order view blockage for various locations in the mean surface level

IV. ANALYSIS

Basic Equations

The basic calculation made in this analysis is the quantity of energy flux intercepted at a differential area for both the model of a rough surface and the ideal case of a flat, diffuse surface. The ratio of the intercepted flux for the rough case to the flat case is used as the indication of the effect of surface roughness. To start the analysis a differential area dA_s in a surface area A_s which is a source of emitted and reflected radiation is considered. The flux at dA_s is defined as

$$f_{dA_s} = \lim_{\Delta A_s \to 0} \left(\frac{\Delta q}{\Delta A_s} \right)$$

where Δq is the quantity of radiation energy leaving ΔA_s. It can be shown from Reference (12) that

$$\frac{df_{dA_s}}{dA_\perp} = \frac{I \cos \beta}{r^2} \qquad (1)$$

where $\frac{df_{dA_s}}{dA_\perp}$ is the portion of the flux from dA_s which

is intercepted at $dA_\perp$. The differential element $dA_\perp$ is a portion of the hemisphere of radius r with center at dA_s . The angle β is measured between the normal to dA_s and the line connecting dA_s and $dA_\perp$. I is the intensity of the radiation from dA_s . To consider a differential area of arbitrary orientation at $dA_\perp$ it is noted that

$$dA_\perp = \cos\beta' dA$$

where β' is the angle between the normal to dA and the line connecting dA and dA_s . So that equation (1) can be written

$$\frac{df_{dA_s}}{dA} = \frac{I \cos\beta\cos\beta'}{r^2} \qquad (2)$$

where by definition $\frac{df_{dA_s}}{dA}$ is the intercepted flux at dA from the source dA_s . The total intercepted flux at dA from area A_s is

$$\frac{df_{A_s}}{dA} = \int_{A_s} \frac{df_{dA_s}}{dA} \, dA_s$$

or

$$f_{dA} = \frac{df_{A_s}}{dA} = \int_{A_s} \frac{I \cos\beta\cos\beta'}{r^2} \, dA_s \qquad (3)$$

The term f_{dA} is the quantity of interest since it represents the total incident energy at dA from a surface A_s . The calculation of the intercepted flux $f_{dA}\left(\frac{df_{A_s}}{dA}\right)$ for the flat, diffuse case is presented in Appendix A. To calculate the incident flux for the rough surface an element of the rough surface as pictured in Figure 3 is considered. If this element is isolated in space so that there are no effects of sun shadowing or view blockage by adjacent elements, a heat balance can be applied to establish the radiosity of the element. First the incident energy on the element is assumed to be a collimated flux of solar radiation represented by the solar constant G_s . With the assumptions of no conduction and no convection, conservation of energy states that for this element

$$J = G \tag{4}$$

where J = the radiosity of the surface (both reflected and emitted energy)

and G = the irradiation of the surface.

Now the irradiation of the element is given by

$$G = G_s \cos \eta \tag{5}$$

where G_s = the solar constant (440 BTU/hr ft^2)

and η = the angle between the normal of the element and incident energy G_s .

This gives

$$J = G_s \cos \eta \tag{6}$$

It can be shown from Reference (12) with the assumption of diffuse emission and reflection for the element that

$$J = I \pi \tag{7}$$

So now the incident energy can be related to intensity of emitted and reflected radiation of the element. This allows the incident flux at dA to be written as

$$f_{dA} = \int_{A_s} \frac{G_s \cos\eta}{\pi} \frac{\cos\beta\cos\beta'}{r^2} dA_s \tag{8}$$

Since the element is flat the angle η will be constant over the surface element or

$$f_{dA} = \frac{G_s \cos\eta}{\pi} \int_{A_s} \frac{\cos\beta\cos\beta'}{r^2} dA_s$$

At this point it can be noted that with the assumptions made the incident flux from any element is determined by its orientation with respect to dA, and its radiosity is determined by the orientation of the element with respect

to the solar flux. If the absorbtivity with respect to the solar energy of the roughness elements and the flat surface reference case is assumed to be constant then the ratio of the rough surface emitted flux to the flat surface emitted flux will be the same as the ratio of the total rough surface flux to the total flat surface flux. This applies to the reflected fluxes as well. Also, the temperature of each element is immaterial to the flux at dA since the temperature of each element must be such that the emitted energy when added to the reflected energy will equal the incident energy (i.e., conservation of energy).

If only small area elements are considered the integration to obtain f_{dA} can be simplified by making the following approximations

$$\cos\beta \cong \cos\beta_c$$

$$\cos\beta' \cong \cos\beta'_c$$

$$r \cong r_c$$

for all portions of the area element A_s . The subscript c denotes the term evaluated at the center of the element (the point at which the element is pivoted). These approximations give

$$f_{dA} \cong \frac{G_s \cos\eta \cos\beta_c \cos\beta'_c}{\pi r_c^2} A_s \qquad (9)$$

This equation will be used to calculate the energy from each rough surface element. It is convenient to convert equation (7) into the variables used to describe the orientation of the elements and the dimensions of the grid system of the mean surface level. This transformation of variables is carried out in Appendix B. The final result after adding subscripts to indicate the grid location is

$$f_{dA_{ij}} = \frac{G_s}{\pi}\left[\cos\alpha_s\cos\theta_{ij} + \cos\varphi_{ij}\sin\alpha_s\sin\theta_{ij}\right]$$

$$\times \frac{\left[\chi_i\cos\gamma - \sin\gamma\right]\left[\cos\theta_{ij} - \sqrt{\xi_j^2 + \chi_i^2}\ \sin\theta_{ij}\cos(\varphi_{ij} + \omega_{ij})\right]}{\left[\xi_j^2 + \chi_i^2 + 1\right]^2}$$

The total flux from a region of the rough surface is

$$F_{dA_{NN}} = \sum_{i}^{M}\sum_{j}^{N} f_{dA_{ij}}$$

where $F_{dA_{NN}}$ is a rough surface flux received at dA with sun shadowing and view blockage not included. The flat surface diffuse case flux f_{dA} can be evaluated from the equations of Appendix A for the same region as considered in the rough surface analysis and the ratio

of the two fluxes gives the effect of surface roughness. As yet the effects of sun shadowing and view blockage have not been included, but this ratio serves a useful purpose in confirming some aspects of the analysis as will be seen in the discussion. To account for sun shadowing and view blockage a factor based on the geometry of the element involved is multiplied by f_{ij} to account for the reduction in the effective area of the element due to incomplete irradiation of the element or the partial visibility of the element at the differential area dA. So the final form for calculating the rough surface flux is

$$F_{dA} = \sum_i \sum_j f_{dA_{ij}} C_{ij}$$

where C_{ij} is the correction factor for sun shadowing and view blockage; F_{dA} is a rough surface flux received at dA with sun shadowing and view blockage included. The detailed calculations of C_{ij} for sun shadowing and view blockage are given in Appendix C.

To calculate the contribution of the energy flux from the region very far from dA an approximation is used. This approximation is used because as the region under consideration becomes farther from dA the higher order view blockage becomes significant and using only first

order view blockage leads to substantial error. The derivation of this approximation is given in Appendix D, and the method of calculating the flux from the region outside of A_g is presented in Appendix F. This leads to the final form for calculating the energy flux from a rough surface of infinite extent as

$$F_{dA} = \sum_{A_g} f_{dA_{ij}} C_{ij} + F_{dA_\ell}$$

where A_g is the area in the mean surface level treated by grid system analysis and F_{dA_ℓ} is the flux from the remaining portion of the infinite surface not treated by grid system analysis.

Method of Solution

To solve the equations for F_{dA} and $F_{dA_{NN}}$ a computer program was written. The program generated the orientations of the grid elements in the region A_g . The orientations of three rows of elements were generated and held in storage. These values provide sufficient information to calculate the energy flux for the center row, and the two adjacent rows provide information for first order sun shadowing and view blockage. After all the elements in the center row had been evaluated the three rows in

storage were updated to include one new row, and the evaluation process was repeated with the new center row. This process was repeated until the flux at dA from all the elements in A_g had been evaluated. A second program was used to calculate the flux at dA from the region outside of A_g using the approximation of Appendix D and the method described in Appendix F. This flux was added to the flux from the region A_g to give the total flux at dA from the model of a rough surface of infinite extent. This flux was divided by the flux received at dA from the flat, infinite surface to get the ratio $\mathcal{F}$. Computer solutions were performed for two height distributions in the surface -- random and normal. The grid size used was $\alpha = .02$. Five values of the differential area orientation angle γ were considered. These were $\gamma = 0$, $\gamma \cong \pm 30°$, and $\gamma \cong \pm 60°$. The range of sun angles α_s investigated was from -75° to +75° with solutions performed at 15° increments of α_s between these two values. The programs were written in Fortran IV and were run on a Burroughs 5500 Digital Computer at the Rice Computer Center.

V. DISCUSSION OF RESULTS

Flat Surface Shape Factor Contours

As a first step in considering the results it is of interest to consider the flat, diffuse case for an infinite surface. This case serves as a reference for all the rough surface results and can be used to indicate the relative importance of different regions in the infinite surface. To accomplish this the shape factor for a differential area in the infinite surface at the mean surface level to a differential area located at a height H above the mean surface level is derived in Appendix A. If this expression is evaluated for constant values of shape factor to determine the resulting points in the surface, a set of curves of equal shape factor result. This set of contours can be plotted in the mean surface level to give an indication of the relative importance of different regions in the surface. In Figures 5, 6 and 7 these sets of contours are plotted for several values of γ used in the final results. These plots indicate that the most important region is near

Figure 5: Differential shape factor contours in the mean surface level ($F_{dA_p \rightarrow dA}$ = constant) for $\gamma = -30°$

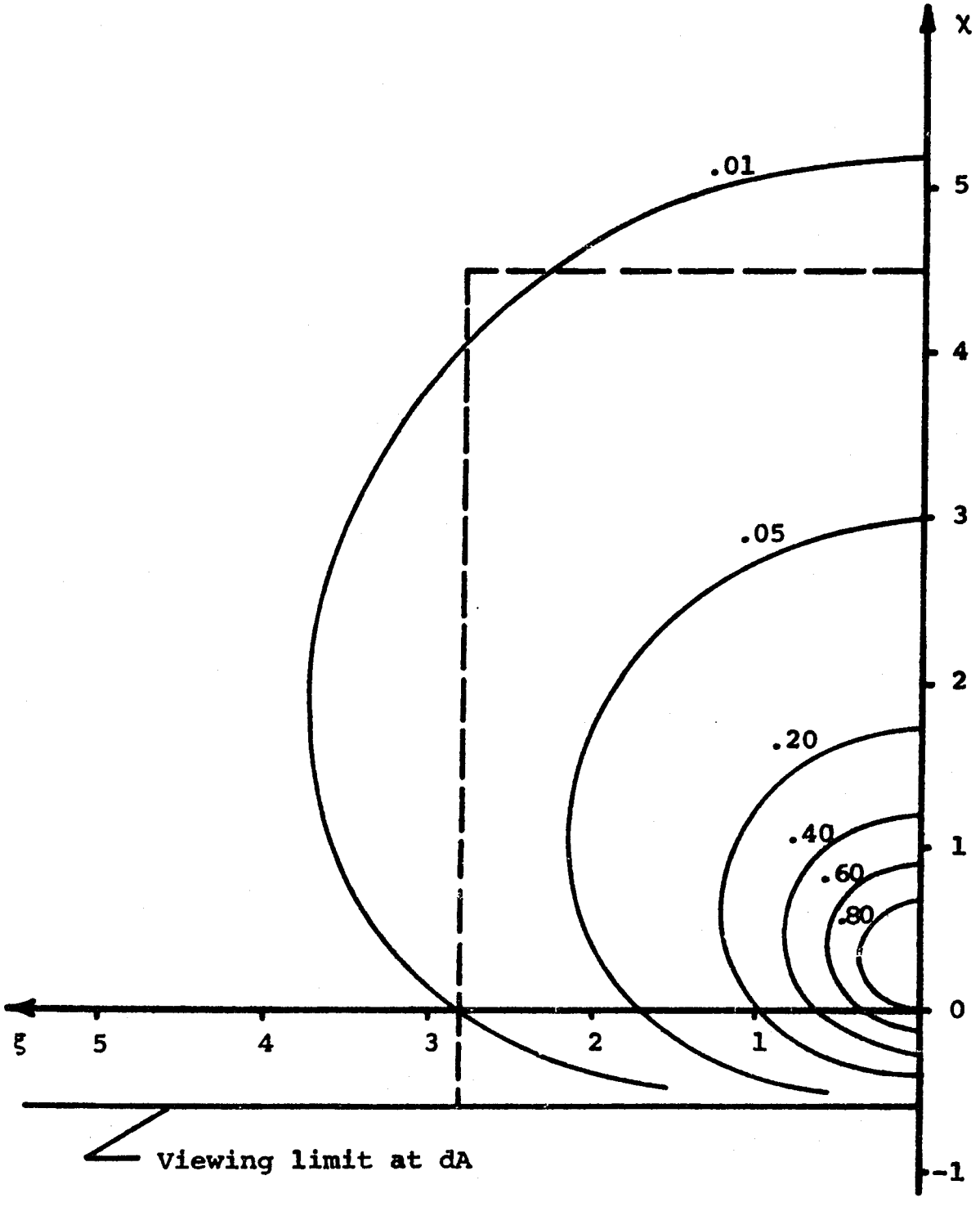

Figure 6: Differential shape factor contours in the mean surface level ($F_{dA_p \rightarrow dA}$ = constant) for $\gamma = 0°$

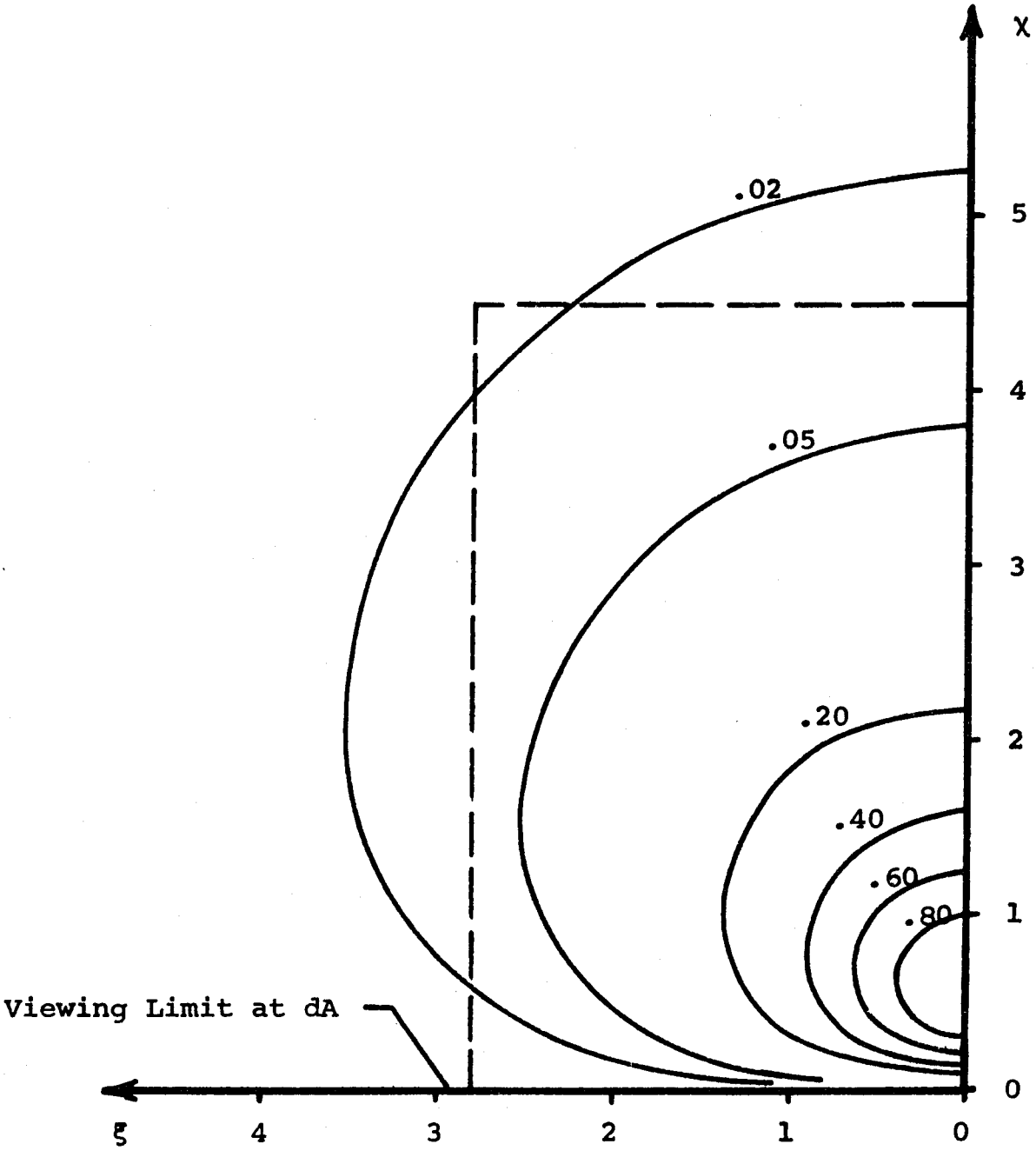

Figure 7: Differential shape factor contours in the mean surface level ($F_{dA_p \rightarrow dA}$ = constant) for $\gamma = 30°$

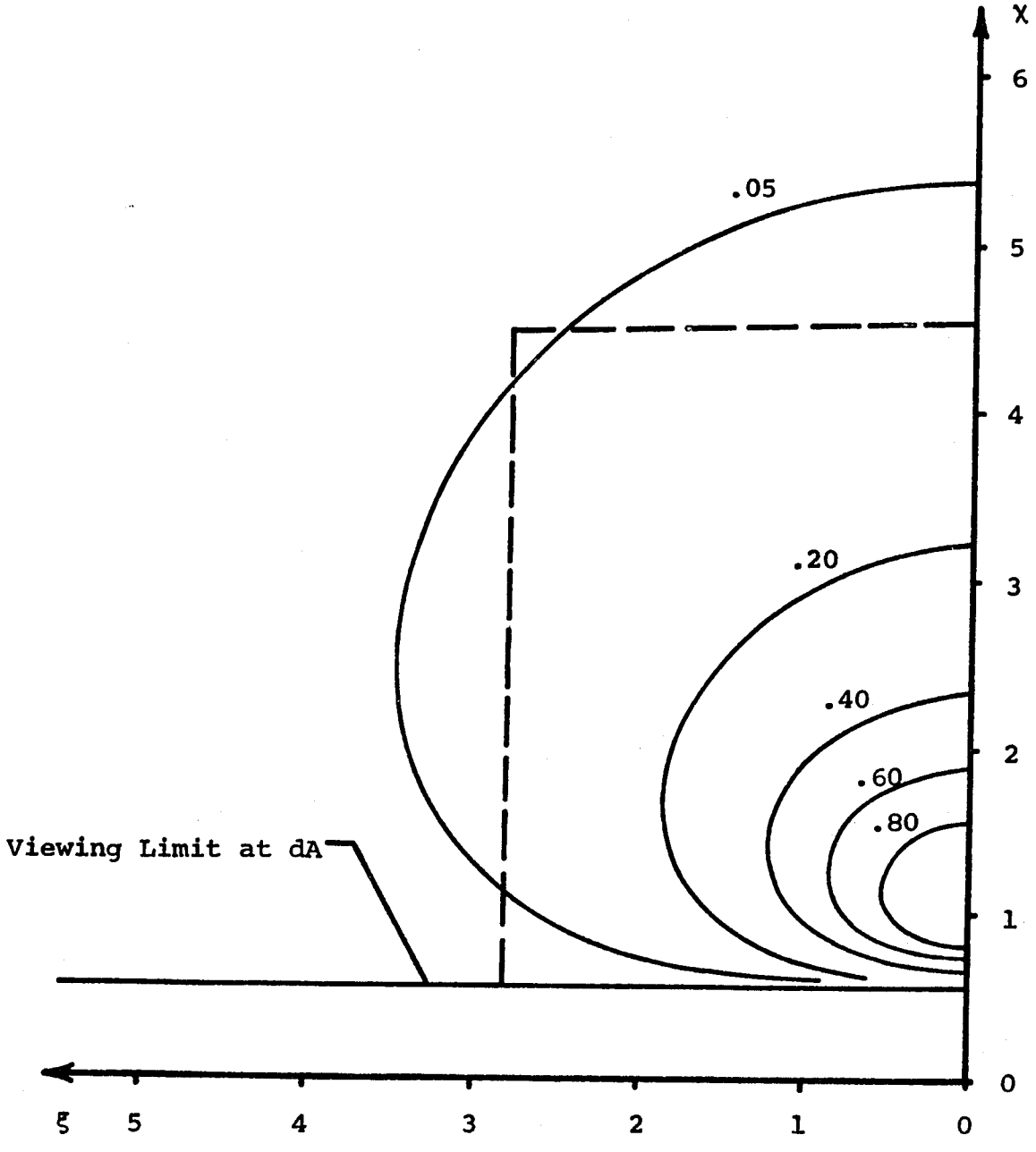

the line of symmetry. Also the value of the shape factor falls off quite rapidly as the distance from the origin of the coordinates gets large. As mentioned in the last chapter, due to higher order view blockage and to conserve computer time only a portion of the infinite surface is treated with a detailed grid system analysis (dividing the mean surface level into grid elements and assigning the orientation from distributions), and the rest is treated with an approximation derived in Appendix D. If it is assumed that the rough surface will show similar trends these plots can be used to show the appropriate shape of the region for grid system analysis. Clearly this shape must be consistent with the square grid system used. The region of detailed analysis is shown superimposed on these plots by dashed lines. Figure A-4 of Appendix A shows the fraction of the flux from the infinite surface included by this region.

Test Area Results

Now to start the analysis of the rough surface the model is considered with view blockage neglected. If the case of $\alpha_s = 0$ ("high noon" sun) is used then sun shadowing will be zero. To analyze different portions of the rough surface a test area is used. The idea of the test

area is to use a large enough number of grid elements so that a reasonable distribution of orientations is contained within the area and the area is still small enough to represent only a small portion of infinite surface. In this analysis the test area is a square region containing 625 grid elements (a square 25 x 25 grid units). If the ratio of the flux from the rough surface model to the flat surface is calculated for test area locations along the line of symmetry the resulting values of F_{dA}/f_{dA} can be plotted as a function of distance from the origin. This plot is made in Figure 8 for several values of the grid dimension α . In Appendix D the ratio of the energy flux is derived for a single inclined element. If this expression is written with average values of the distribution determining the orientation of the elements and applied to a test area the result is equation D-6. It is clear that the form of the equation will give a straight line. This line is plotted in Figure 8 as a dashed line. From this figure it is seen that as α becomes small the results of the test area analysis approach the results of equation D-6 very closely. With values of $\alpha \leq .02$ the points determined from the test area analysis form a straight line with slope and intercept very close to the results of equation D-6. This plot is for a normal height distribution, but a random distribution gives the same

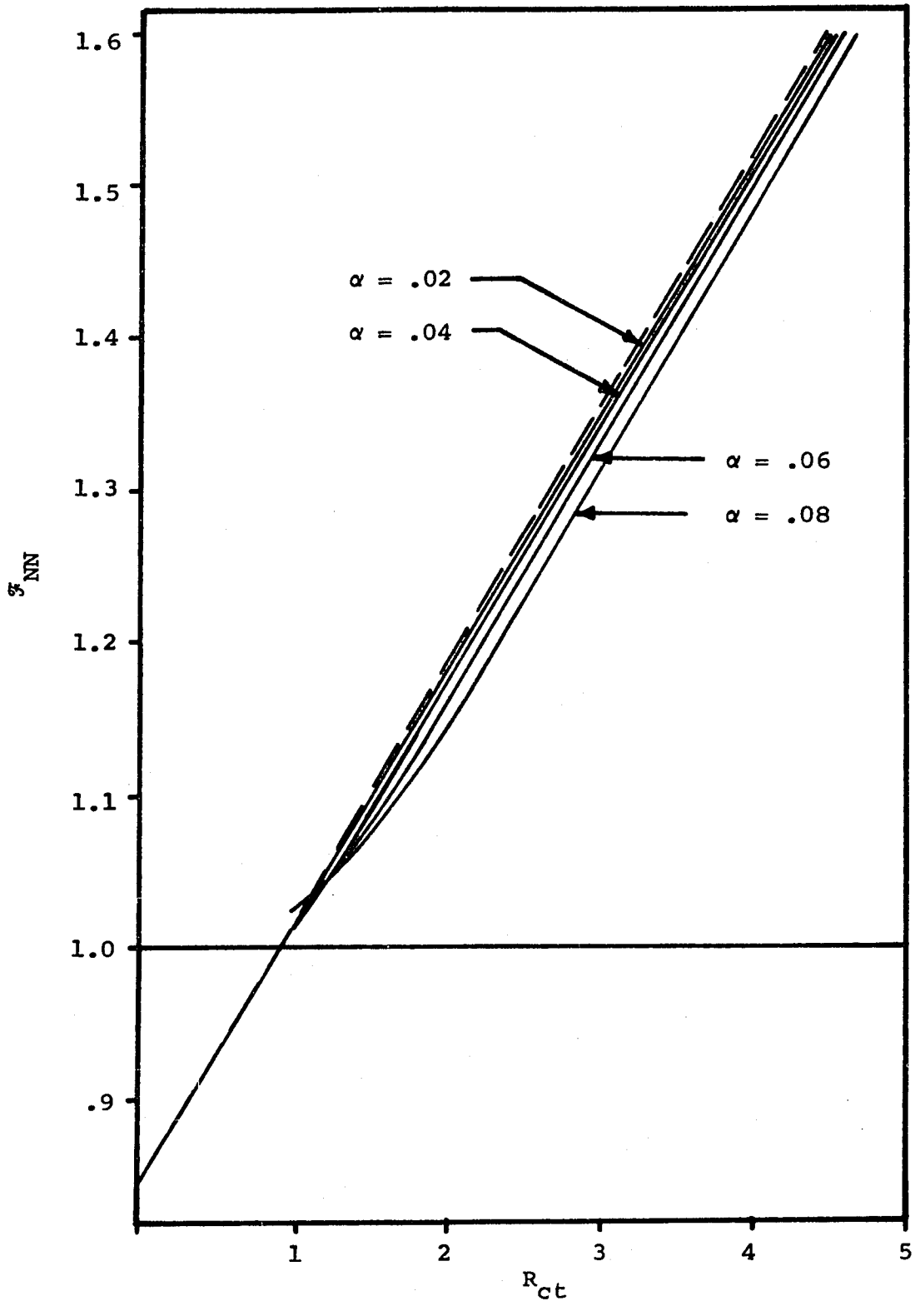

Figure 8: Plot of the rough surface energy flux to the flat surface flux with sun shadowing and view blockage neglected ($\mathcal{F}_{NN}$) vs. R_{ct} for a normal distribution of heights with grid size as indicated for w_{ct} = 0

agreement. Also this agreement is not restricted to the line of symmetry or to $\alpha_s = 0$ (if sun shadowing is not included in the analysis). This can be seen in Table D-1 of Appendix D. From these results it is concluded that for this model of surface roughness the ratio F_{dA}/f_{dA} is essentially independent of grid size for $\alpha \leq .02$. Also it is concluded that average values of the distributions are meaningful in calculating the energy flux and can be used in the approximation of the limiting case as derived in the second part of Appendix D. It should be noted that the ratio F_{dA}/f_{dA} tends to infinity as the distance from the origin tends to infinity. This is physically unrealistic since it indicates that a rough surface of infinite extent would cause an infinite flux at the differential area dA . The reason this occurs is that view blockage has been neglected in the analysis so far. At this point it should be emphasized that this analysis does not apply to height variations of the rough surface on the order of magnitude of the radiation wavelengths under consideration. Only macroscopic height variations are considered. The assumption of diffuse elements composing the rough surface precludes any attempt to describe height variations on the scale of the radiation wavelengths. Although the grid size is not important to the

ratio F_{dA}/f_{dA} , the resulting distribution of slopes in the surface is significant to this ratio. If the maximum value of the polar angle is restricted to less than 90°, the ratio is closer to the flat surface case as can be seen in Figure 13. As the maximum polar angle tends to zero the results tend to the flat surface case.

To complete the analysis of the rough surface model, first order view blockage is introduced into the test area analysis. The equations used to establish the reduction in effective area of the grid elements are given in Appendix C. Figures 9 through 12 show the effect of view blockage on the ratio F_{dA}/f_{dA} . As the distance from the origin becomes large the ratio begins to increase due to the neglection of higher order view blockage. For this reason an approximation is used to calculate the energy flux from the region far from the origin. This approximation is derived in Appendix D and the values from this approximation are also indicated in Figures 9 through 12.

This model is oriented mainly toward the evaluation of the flux from the lunar surface subjected to solar irradiation. To evaluate this model of surface roughness experimental data is available to compare with the results of test area analysis. This data is derived from the results of earth observation of lunar emissions by Saari

Figure 9: Plots of $\mathcal{F}$, $\mathcal{F}_N$, and $\mathcal{F}_{NN}$ vs. distance from origin R_{ct} for normal distribution with $\omega_{ct} = 0°$

——————— $\mathcal{F}_{NN}$ (sun shadowing and view blockage neglected)

— — — — $\mathcal{F}_N$ (view blockage neglected)

Points represent values of $\mathcal{F}$

○ — $\alpha_s = 0°$ Δ — $\alpha_s = -45°$

□ — $\alpha_s = -30°$ ● — $\alpha_s = -60°$

◀— Values of approximation from Appendix D

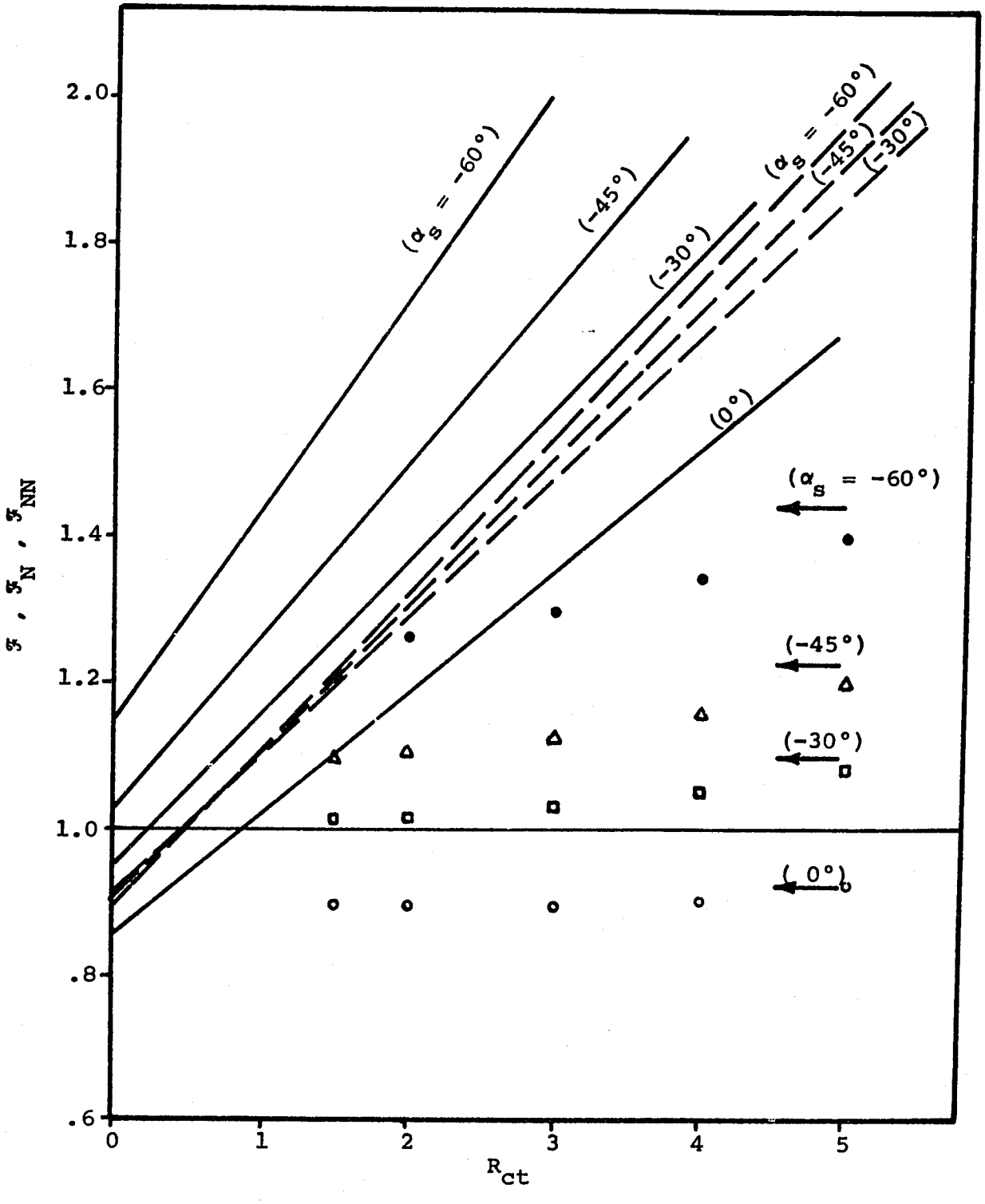

Figure 10: Plots of $\mathcal{F}$, $\mathcal{F}_N$, and $\mathcal{F}_{NN}$ vs. distance from the origin R_{ct} for a random distribution with $\omega_{ct} = 0°$

——— $\mathcal{F}_{NN}$ (sun shadowing and view blockage neglected)

— — — $\mathcal{F}_N$ (view blockage neglected)

Points represent values of $\mathcal{F}$

o — $\alpha_s = 0°$ Δ — $\alpha_s = -45°$

□ — $\alpha_s = -30°$ ● — $\alpha_s = -60°$

← Value of approximation from Appendix D

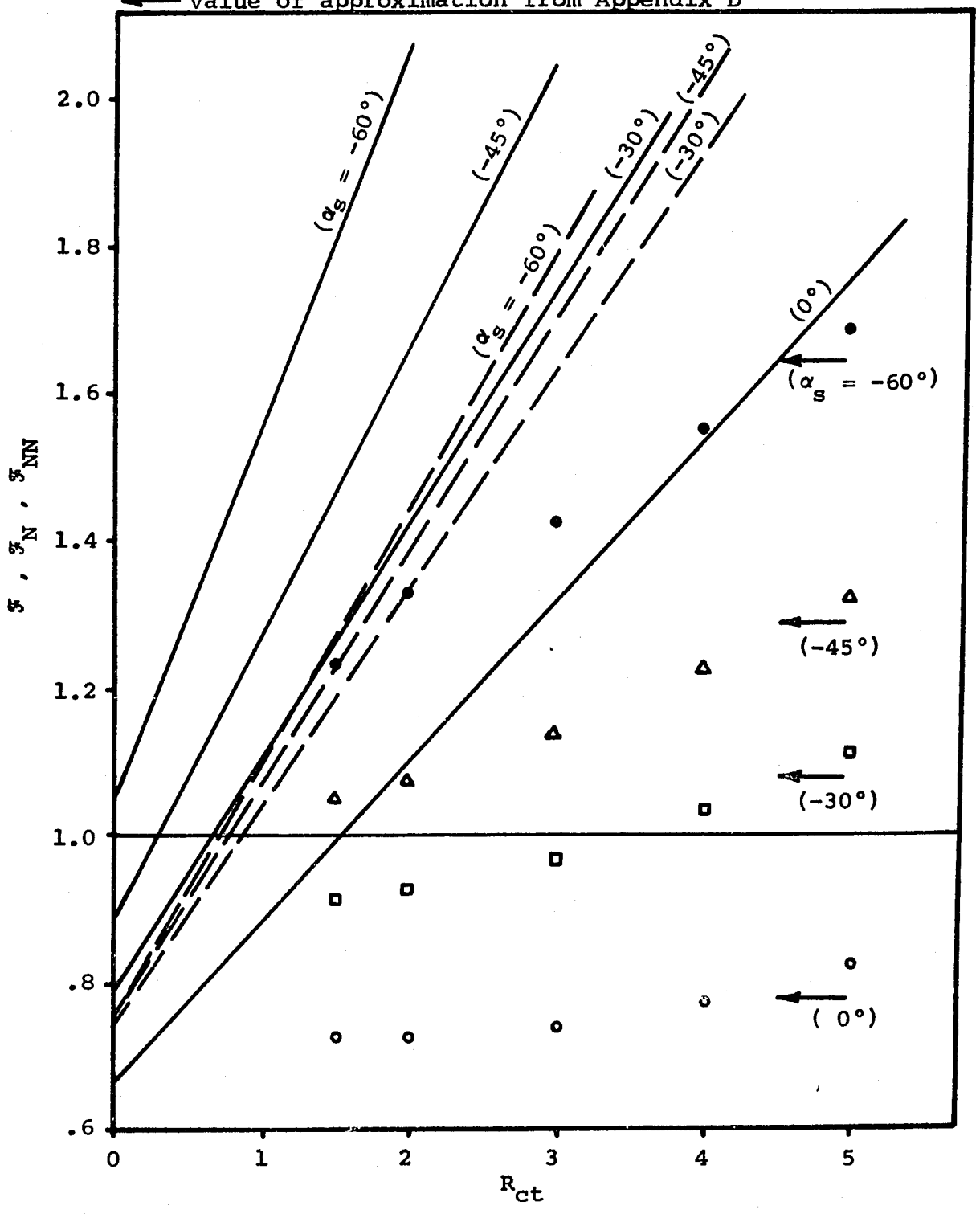

Figure 11: Plots of $\mathcal{F}$ and $\mathcal{F}_{NN}$ vs. distance from the origin R_{ct} for normal distribution with $\omega_{ct} = 45°$

——— $\mathcal{F}_{NN}$ (sun shadowing and view blockage neglected)

Points represent values of $\mathcal{F}$

□ — $\alpha_s = -30°$ ● — $\alpha_s = -60°$

◀— Values of approximation from Appendix D

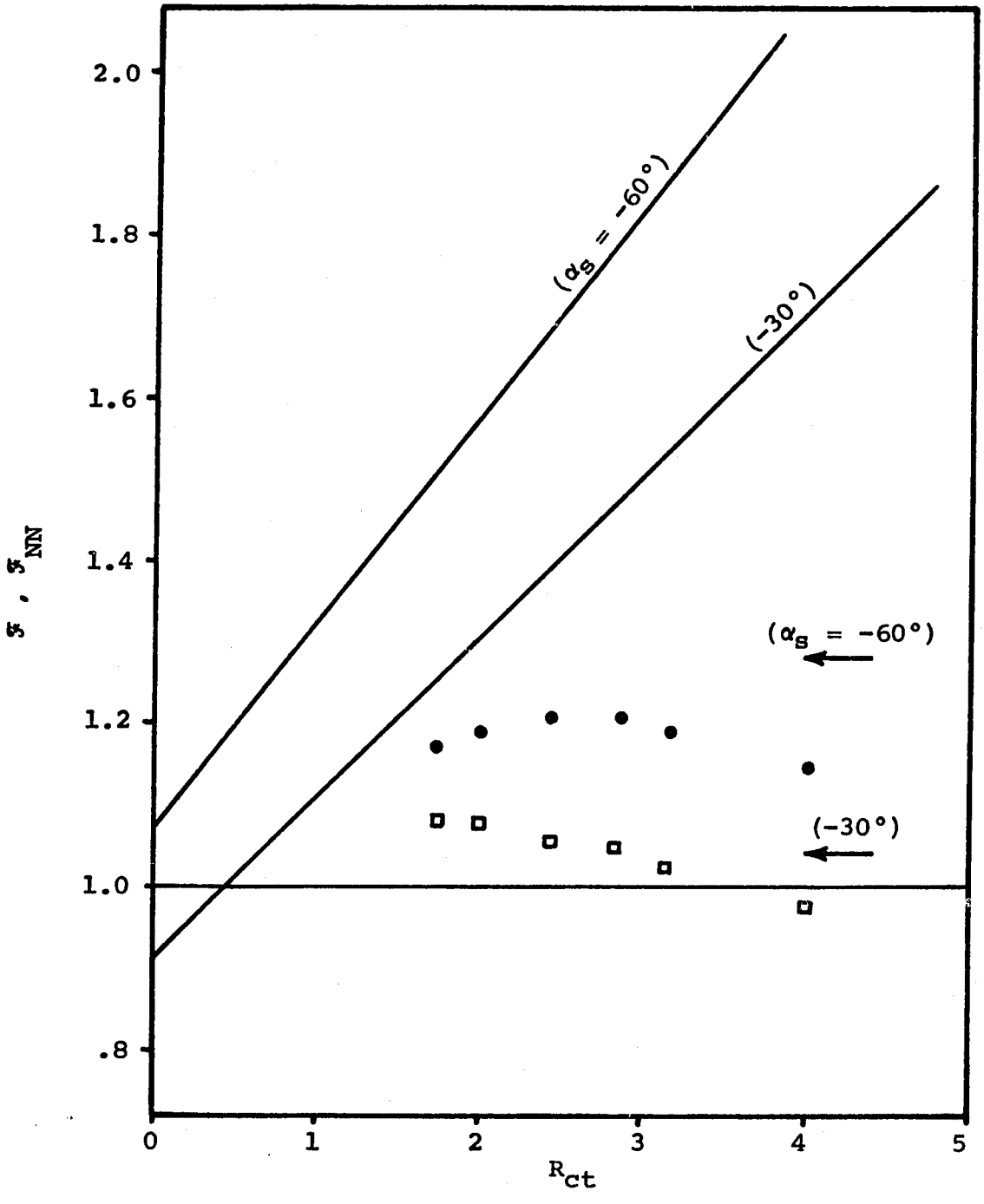

Figure 12: Plots of $\mathcal{F}$ and $\mathcal{F}_{NN}$ vs. distance from the origin R_{ct} for random distribution with $\omega_{ct} = 45°$

——— $\mathcal{F}_{NN}$ (sun shadowing and view blockage neglected)

Points represent values of $\mathcal{F}$

□ — $\alpha_s = -30°$ ● — $\alpha_s = -60°$

◄—— Values of approximation from Appendix D

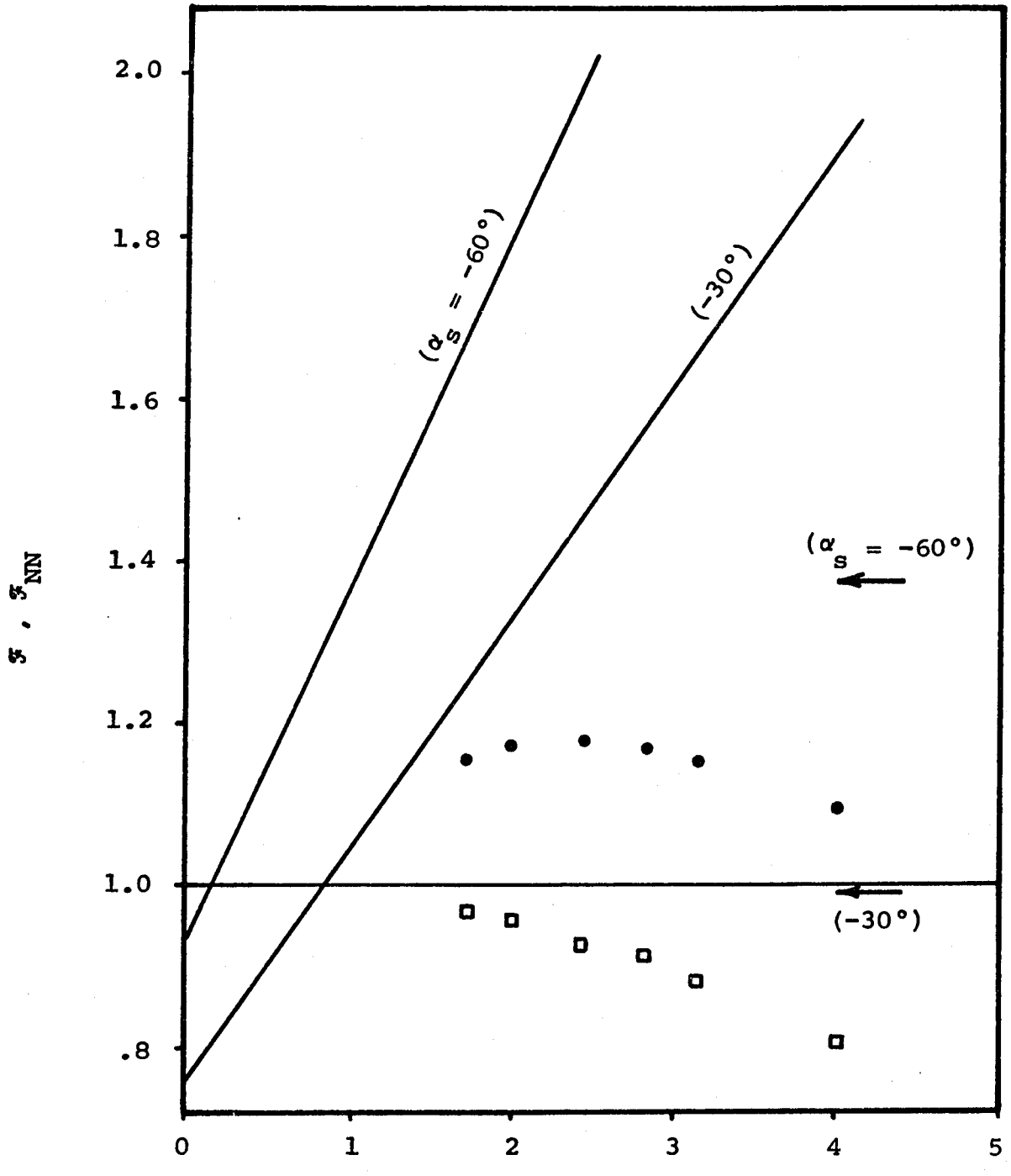

Figure 13: Plot of $\mathcal{F}_{NN}$ vs. R_{ct} for a normal distribution with various values of maximum polar angle and $\omega_{ct} = 0°$

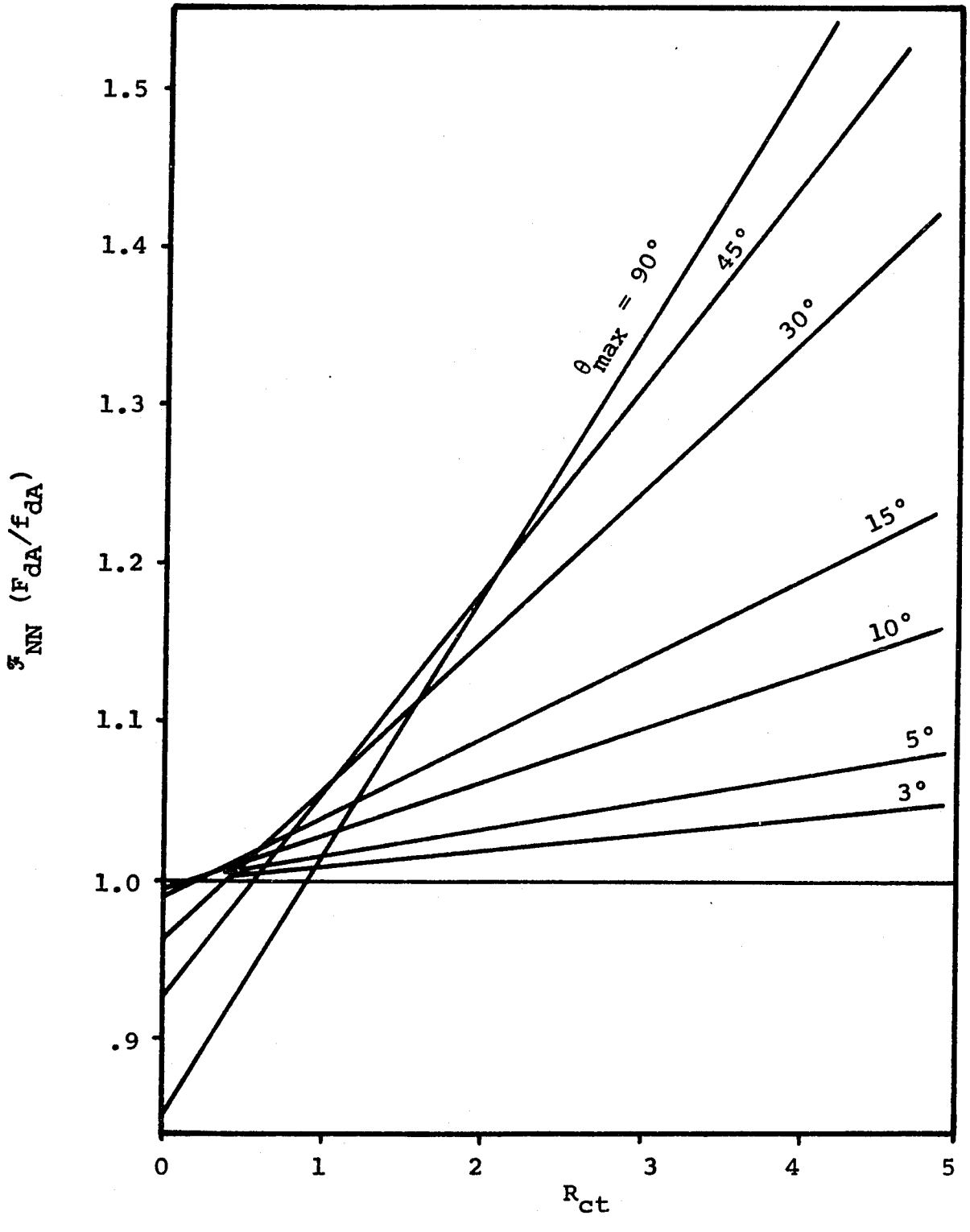

and Shorthill[10]. In these experimental measurements the sun angle and orientation of the observation point were allowed to vary, but since the earth and moon orbits are essentially in the same plane measurements were made only for locations corresponding to the line of symmetry in the mean surface level. The results of Saari and Shorthill consisted of curves which represented least square fits to the measured values. A first comparison of results is given in Figure 14. This plot is of the limiting case approximation of Appendix D for both normal and random distributions and the corresponding data points of Saari and Shorthill. Both distributions show good agreement with the trend of experimental data, and the random distribution fits the data a little more closely in certain portions of the curve. To continue the comparison Figures 15, 16 and 17 give plots of the results of the test area analysis and appropriate experimentally derived curves of Saari and Shorthill.

Infinite Surface Results

Now to consider the final results of this analysis. The energy flux from the region outlined with dashed lines in Figures 5, 6 and 7 is calculated using normal and random height distributions of grid elements and the energy

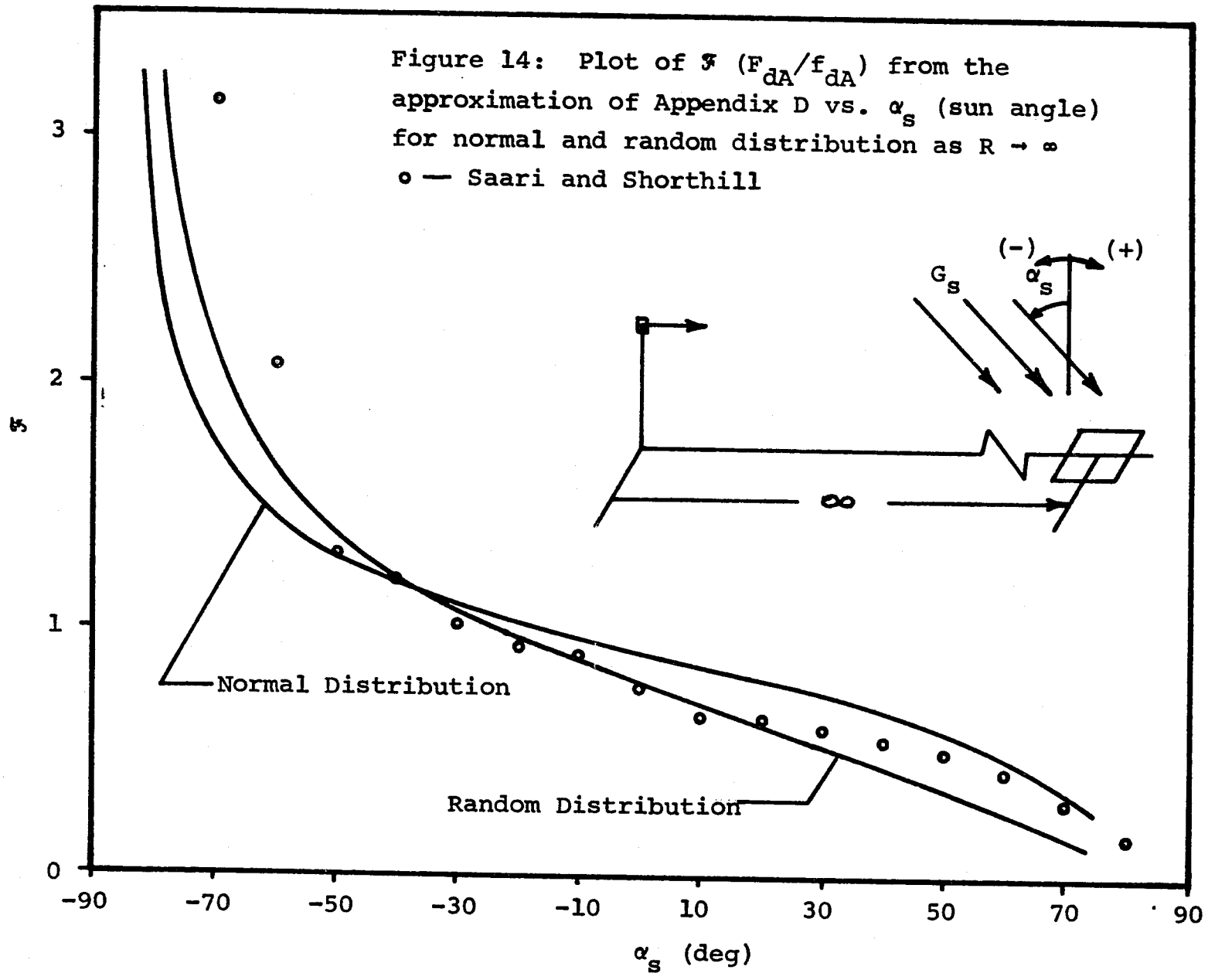
Figure 14: Plot of $\mathfrak{F}$ (F_{dA}/f_{dA}) from the approximation of Appendix D vs. α_s (sun angle) for normal and random distribution as R → ∞
o — Saari and Shorthill
(-)
(+)
G_s
α_s
∞
Normal Distribution
Random Distribution
$\mathfrak{F}$
0
1
2
3
-90
-70
-50
-30
-10
10
30
50
70
90
α_s (deg)

Figure 15: $\mathcal{F}$ vs. observation angle for sun elevation angle = 90° (α_s = 0°)

– – – – – Saari and Shorthill data

o ——— Normal distribution

● ——— Random distribution

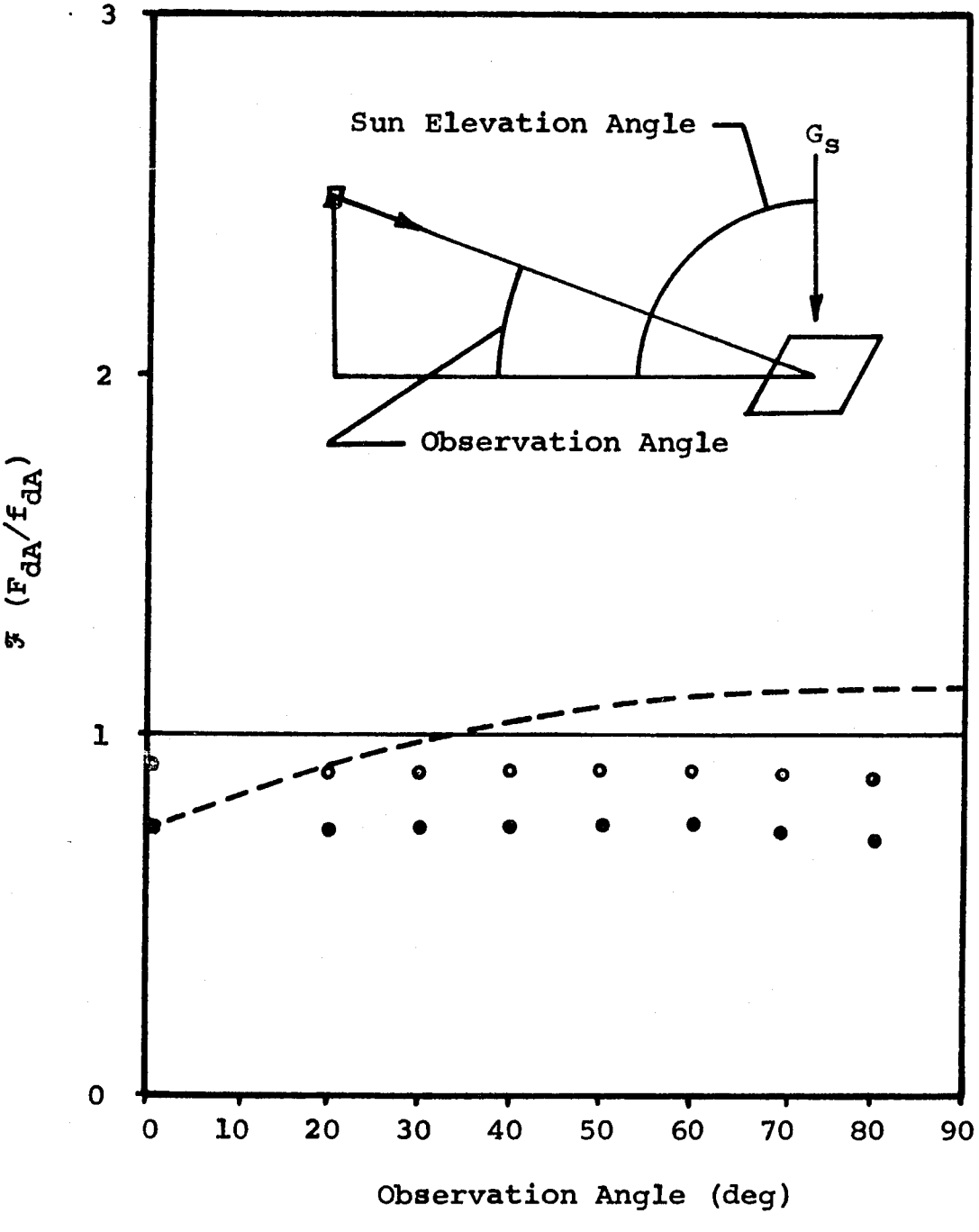

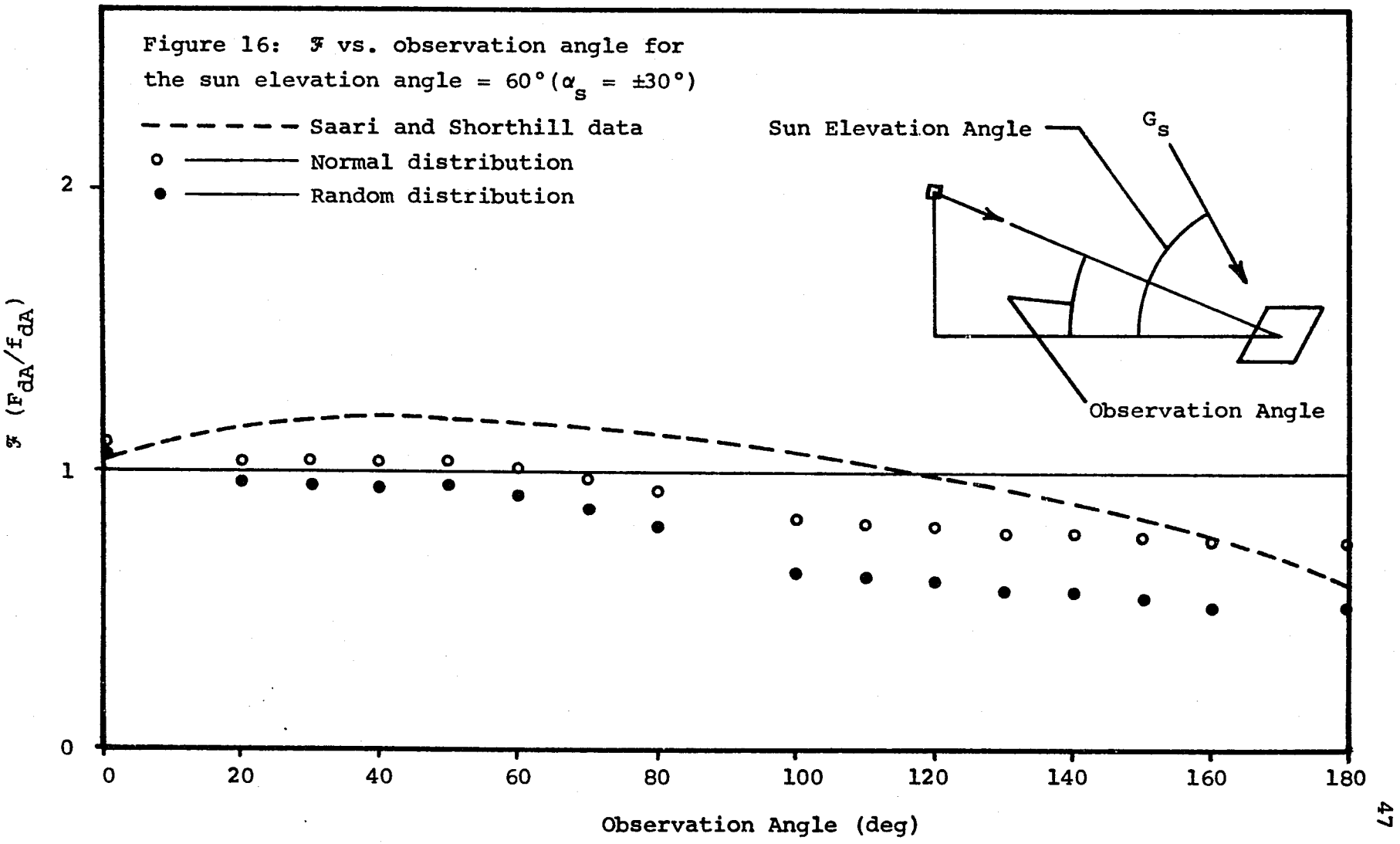
Figure 16: ℱ vs. observation angle for
the sun elevation angle = 60° (α_s = ±30°)
Saari and Shorthill data
Normal distribution
Random distribution
Sun Elevation Angle
G_s
Observation Angle
ℱ (F_{dA}/f_{dA})
2
1
0
0
20
40
60
80
100
120
140
160
180
Observation Angle (deg)

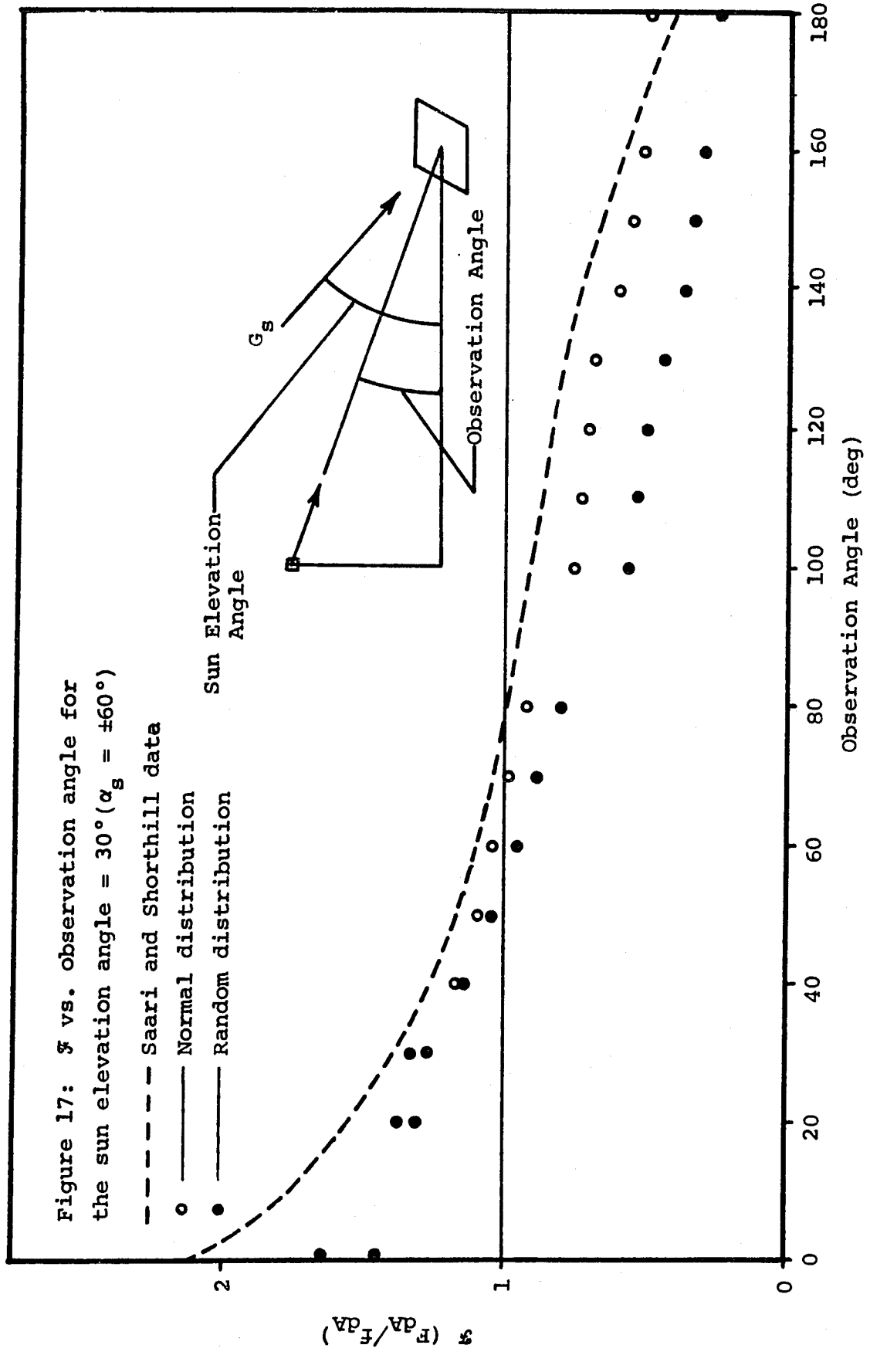
Figure 17: $\mathcal{F}$ vs. observation angle for the sun elevation angle = 30°(α_s = ±60°)
Saari and Shorthill data
Normal distribution
Random distribution
Sun Elevation Angle
G_s
Observation Angle
$\mathcal{F}$ (F_{dA}/F_{dA})
Observation Angle (deg)
0
1
2
0
20
40
60
80
100
120
140
160
180

flux from the region outside this rectangle is calculated by the method described in Appendix F. The sum of these fluxes represents the energy flux from a rough surface of infinite extent. The ratio of this sum to the energy flux from a flat, diffuse surface of infinite extent gives the value of F_{dA}/f_{dA} for an infinite surface. This ratio for normal and random height distributions is plotted in Figures 18 and 19. There are no direct experimental values for this quantity, but some empirically derived results for this quantity have been made by Harrison.[13] In this work an empirically derived expression developed by Ashby and Burkhard[14] for the intensity of radiation from the lunar surface was used. The data was from the experimental work of Saari and Shorthill[8] and some limited thermal radiation measurements by Surveyor I[15] on the moon's surface. These data were used as a basis for a curve fitting process to determine the directional properties of the intensity of lunar emissions. These empirically derived equations for lunar intensity were integrated by Harrison[13] over a surface which consisted of a disk of radius = 1000 H where H is the height of the receiving differential area above this disk to get a value of the energy flux at the differential area. This size disk is an infinite surface for all practical purposes. The ratio of Harrison's empirically derived

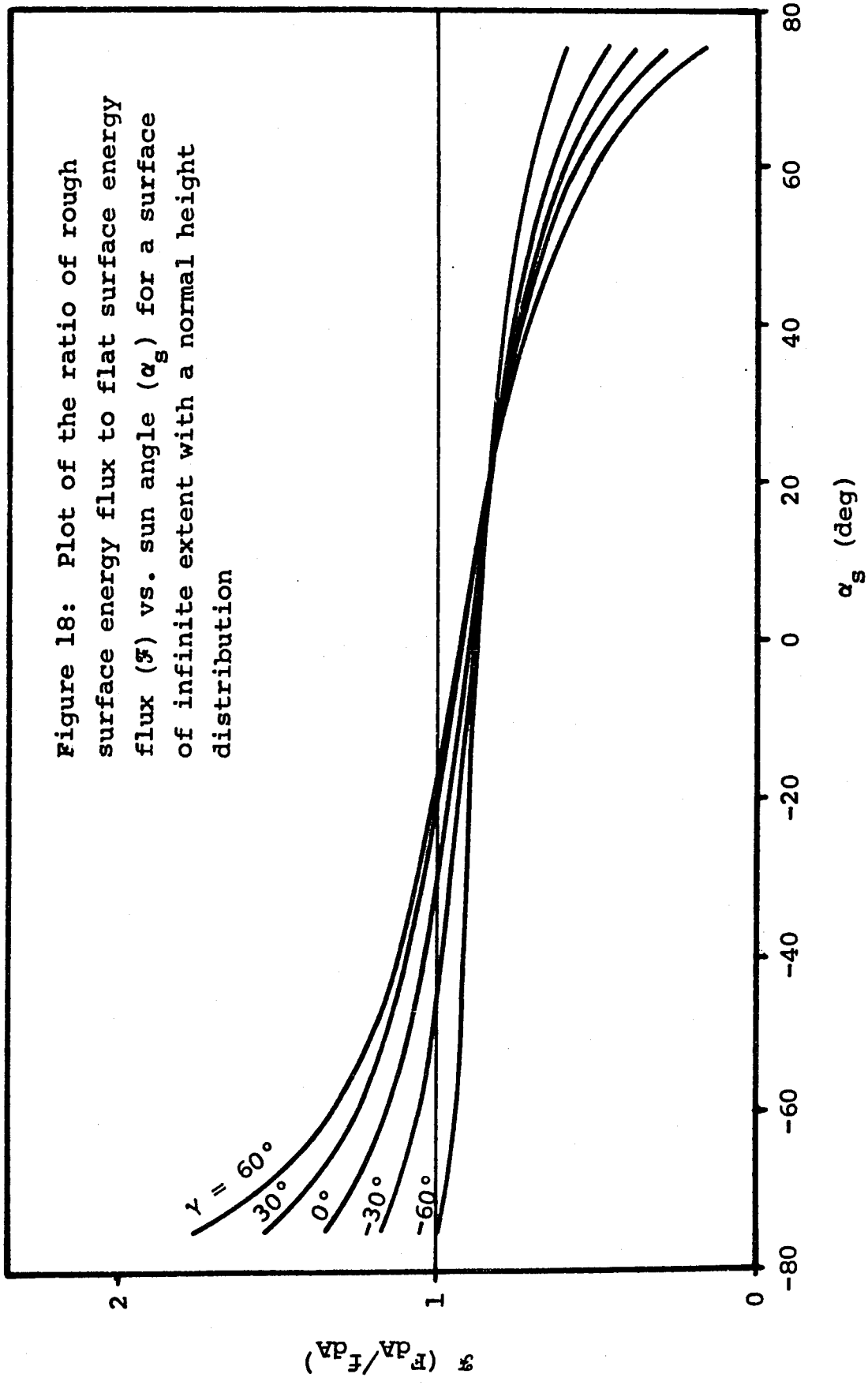
Figure 18: Plot of the ratio of rough surface energy flux to flat surface energy flux (ℱ) vs. sun angle (α_s) for a surface of infinite extent with a normal height distribution
$\mathcal{F}$ (F_{dA}/f_{dA})
2
1
0
γ = 60°
30°
0°
-30°
-60°
80
60
40
20
0
-20
-40
-60
-80
α_s (deg)

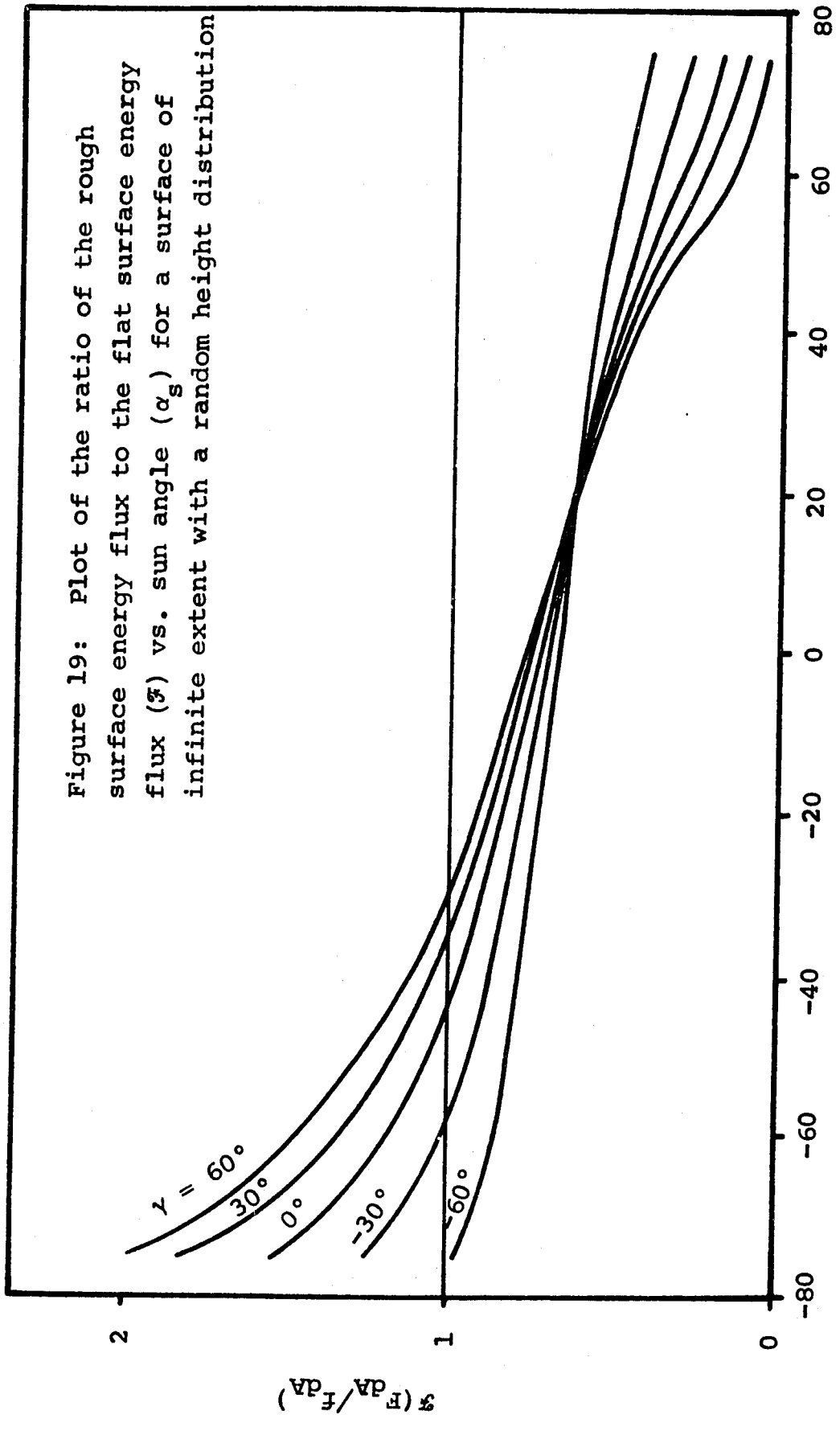

Figure 19: Plot of the ratio of the rough surface energy flux to the flat surface energy flux ($\mathcal{F}$) vs. sun angle (α_s) for a surface of infinite extent with a random height distribution

flux to the flux from a flat, diffuse surface is plotted in Figure 22. Also plotted are the results of the analytical model for this ratio with the same orientation of the differential area for both normal and random height distributions. The plots show generally good agreement with the normal distribution showing closer agreement to Harrison's results. In Figures 20 and 21 the ratio F_{dA}/f_{dA} is plotted for normal and random height distributions considering only the energy flux from region A_g bounded by the dashed lines in Figures 5, 6 and 7. Comparison of these plots with Figures 18 and 19 (the infinite surface cases) shows only minor modification by the inclusion of the remaining part of the infinite surface.

A minor point concerning the differential area orientation angle γ should be explained. The curves of Figures 18, 19, 20 and 21 labelled $\gamma = \pm 30°$ and $\pm 60°$ should actually be $\pm 30.1137°$ and $\pm 60.1135°$ respectively. The reason these curves were calculated at these odd angles resulted from a method of saving computer time in the calculations. Only one position of the grid system with respect to the coordinate axes was used for all values of γ and to avoid considering fractional grid elements the values of γ were not set equal to $\pm 30°$ and $\pm 60°$ but to the values of γ which were nearest to these values and still consistent with the grid lines.

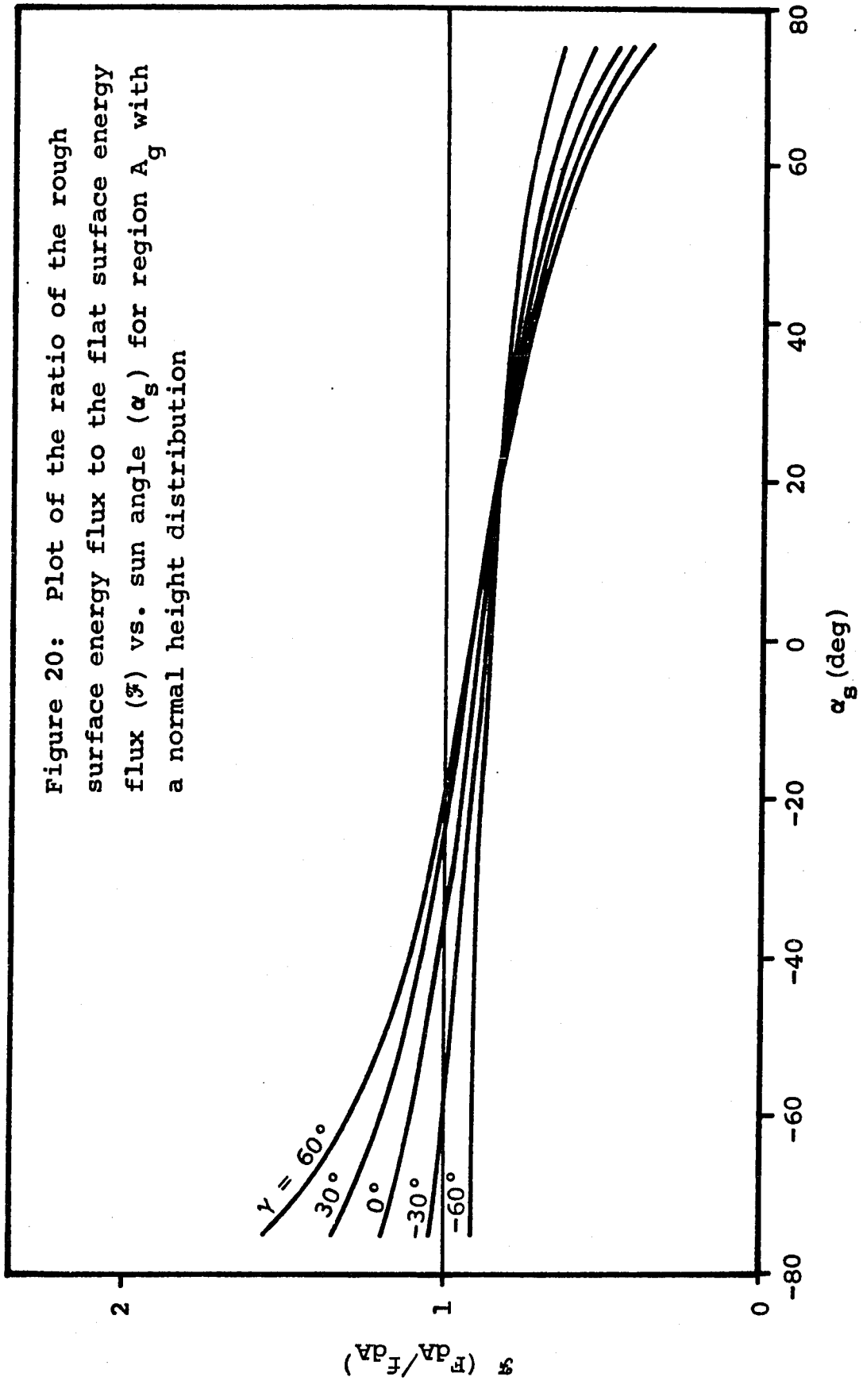

Figure 20: Plot of the ratio of the rough surface energy flux to the flat surface energy flux ($\mathfrak{F}$) vs. sun angle (α_s) for region A_g with a normal height distribution

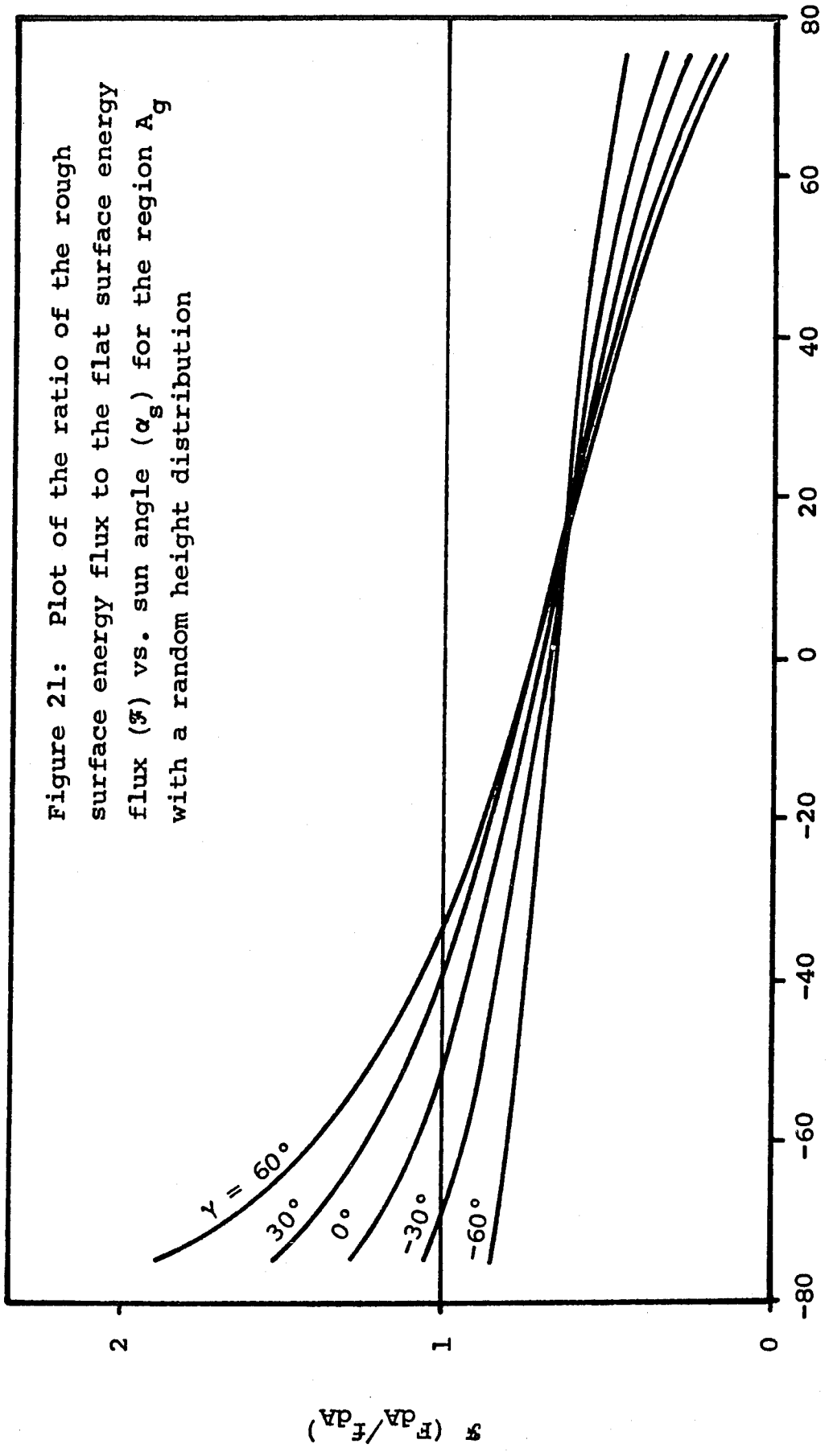
Figure 21: Plot of the ratio of the rough surface energy flux to the flat surface energy flux (F) vs. sun angle (α_s) for the region A_g with a random height distribution
γ = 60°
30°
0°
-30°
-60°
$\mathcal{F}$ (F_{dA}/F_{dA})
α_s (deg)
2
1
0
80
60
40
20
0
-20
-40
-60
-80

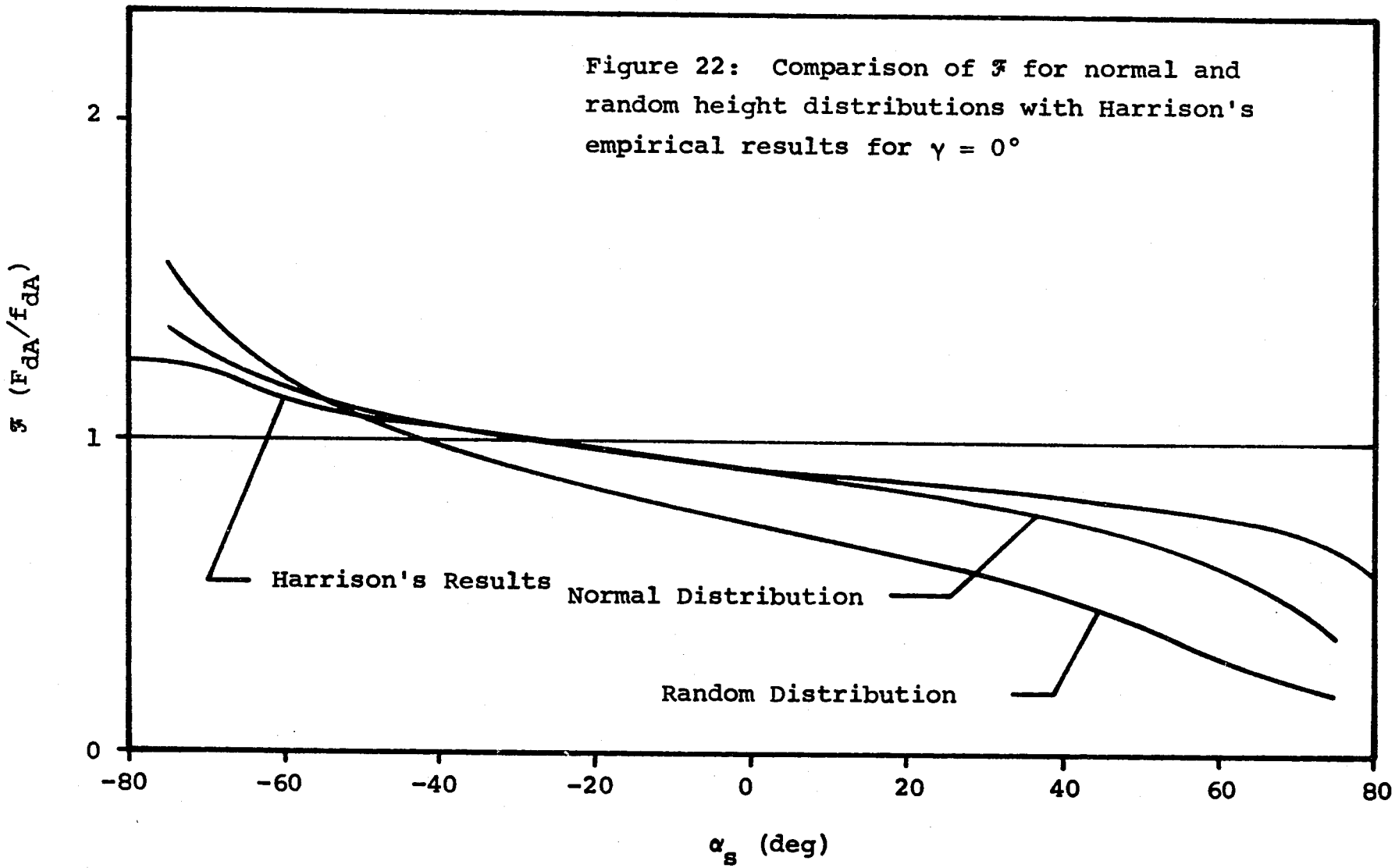

Figure 22: Comparison of $\mathcal{F}$ for normal and random height distributions with Harrison's empirical results for $\gamma = 0°$

VI. CONCLUSIONS

An analysis of the heat transfer from the model of a surface which contains roughness but still retains the simplifying assumption of diffuse reflection and emission has been investigated. The results indicate a higher flux in the general direction of the incident energy. This is consistent with the lunar emission measurements of Saari and Shorthill[10]. No direct measurements of infinite surface case are available, but Harrison's empirical results for this case show this trend and agree well with the results of this analysis for the normal distribution case. From the Figures 9 through 12 it is concluded that view blockage is an important aspect of the analysis for the infinite surface case since the flux, when view blockage is neglected, becomes indeterminate as the distance from the differential area tends to infinity. The analysis of both random and normal height distributions show the same trends in the results with the normal distribution having a better overall agreement with the available data. From this similarity of trends it is

concluded that the exact nature of the roughness height distribution is not critical to the results indicating higher fluxes in the incident direction.

As further study a possible extension of the analysis would be to consider the case of the sun not in the plane of symmetry. This would require more computer time for solution because some of the basic symmetry is lost in this case. Another extension would be to consider non-planar roughness elements (i.e., hemispherical or pyramid shaped roughness elements). An additional investigation of interest would be to retain the planer grid elements but restrict the maximum polar angle allowed to some value less than 90° as was used in this analysis. This case would be of interest if a rough surface were covered with an unconsolidated layer of dust or sand which would have maximum slope determined by the particle's angle of internal friction.

VII. REFERENCES

[1]Harrison, W. N.: "Pitfalls in Thermal Emission Studies." Measurement of Thermal Radiation Properties of Solids. J. C. Richmond ed., NASA SP-31, 1963, pp 3-10.

[2]Sparrow, E. M.; and Cess, R. D.: Radiation Heat Transfer. Brooks/Cole Publishing Company, Belmont, California, 1966, pp 44-48.

[3]Gubareff, G. G.; Janssen, J. E.; and Torborg, R. H.: Thermal Radiation Properties Survey, second edition. Honeywell Research Center, Minneapolis, Minn., 1960.

[4]Beckmann, P.; and Spizzichino, A.: The Scattering of Electromagnetic Waves from Rough Surfaces. The Macmillan Company, 1963, Chapter 2.

[5]Siegel, R.; and Howell, J. R.: Thermal Radiation Heat Transfer. Vol. 1, NASA SP-164, 1968, Chapter 4.

[6]Hering, R. G.; and Smith, T. F.: "Surface Roughness Effects on Radiant Transfer between Surfaces." Int. J. Heat Mass Transfer, Vol. 13, No. 4, April 1970, pp 725-739.

[7]Black, W. Z.; and Schoenhals, R. J.: "An Experimental Study of Radiation Heat Transfer from Parallel Plates with Direction-Dependent Properties." A.S.M.E. No. 70-HT/SpT-1, 1970.

[8]Smith, T. F.; and Hering, R. G.: "Bidirectional Reflectance of a Randomly Rough Surface." AIAA No. 71-465, 1971.

[9]Petit, E.; and Nicholson, Seth B.: "Lunar Radiation and Temperatures." Journal of Astrophysics, Vol. 71, 1930, p 102.

[10]Saari, J. M.; and Shorthill, R. W.: "Review of Lunar Infrared Observations." Physics of the Moon, ed. S. Fred Singer, AAS Science and Technology Series, Vol. 13, 1967.

[11]Orlova, N. S.: "Photometric Relief of the Lunar Surface." Astron. Zhur., Vol. 33, No. 1, Jan/Feb 1956, pp 93-100.

[12]Chapman, A. J.: Heat Transfer. The Macmillan Company, 1967, Chapter 11.

[13]Harrison, J. K.: "Calculations of Non-Diffuse Infrared Radiation from the Lunar Surface Incident onto a Unit Element Above the Surface." NASA Technical Memorandum X-1567, 1968.

[14]Ashby, Neil; and Burkhard, D. G.: "Study of Radiative Aspects of Lunar Materials." Final Report on Contract NAS8-20385 covering Period April 26, 1966 to January 26, 1967. P.E.C. Research Associates, Inc.

[15]Lucas, J. W., et al.: "Lunar Surface Thermal Characteristics." Chapter IV, Surveyor I Mission Report, Part II: Scientific Data and Results. Technical Report No. 32-1023, Jet Propulsion Laboratory, California Institute of Technology, Pasadena, California, 1966.

[16]Spiegel, M. R.: Mathematical Handbook of Formulas and Tables. Schaum's Outline Series. McGraw-Hill Book Company, New York, 1968.

[17]Dwight, H. B.: Tables of Integrals and Other Mathematical Data. The Macmillan Company, New York, 1947.

[18]Communications of the Association of Computing Machinery's Collected Algorithms. Algorithm #266.

[19]Howell, J. R.; and Siegel, R.: Thermal Radiation Heat Transfer. Vol. 2, NASA SP-164, 1968.

[20]Abramowitz, M.; and Stegun, I. A.: Handbook of Mathematical Functions. Dover Publications, Inc., New York, 1965.

APPENDIX A

Energy Flux From a Rectangle in the Mean Surface Level

From equation (3) the heat flux at dA from a flat, diffuse surface of area A_p can be written as

$$f_{dA} = \int_{A_p} \frac{I \cos\beta \cos\beta'}{r^2} \, dA_p \qquad \text{(A-1)}$$

where A_p = an arbitrary area in the plane of the mean surface level

dA_p = a differential segment of area A_p

I = the intensity of the radiosity from dA_p

If the source of incident energy provides a constant, collimated energy flux of magnitude G and the reflections and emissions of the surface are diffuse then from equations (6) and (7)

$$I = \frac{G_s \cos\eta}{\pi} \qquad \text{(A-2)}$$

And so equation (A-1) can be written

$$f_{dA} = \frac{G_s}{\pi} \int_{A_p} \frac{\cos\eta\cos\beta\cos\beta'}{r^2} \, dA_p \qquad \text{(A-3)}$$

where G_s = solar constant at the mean earth radius from the sun

η = angle between the incident solar flux and the normal to dA_p

For an area in the mean surface level η is constant over the entire area and equal by definition to the sun angle α_s. So equation (A-3) becomes

$$f_{dA} = \frac{G \cos\alpha_s}{\pi} \int_{A_p} \frac{\cos\beta\cos\beta'}{r^2} \, dA_p \qquad \text{(A-4)}$$

To evaluate the integral the geometry in Figure A-1 is considered. The rectangle is assumed to be oriented so that each pair of sides is parallel to one of the coordinate axes. The center of the rectangle is allowed to have an arbitrary location in the mean surface level. In this derivation the normal to the receiving differential area dA will be allowed to have a value of the angle γ between $-\frac{\pi}{2}$ and $\frac{\pi}{2}$. Since the area is in the mean surface level equation (A-4) is applicable. Now to evaluate

$\frac{\cos\beta\ \cos\beta'}{r^2}$ for this case the geometry in Figure A-2 is considered. Using rectangular coordinates

$$\cos\beta = \frac{1}{\sqrt{\xi^2 + \chi^2 + 1}}$$

$$r = \sqrt{\xi^2 + \chi^2 + 1}$$

The projection of the normal N′ on the line joining dA and dA_p is N′cosβ′ and from geometry of Figure A-3 this can be written

$$N'\cos\beta' = N'\cos\gamma\cos\beta'' + N'\sin\gamma(-\cos\beta)$$

where

$$\cos\beta'' = \frac{\chi}{\sqrt{\xi^2 + \chi^2 + 1}}$$

and from above

$$\cos\beta = \frac{1}{r} = \frac{1}{\sqrt{\xi^2 + \chi^2 + 1}}$$

So now cosβ′ can be written

$$\cos\beta' = \frac{\chi\cos\gamma - \sin\gamma}{\sqrt{\xi^2 + \chi^2 + 1}} \qquad \text{(A-5)}$$

This gives

$$\frac{\cos\beta\cos\beta'}{r^2} = \frac{\chi\cos\gamma - \sin\gamma}{(\xi^2 + \chi^2 + 1)^2}$$

And since

$$dA_p = d\chi\, d\xi \quad ,$$

equation (A-4) can be written

$$f_{dA} = \frac{G_s\cos\alpha_s}{\pi} \int\int_{A_p} \frac{\chi\cos\gamma - \sin\gamma}{(\xi^2 + \chi^2 + 1)^2}\, d\chi\, d\xi \qquad \text{(A-6)}$$

Before evaluating the limits of integration it should be pointed out that for the area A_p to contribute to the heat flux at dA the area must be in the "field of view" at dA as indicated in Figure A-1. The viewing limit for any angle γ is determined by equation (A-5) for $\cos\beta' = 0$. This requires

$$\chi_{min} \geq \tan\gamma$$

where χ_{min} is the smallest value of χ in A_p, for the entire area A_p to be in the field of view. In this derivation A_p is assumed to be in the field of view (this can be adjusted by redefining the area A_p such that

$\chi_{min} = \tan\gamma)$. Now rewriting equation (A-6) with the limits of integration from Figure A-1,

$$f_{dA} = \frac{G_s \cos\alpha_s}{\pi} \int_{\chi_-}^{\chi_+} \int_{\xi_-}^{\xi_+} \frac{\chi\cos\gamma - \sin\gamma}{(\xi^2 + \chi^2 + 1)^2} \, d\xi \, d\chi$$

or

$$f_{dA} = \frac{G \cos\gamma}{\pi} \int_{\xi_-}^{\xi_+} \int_{\chi_-}^{\chi_+} \frac{\chi \, d\chi \, d\xi}{(\xi^2 + \chi^2 + 1)^2} - \frac{G \sin\gamma}{\pi} \int_{\xi_-}^{\xi_+} \int_{\chi_-}^{\chi_+} \frac{d\chi \, d\xi}{(\xi^2 + \chi^2 + 1}$$

and in abbreviated form

$$f_{dA} = G \cos\gamma \, S_1 - G \sin\gamma \, S_2$$

Using equation (14.133) from Reference (10) gives for the first integration of S_1

$$2S_1 = - \int_{\xi_-}^{\xi_+} \frac{d\xi}{(\xi^2 + \chi_+^2 + 1)} + \int_{\xi_-}^{\xi_+} \frac{d\xi}{(\xi^2 + \chi_-^2 + 1)}$$

Equation (14.125) from (16) gives

$$2S_1 = \frac{1}{\sqrt{\chi_-^2 + 1}} \tan^{-}\left(\frac{\xi_+}{\sqrt{\chi_-^2 + 1}}\right) - \frac{1}{\sqrt{\chi_-^2 + 1}} \tan^{-1}\left(\frac{\xi_-}{\sqrt{\chi_-^2 + 1}}\right)$$

$$- \frac{1}{\sqrt{\chi_+^2 + 1}} \tan^{-1}\left(\frac{\xi_+}{\sqrt{\chi_+^2 + 1}}\right) + \frac{1}{\sqrt{\chi_+^2 + 1}} \tan^{-1}\left(\frac{\xi_-}{\sqrt{\chi_+^2 + 1}}\right)$$

Now for integral S_2 using equation (14.125) of (16) gives

$$2S_2 = \int_{\xi_-}^{\xi_+} \frac{\chi}{(\xi^2 + 1)(\xi^2 + \chi^2 + 1)} \Big/_{\chi_-}^{\chi_+} d\xi$$

$$+ \int_{\xi_-}^{\xi_+} \frac{1}{(\xi^2 + 1)^{3/2}} \tan^{-1}\left(\frac{\chi}{(\xi^2 + 1)^{1/2}}\right) \Big/_{\chi_-}^{\chi_+} d\xi$$

or in abbreviated form

$$2S_2 = S_{2A} + S_{2B}$$

S_{2A} is of the form

$$S_{2A} = \int_{\xi_-}^{\xi_+} \frac{a}{(\xi^2 + 1)(\xi^2 + b)} d\xi$$

which can be written

$$S_{2A} = \frac{a}{b^2 - 1} \int_{\xi_-}^{\xi_+} \frac{d\xi}{\xi^2 + 1} - \frac{a}{b^2 - 1} \int_{\xi_-}^{\xi_+} \frac{d\xi}{\xi^2 + b^2}$$

and from equation (14.125) of (10) is

$$S_{2A} = \frac{a}{b^2 - 1}\left[\tan^{-1}(\xi)\Big|_{\xi_-}^{\xi_+} - \frac{1}{b}\tan^{-1}\left(\frac{\xi}{b}\right)\Big|_{\xi_-}^{\xi_+}\right]$$

or

$$S_{2A} = \frac{1}{\chi_+} \tan^{-1}(\xi)\Big|_{\xi_-}^{\xi_+} - \frac{1}{\chi_-} \tan^{-1}(\xi)\Big|_{\xi_-}^{\xi_+}$$

$$+ \frac{1}{\chi_-\sqrt{\chi_-^2 + 1}} \tan^{-1}\left(\frac{\xi}{\sqrt{\chi_-^2 + 1}}\right)_{\xi_-}^{\xi_+} - \frac{1}{\chi_+\sqrt{\chi_+^2 + 1}} \tan^{-1}\left(\frac{\xi}{\sqrt{\chi_+^2 + 1}}\right)_{\xi_-}^{\xi_+}$$

To complete the integration of S_2 it is noted that S_{2B} is of the form

$$2S_{2B} = \int \frac{u}{\sqrt{1 - u^2}} \tan^{-1}(au)\, du$$

where

$$u = \frac{1}{\sqrt{1 - \xi^2}}$$

Using integration by parts gives

$$2S_{2B} = -\sqrt{1 - u^2} \tan^{-1}(au) + a \int \frac{\sqrt{1 - u^2}}{(1 + a^2u^2)}\, du$$

letting

$$v = (1 - u^2)^{1/2} \qquad c^2 = \frac{a^2 + 1}{a^2}$$

$$a \int \frac{\sqrt{1 - u^2}}{1 + a^2u^2}\, du = \frac{1}{a} \int \frac{v^2}{(v^2 - c^2)} \frac{1}{(1 - v^2)^{1/2}}\, dv$$

From equation (197) of Reference (17) this becomes

$$2S_{2B} = -a \int \frac{w^2\, dw}{[w^2 + (a^2 + 1)](w^2 + 1)}$$

where

$$w = \frac{u}{\sqrt{1 - u^2}}$$

This can be written as

$$2S_{2B} = -\frac{(a^2 + 1)}{a} \int \frac{dw}{w^2 + (a^2 + 1)} - \frac{1}{a} \int \frac{dw}{w^2 + 1}$$

and from equation (14.125) of Reference (10) is

$$2S_{2B} = -\frac{\sqrt{a^2 + 1}}{a} \tan^{-1} \left(\frac{w}{\sqrt{a^2 + 1}} \right)_{w_-}^{w_+} + \frac{1}{a} \tan^{-1}(w)_{w_-}^{w_+}$$

Rewriting this in terms of ξ gives

$$2S_{2B} = \frac{-\xi}{\sqrt{\xi^2 + 1}} \tan^{-1} \left(\frac{a}{\sqrt{\xi^2 + 1}} \right)_{\xi_-}^{\xi_+} - \frac{\sqrt{a^2 + 1}}{a} \tan^{-1} \left(\frac{\xi}{\sqrt{a^2 + 1}} \right)_{\xi_-}^{\xi_+}$$

$$+ \frac{1}{a} \tan^{-1}(\xi)_{\xi_-}^{\xi_+}$$

or

$$2S_{2B} = \frac{\tan^{-}(\xi)\Big|_{\xi_-}^{\xi_+}}{\chi_-} - \frac{\tan^{-1}(\xi)\Big|_{\xi_-}^{\xi_+}}{\chi_+} - \frac{\chi_-}{\sqrt{\chi_-^2+1}}\tan^{-1}\left(\frac{\xi}{\sqrt{\chi_-^2+1}}\right)_{\xi_-}^{\xi_+}$$

$$+ \frac{\chi_+}{\sqrt{\chi_+^2+1}}\tan^{-1}\left(\frac{\xi}{\sqrt{\chi_+^2+1}}\right)_{\xi}^{\xi_+} + \frac{\sqrt{\xi^2+1}}{\xi}\tan^{-1}\left(\frac{\chi_+}{\sqrt{\xi^2+1}}\right)_{\xi_-}^{\xi_+}$$

$$- \frac{\sqrt{\xi^2+1}}{\xi}\tan^{-1}\left(\frac{\chi}{\sqrt{\xi^2+1}}\right)_{\xi_-}^{\xi_+}$$

Now combining S_{2A} and S_{2B} and some manipulation gives

$$2S_2 = -\frac{\xi_-}{\sqrt{\xi_-^2+1}}\left[\tan^{-1}\left(\frac{\sqrt{\xi_-^2+1}}{\chi_-}\right) - \tan^{-1}\left(\frac{\sqrt{\xi_-^2+1}}{\chi_+}\right)\right]$$

$$- \frac{\xi_+}{\sqrt{\xi_+^2+1}}\left[\tan^{-1}\left(\frac{\sqrt{\xi_+^2+1}}{\chi_+}\right) - \tan^{-1}\left(\frac{\sqrt{\xi^2+1}}{\chi_-}\right)\right]$$

$$- \frac{\chi_-}{\sqrt{\chi_-^2+1}}\left[\tan^{-1}\left(\frac{\xi_+}{\sqrt{\chi_-^2+1}}\right) - \tan^{-1}\left(\frac{\xi_-}{\sqrt{\chi_-^2+1}}\right)\right]$$

$$- \frac{\chi_+}{\sqrt{\chi_+^2+1}}\left[\tan^{-1}\left(\frac{\xi_-}{\sqrt{\chi_+^2+1}}\right) - \tan^{-1}\left(\frac{\xi_+}{\sqrt{\chi_+^2+1}}\right)\right]$$

So the final form of f_{dA} is

$$
\begin{aligned}
f_{dA} = {} & \frac{G_s \cos\alpha_s \cos\gamma}{2\pi} \left\{ \frac{1}{\sqrt{\chi_-^2 + 1}} \left[\tan^{-1}\left(\frac{\xi_-}{\sqrt{\chi_-^2 + 1}} \right) - \tan^{-1}\left(\frac{\xi_-}{\sqrt{\chi_-^2 + 1}} \right) \right] \right. \\
& \left. - \frac{1}{\sqrt{\chi_+^2 + 1}} \left[\tan^{-1}\left(\frac{\xi_+}{\sqrt{\chi_+^2 + 1}} \right) - \tan^{-1}\left(\frac{\xi_-}{\sqrt{\chi_+^2 + 1}} \right) \right] \right\} \\
& + \frac{G_s \cos\alpha_s \sin\gamma}{2\pi} \left\{ \frac{\xi_-}{\sqrt{\xi_-^2 + 1}} \left[\tan^{-1}\left(\frac{\sqrt{\xi_-^2 + 1}}{\chi_-} \right) - \tan^{-1}\left(\frac{\sqrt{\xi_-^2 + 1}}{\chi_+} \right) \right] \right. \\
& + \frac{\xi_+}{\sqrt{\xi_+^2 + 1}} \left[\tan^{-1}\left(\frac{\sqrt{\xi^2 + 1}}{\chi_+} \right) - \tan^{-1}\left(\frac{\sqrt{\xi_+^2 + 1}}{\chi_-} \right) \right] \\
& + \frac{\chi_-}{\sqrt{\chi_-^2 + 1}} \left[\tan^{-1}\left(\frac{\xi_+}{\sqrt{\chi_-^2 + 1}} \right) - \tan^{-1}\left(\frac{\xi_-}{\sqrt{\chi_-^2 + 1}} \right) \right] \\
& \left. + \frac{\chi_+}{\sqrt{\chi_+^2 + 1}} \left[\tan^{-1}\left(\frac{\xi_-}{\sqrt{\chi_+^2 + 1}} \right) - \tan^{-1}\left(\frac{\xi_+}{\sqrt{\chi_+^2 + 1}} \right) \right] \right\}
\end{aligned}
$$

(A-7)

To consider the fraction of the infinite, flat surface flux provided by a finite area in the mean surface level, the following special case is investigated. If $\gamma = 0$ and the rectangle location is such that one side is colinear with the ξ axis ($\chi_- = 0$) and another side is colinear with the χ axis ($\xi_- = 0$) then equation (A-7) becomes

$$f_{dA} = \frac{G_s \cos\alpha_s}{2\pi} \left[\tan^{-1}(\xi_+) - \frac{1}{\sqrt{\chi_+^2 + 1}} \tan^{-1}\left(\frac{\xi_+}{\sqrt{\chi_+^2 + 1}} \right) \right]$$

Letting $\chi_+ = L$ and $\xi_+ = Z\chi_+ = ZL$ with rearrangement gives

$$f_{dA_L} = \frac{f_{dA}}{G_s \cos\alpha_s} = \frac{1}{2\pi} \left[\tan^{-1}(ZL) - \frac{1}{\sqrt{L^2 + 1}} \tan^{-1}\left(\frac{ZL}{\sqrt{L^2 + 1}} \right) \right]$$

The infinite flat surface case ($L \to \infty$ for any non-zero value of Z) gives

$$f_{dA_{L\to\infty}} = \left. \frac{f_{dA}}{G_s \cos\alpha_s} \right|_{L\to\infty} = \frac{1}{4}$$

(note that this case represents only one quadrant of the coordinate system (ξ,χ) and therefore is 1/4 instead of

1/2 as would be the case for the entire surface.) The ratio of these two quantities is plotted in Figure A-4 with Z as parameter. This plot shows how the finite area case tends to the infinite area case.

Contour Plots for a Differential Area in the Mean Surface Level

From equation (A-4) it is clear that

$$f_{dA_p \rightarrow dA} = \frac{G_s \cos\alpha_s}{\pi} \frac{\cos\beta \cos\beta'}{r^2}$$

where $f_{dA_p \rightarrow dA}$ = the heat flux per square foot received at dA from a differential area dA_p. Rearranging and evaluating terms with rectangular coordinates ξ, χ gives

$$\frac{f_{dA_p \rightarrow dA}}{G_s \cos\alpha_s} = \frac{1}{\pi} \frac{\chi\cos\gamma - \sin\gamma}{(\xi^2 + \chi^2 + 1)^2}$$

The quantity on the right (actually this is a differential shape factor) gives the relative importance to the heat flux at dA of a differential area in the mean surface level as a function of position in the mean surface level. Contour plots of this quantity for several values of γ are given in Figures 5, 6 and 7. These curves are of interest

in establishing the shape of the region in the mean surface level to be treated by the grid system analysis.

Sizing of A_g

The area A_g is the area in the mean surface level which is treated by grid system analysis in calculating rough surface heat flux. The remaining portion of the infinite surface is treated by an approximation derived in Appendix D with the method explained in Appendix F. The area is actually a function of γ , but for this analysis only the case of $\gamma = 0$ will be considered. First it is assumed that the rough surface results will be similar to the flat surface results for the fraction of the infinite surface flux contributed by a finite rectangular region. Obviously this is not exactly correct, but the plots of Figures 9 through 12 indicate this assumption is not too unreasonable. There are several considerations in sizing A_g . First the computer time required for solutions is proportional to the area A_g . Secondly the maximum length L is restricted by neglection of second order view blockage. The maximum value of L for which this becomes significant is difficult to calculate, but a value between 4 and 5 is reasonable. Thirdly, the agreement of limiting values and grid analysis results at the

boundaries of A_g is important, but the plots in Figures 9 and 10 indicate close agreement for R greater than about 3. From the second consideration the value of L was set at 4.5. To determine the value of Z Figure A-4 and contour plots of Figures 5, 6 and 7 are considered. Figure A-4 shows that for Z greater than about .6 the addition of area adds little to the total flux. The contour plots confirm this conclusion and from computer time considerations, the value of Z was set at about .6 (the value must be compatible with the grid size used). Rectangles of those dimensions are drawn on the contour plots of Figures 5, 6 and 7.

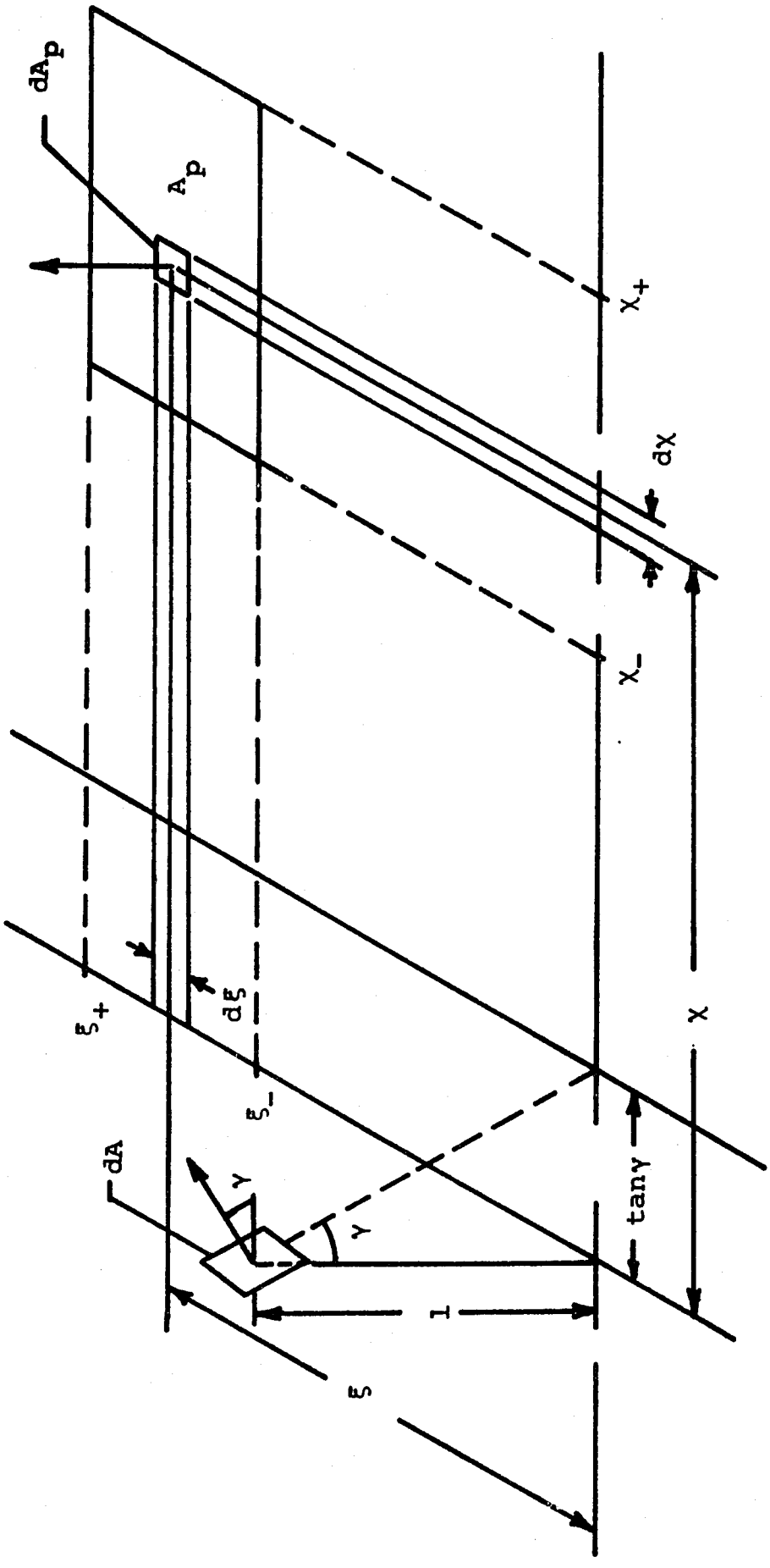

Figure A-1: Area A_p in the mean surface level

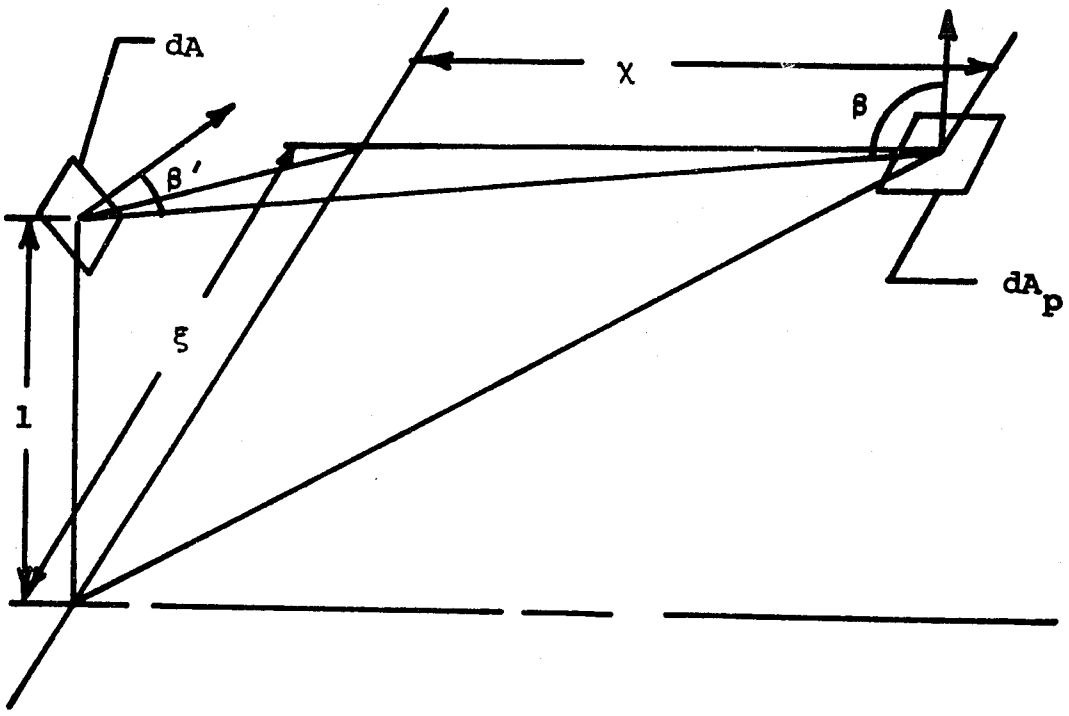

Figure A-2: Detail of dA_p in the mean surface level

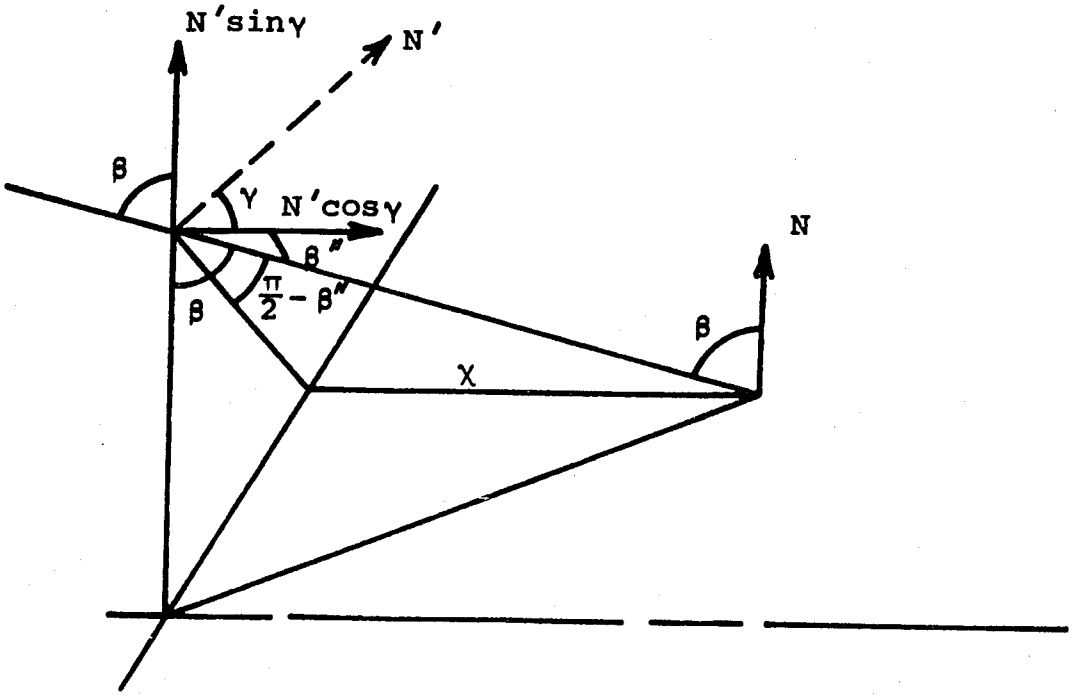

Figure A-3: Detail of angles involved in flux calculations for dA

Figure A-4: Plot of the ratio of the energy flux from a rectangle in the mean surface level of dimension L x ZL to the energy flux of this rectangle as $L \to \infty$

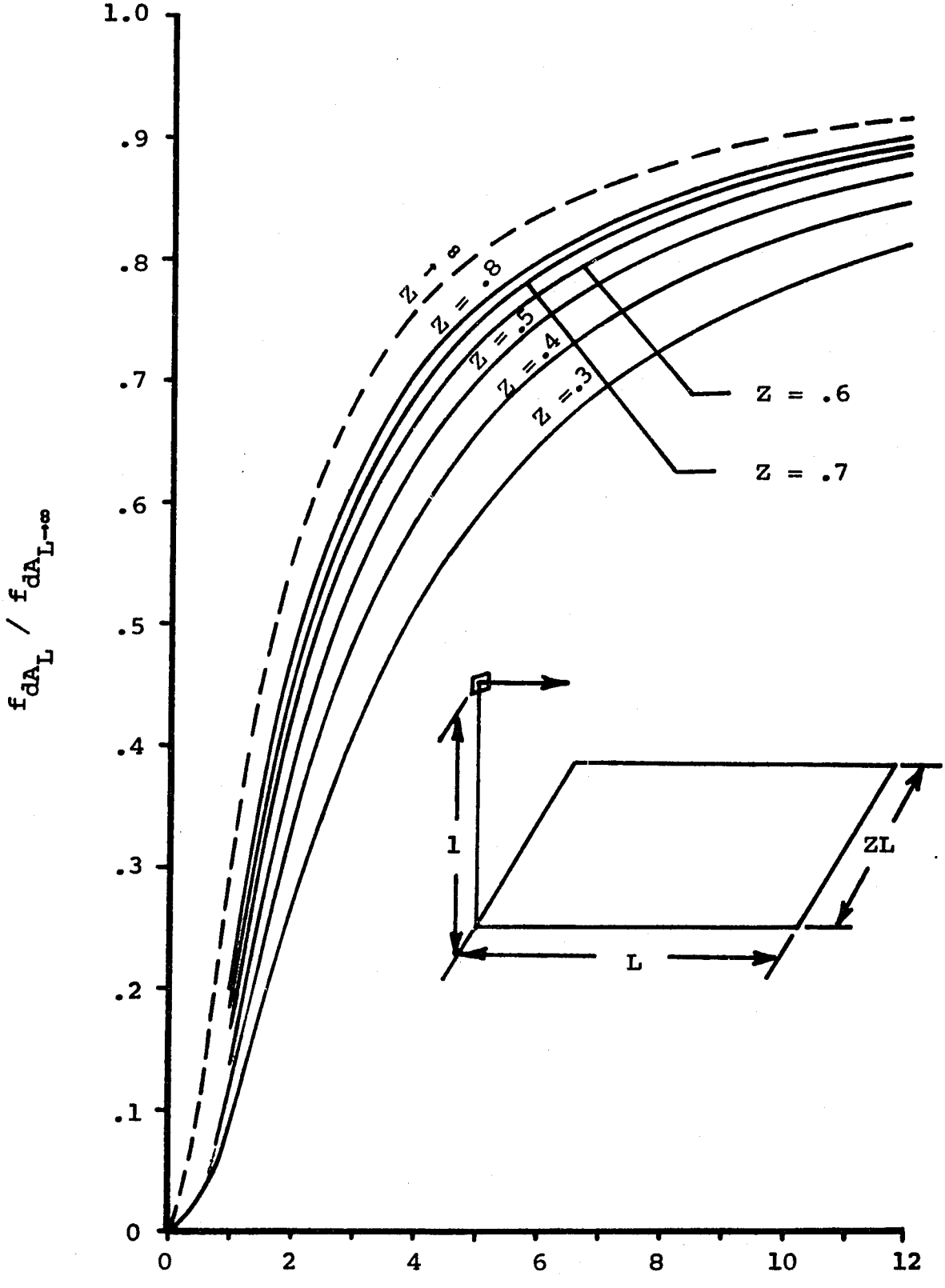

APPENDIX B

Evaluation of $f_{dA_{ij}}$

If an arbitrary square element of the grid system with coordinate i and j of the ξ,χ system is considered, then from equation (7)

$$f_{dA_{ij}} = \frac{G_s \cos\eta_{ij} \cos\beta_{c_{ij}} \cos\beta'_{c_{ij}}}{r_{c_{ij}}} A_s \qquad \text{(B-1)}$$

where A_s is not subscripted since in this analysis the grid elements all have the same size. It is assumed that the element is within the field of view at the receiving differential area dA. From Appendix A it was shown that this will be the case if

$$\chi_{i_{min}} \geq \tan\varphi$$

For all practical purposes this will be the case if

$$\chi_i - \frac{\alpha}{2} \geq \tan\varphi$$

If the element ij is not within the field of view then

$$f_{ij} = 0 .$$

To evaluate equation (B-1) Figure B-1 is considered. The angle $\beta_{c_{ij}}$ is the angle between the normal N_{ij} and the line $0' - P$. Evaluation of the projection of the normal N_{ij} onto this line gives

$$N\cos\beta_{c_{ij}} = N_V\cos\epsilon_{ij} + N_H\cos\zeta_{ij}\cos\left(\frac{\pi}{2} - \epsilon_{ij}\right)$$

where N_V = vertical component of N

N_H = horizontal component of N

or

$$\cos\beta_{c_{ij}} = \cos\theta_{ij}\cos\epsilon_{ij} + \sin\theta_{ij}\cos\zeta_{ij}\sin\epsilon_{ij} \qquad \text{(B-2)}$$

From geometry

$$\cos\epsilon_{ij} = \frac{1}{\sqrt{\xi_j^2 + \chi_i^2 + 1}}$$

$$\sin\epsilon_{ij} = \frac{\sqrt{\xi_j^2 + \chi_i^2}}{\sqrt{\xi_j^2 + \chi_i^2 + 1}}$$

$$\cos\zeta_{ij} = \cos(\varphi_{ij} + \omega_{ij} - \pi) = -\cos(\varphi_{ij} + \omega_{ij}) \qquad \text{(B-3)}$$

$$\cos\omega_{ij} = \frac{\chi_i}{\sqrt{\xi_j^2 + \chi_i^2}}$$

$$\sin\omega_{ij} = \frac{\xi_j}{\sqrt{\xi_j^2 + \chi_i^2}}$$

so

$$\cos\beta_{c_{ij}} = \frac{1}{\sqrt{\xi_j^2 + \chi_i^2 + 1}} \left[\cos\theta_{ij} + \sin\theta_{ij} \cdot \left(\chi_i\cos\varphi_{ij} - \xi_j\sin\varphi_{ij}\right)\right]$$

From Appendix A with subscripts added

$$\cos\beta'_{c_{ij}} = \frac{\chi_i\cos\gamma - \sin\gamma}{\sqrt{\xi_j^2 + \chi_i^2 + 1}}$$

and

$$r_{c_{ij}} = \sqrt{\xi_j^2 + \chi_i^2 + 1}$$

Now using the same method as for $\cos\beta_{c_{ij}}$ gives

$$\cos\eta_{ij} = \cos\alpha_s\cos\theta_{ij} + \cos\varphi_{ij}\sin\alpha_s\sin\theta_{ij}$$

where φ_{ij} is measured from the positive sun direction. Equation (B-1) can be written

$$f_{dA_{ij}} = \frac{G_s}{\pi}\left[\cos\alpha_s\cos\theta_{ij} + \cos\varphi_{ij}\sin\alpha_s\sin\theta_{ij}\right]$$

$$\cdot\left\{\frac{\left(\chi_i\cos\gamma - \sin\gamma\right)\left[\cos\theta_{ij} - \sqrt{\xi_j^2 + \chi_i^2}\,\sin\theta_{ij}\cos\left(\varphi_{ij} + w_{ij}\right)\right]}{\left(\xi_j^2 + \chi_i^2 + 1\right)^2}\right\}$$

(B-4)

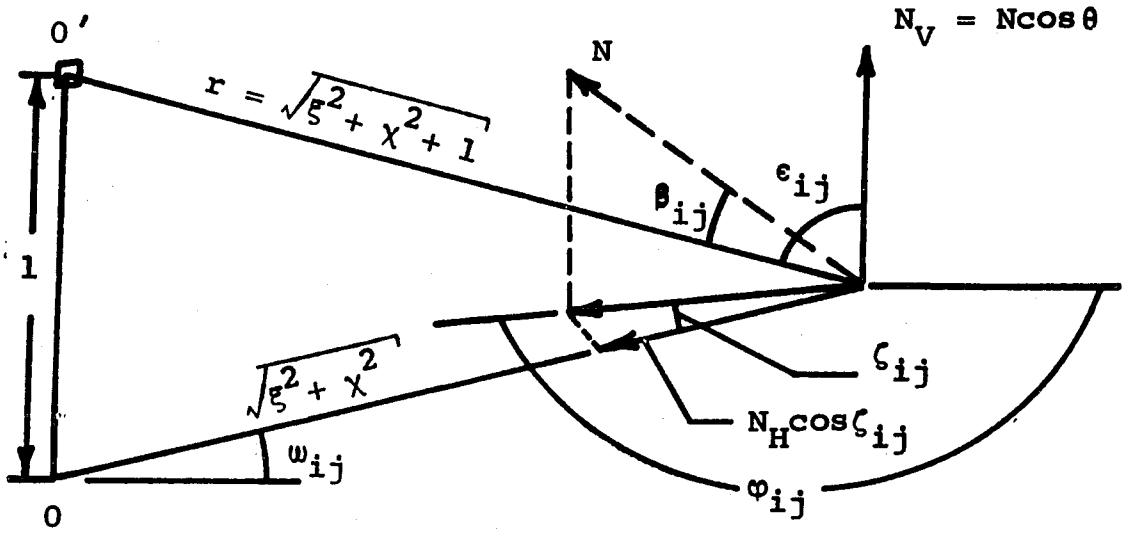

Figure B-1: Detail of angles involved in calculation of the flux from a grid area element

APPENDIX C

Derivation of C_{ij}

In the derivation of f_{ij} the total area of the grid element is used in determining the energy flux at dA. To account for shadowing of the sun's rays by an adjacent element and view blockage at the receiving differential area by an adjacent element, a correction factor based on the geometry of the element orientations is used to reduce the grid area element to an effective area for flux calculations. This can be written as

$$A_{e_{ij}} = C_{ij} A_s$$

where

C_{ij} is the correction factor for view blockage and sun shadowing at element ij caused by adjacent elements

$A_{e_{ij}}$ is the effective area of element ij for flux calculations.

To simplify the analysis for negative sun angles ($\alpha_s < 0$) the value of C_{ij} is set equal to the correction for sun

shadowing or the correction for view blockage,whichever causes the greatest reduction in area. This is equivalent to assuming that the same general portion of the grid element will be subject to sun shadowing and view blockage which is a good approximation for negative sun angles. If the sun angle is positive ($\alpha_s > 0$) the value of C_{ij} is set equal to the sum of the sun shadowing and view blockage corrections. It should be noted that if $\alpha_s = 0$ there is no sun shadowing so C_{ij} is equal to the view blockage correction factor. This is summarized as follows

$$\alpha_s \leq 0 : \quad C_{ij} = \begin{cases} (1 - V_{ij}) & \text{if } V_{ij} \geq S_{ij} \\ (1 - S_{ij}) & \text{if } S_{ij} > V_{ij} \end{cases}$$

and

$$\alpha_s > 0 : \quad C_{ij} = (1 - V_{ij}) + (1 - S_{ij})$$

The evaluation of V_{ij} and S_{ij} is made essentially in the same manner except that for sun shadowing the geometry is a little easier because there is only one case to consider.

Derivation of S_{ij}

The term S_{ij} represents the fraction of grid element ij which does not receive solar irradiation due to the shadow of an adjacent element. For a "high noon" sun ($\alpha_s = 0$) there is no shadowing, but as the absolute magnitude of α_s gets large the shadowing becomes important. For values of α_s near $\pm 90°$ several elements can cause a shadow on the element of interest. In this analysis only the shadow caused by the adjacent element is considered and for this reason is termed first order shadowing. The first step in calculating the shadow is to calculate the apparent area (to the sun's direction) of the two elements involved. This area will be the area in a plane perpendicular to a line joining the center of the element and the center of the sun. For grid sizes small with respect to the distance of the sun the two planes will be essentially parallel. This geometry is shown in Figure C-1. If the apparent area of the shadowing element is projected onto the second plane then the region of overlap will represent the shadowed portion of the element of interest. To construct the shape of the apparent area two cases are considered. If $\theta \leq 45°$ then the width is set equal to α (the actual width of the element) and the height is then

$$h_a = \frac{A_a}{2w_a} = \frac{\alpha(\sin\theta\cos\zeta\cos\lambda + \cos\theta\sin\lambda)}{2}$$

If $\theta > 45°$ the width is

$$w_a = \alpha\cos\xi$$

and

$$h_a = \frac{A_a}{2w_a} = \frac{\alpha(\sin\theta\cos\zeta\cos\lambda + \cos\theta\sin\lambda)}{2\cos\zeta}$$

with the restriction that

$$h_a \leq \frac{\alpha}{2}$$

To calculate the height shadow factor F_H from the geometry of Figure C-2 it is clear

$$d_{is} = \frac{h_{a(3)}}{\sin\lambda}$$

where the subscript (3) represents the (i-1,j) element for negative sun angles ($\alpha_s < 0$) and the (i+1,j) element for positive sun angles, and

$$h_s = h_a - (d - d_{i_s}) \sin\lambda$$

The height shadow factor is defined as

$$F_H = \frac{h_s}{2h_a}$$

so

$$F_H = \frac{h_a - (d - d_{i_s}) \sin\lambda}{2h_a}$$

with the restriction that if the formula gives a value > 1 then

$$F_H = 1$$

(Physically this means that the projection of the shadowing element height is greater than the height of the element of interest) and if the value is < 0 then

$$F_H = 0$$

(i.e., the shadow does not reach the element of interest). The width shadow factor F_W is given by

$$F_W = \frac{w_{a(3)}}{w_a}$$

where $w_{a(3)}$ = the apparent width of the shadowing element

w_a = the apparent width of the shadowed element,

with the restriction that the maximum value of F_W is 1.

Now the shadow factor for the ij element can be written

$$S_{ij} = (F_H)_{ij} (F_W)_{ij}$$

Derivation of V_{ij}

View blockage is treated in the same manner as sun shadowing except that more than one element is significant in occulting the element of interest. In first order view blockage three elements are considered. These are the two adjacent elements and one diagonally adjacent element. The elements considered in various locations in the mean surface level are shown in Figure C-3. The total occulted portion of the element of interest is taken to be the sum of the effects of the three contributing elements. Since the method of calculating view blockage for each occulting element is the same only one set of equations will be derived and the required modifications for the other two will be given. Again the apparent areas are calculated but now with respect to the receiving differential area dA . If the grid size is small with respect to the distance to dA then the apparent areas can be considered to be in parallel planes. To show the derivation of V_{ij} the diagonally adjacent element is used. This element is subscripted with (2) which from Figure C-3 is the (i-1,j+1) element. The first set of equations is exactly the same

as in sun shadowing

$$A_a = \alpha^2(\sin\theta\cos\zeta\cos\lambda + \cos\theta\sin\lambda)$$

for $\theta < 45°$

$$w_a = \alpha$$

$$h_a = \frac{A_a}{2\alpha}$$

for $\theta \geq 45°$

$$w_a = \alpha\cos\zeta$$

$$h_a = \frac{A_a}{2\alpha\cos\zeta}$$

Now to calculate F_H Figure C-4 is considered. From geometry the perpendicular distance between the intersections of the apparent area planes with mean surface level is

$$d = \alpha(\cos\omega + \sin\omega)$$

and

$$d_{i_v} = \frac{h_{a(2)}}{\sin\lambda}$$

where the value of ω is for the center of element of interest. The height view blockage factor is defined as

$$F_{H_v} = \frac{h_{a_v}}{2h_a}$$

and from geometry

$$h_{a_v} = h_a - (d - d_{i_v}) \sin\lambda$$

$$= h_a - \alpha\sin\lambda\ (\cos\omega + \sin\omega) + h_{a(2)}$$

so

$$F_{H_v} = \frac{h_a - \alpha\sin\lambda\ (\cos\omega + \sin\omega) + h_{a(2)}}{2h_a}$$

It should be noted that this equation is still correct if $d_{i_v} > d$. Again restrictions are placed on F_{H_v} such that if the formula gives a value > 1 then F_{H_v} is set equal to 1 and if a negative value results then F_{H_v} is set equal to 0. Now to calculate the width view blockage factor. This quantity is a little more complicated than in sun shadowing since the line joining the centers of the two elements is not colinear with the projection in the mean surface of the line connecting dA and center of the grid element of interest as can be seen in Figure C-5. For this reason adjustment can be necessary to account for this aspect. If no adjustment is necessary the equation for F_{W_v} is the same as for the sun shadowing case

$$F_{W_v} = \frac{w_{a(2)}}{w_a}$$

with the restriction on the maximum value to $F_{W_v} = 1$. The test for the necessity of adjustment is

$$w_{s(2)} + d_c - w_s \begin{cases} > 0 & \text{requires adjustment} \\ \leq 0 & \text{no adjustment} \end{cases}$$

and from Figure C-4

$$d_c = \alpha \sqrt{1 - 2\sin\omega\cos\omega}$$

The value of F_{W_v} with adjustment is

$$F_{W_v} = \frac{w_{a(2)} - 2\alpha\sqrt{1 - 2\cos\omega\sin\omega} + w_a}{2w_a}$$

Now with these calculations the value of the view blockage for the diagonal elements is

$$V_{(2)} = F_{W_v} F_{H_v}$$

The other two elements in view blockage are treated in the same way with different equations for d and d_c . The formulas for the other two elements for d and d_c are as follows:

element (1)

$$d = \alpha \sin\omega$$

$$d_c = \alpha \cos\omega$$

element (3)

$$d = \alpha \cos\omega$$

$$d_c = \alpha \sin\omega$$

The final value of view blockage for the element of interest is the sum of the view blockage by each element or

$$V_{ij} = V_{(1)} + V_{(2)} + V_{(3)}$$

Again a restriction is placed on V_{ij} such that $V_{ij} \leq 1$.

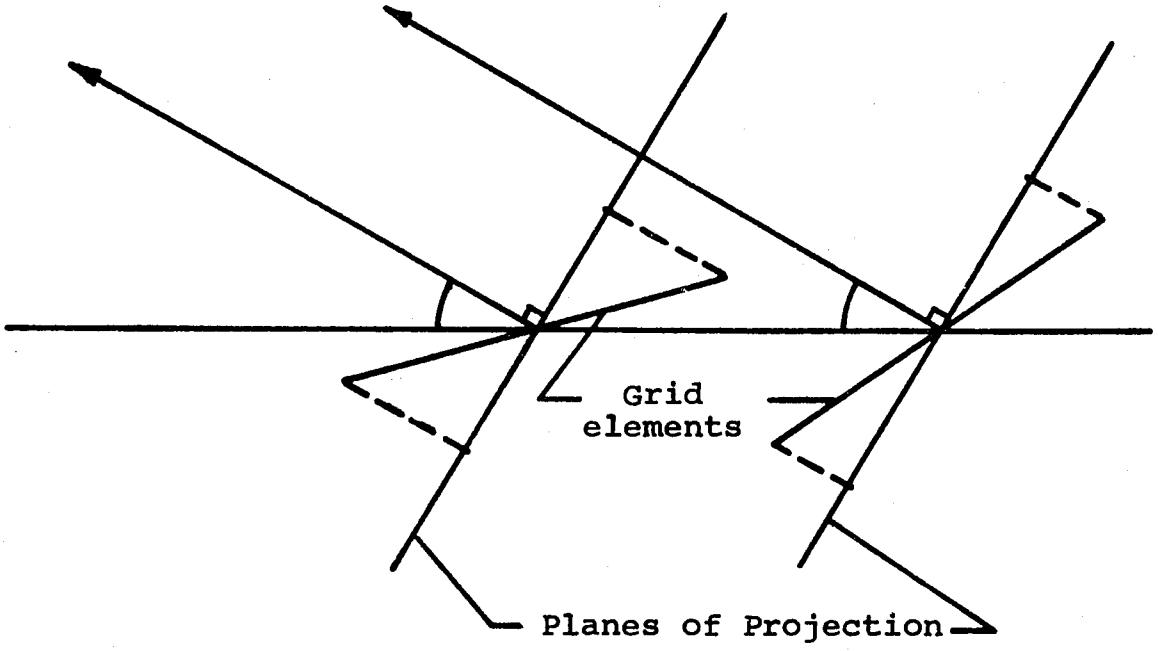

Figure C-1: Cross section of two grid elements with planes of projection for sun shadowing.

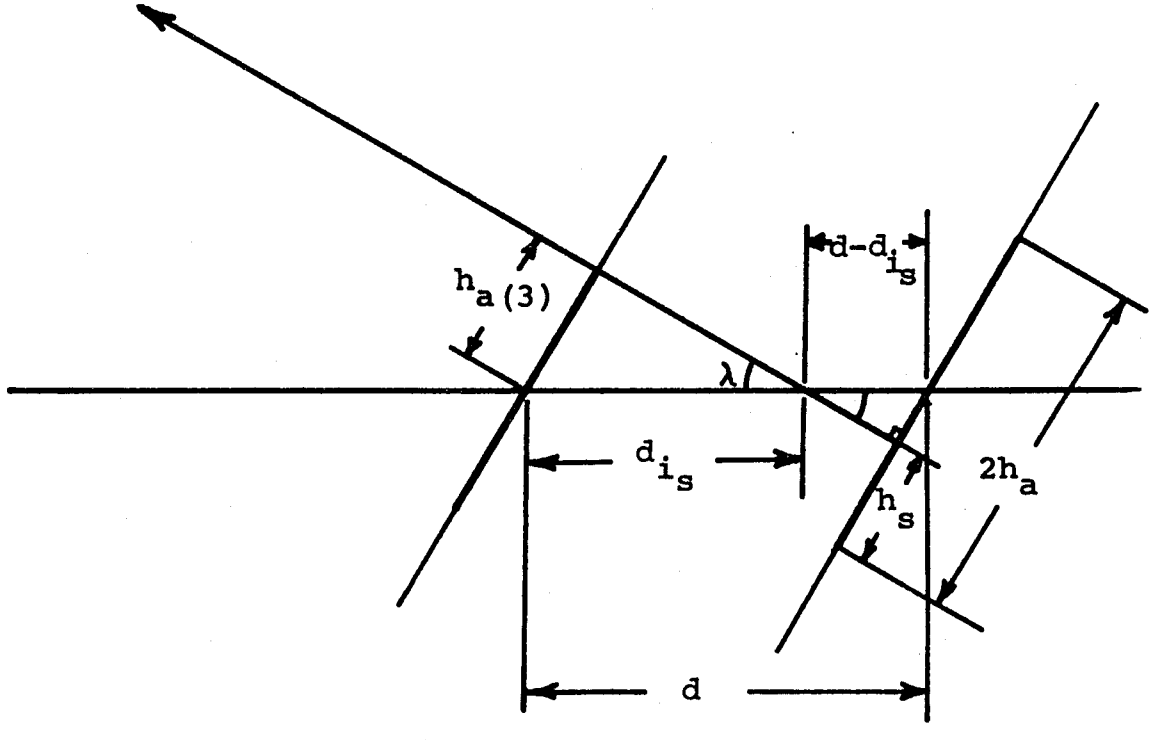

Figure C-2: Detail of geometry required in sun shadowing calculation

Figure C-3: Elements involved in view blockage for several locations in the mean surface level

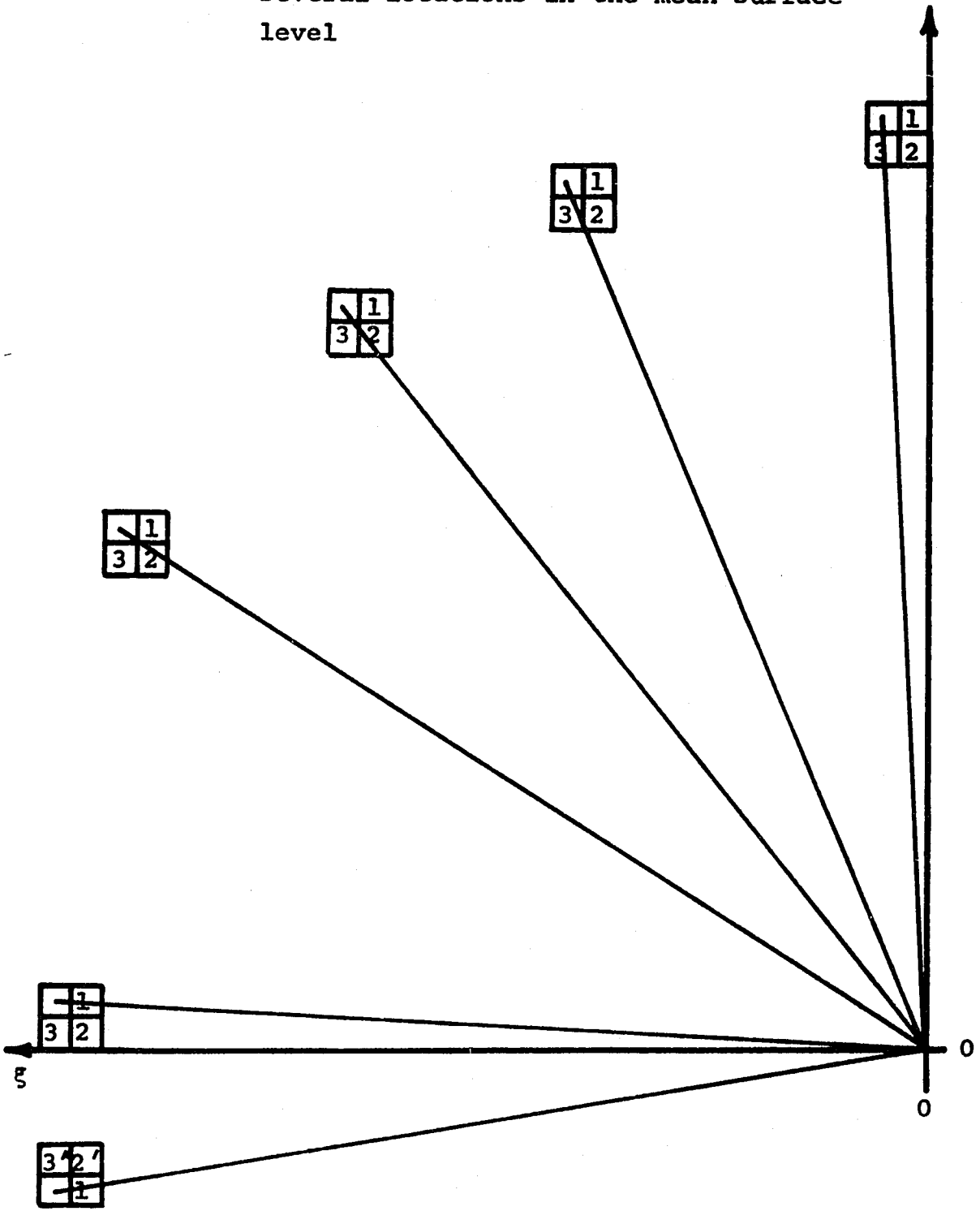

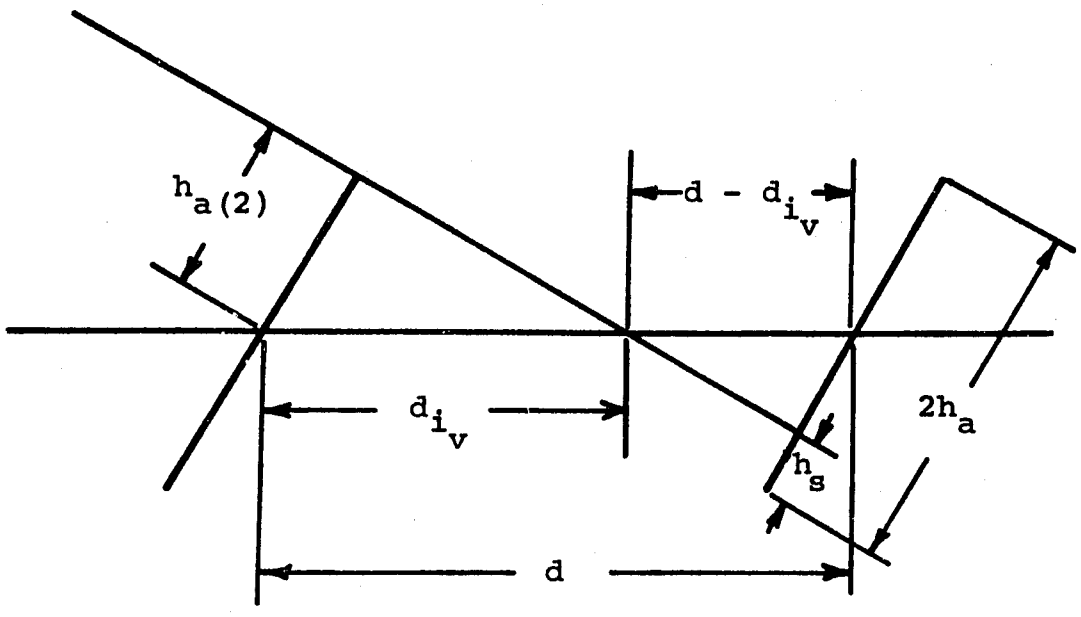

Figure C-4: Detail of geometry involved in view blockage calculations

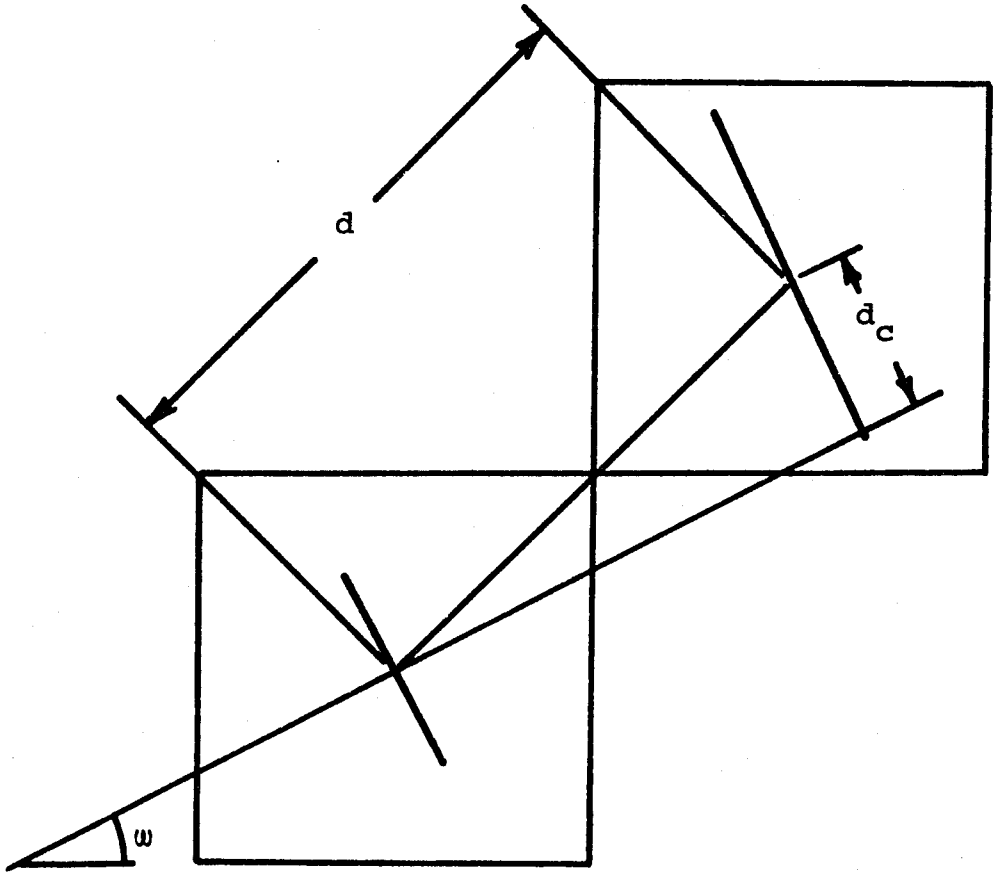

Figure C-5: Diagonally adjacent elements with associated geometry for view blockage

APPENDIX D

Derivation of $\mathcal{F}_{NN}$ Using Average Values of the Height Distribution

In this analysis a single grid element as shown in Figure D-1 is investigated. The flux at dA from the inclined element is calculated and divided by the flux of the element if the element were flat (i.e., $\theta = 0$). From equation (7)

$$f_{dA} = \frac{G_s \cos\eta \cos\beta_c \cos\beta_c'}{\pi r_c^2} A_s$$

For the flat element case from Appendix A

$$\cos\eta_c = \cos\alpha_s$$

$$r_c = \sqrt{\xi_c^2 + \chi_c^2 + 1}$$

$$\cos\beta_c = \frac{1}{r_c}$$

$$\cos\beta_c' = \frac{\chi_c \cos\gamma - \sin\gamma}{\sqrt{\xi_c^2 + \chi_c^2 + 1}}$$

Noting that

$$\cos\omega = \frac{\chi_c}{\sqrt{\xi_c^2 + \chi_c^2}}$$

and

$$R_c = \sqrt{\xi_c^2 + \chi_c^2}$$

then

$$\cos\beta_c' = \frac{R_c\cos\omega\cos\gamma - \sin\gamma}{r_c}$$

and

$$r_c = \sqrt{R_c^2 + 1}$$

gives

$$f_{dA_{flat}} = \frac{G_s\cos\alpha_s(R_c\cos\omega_c\cos\gamma - \sin\gamma)\ \alpha^2}{(R_c^2 + 1)^2} \qquad \text{(D-1)}$$

For the inclined element from Appendix B

$$\cos\beta_c = \frac{R_c\sin\theta\cos\zeta + \cos\theta}{r_c}$$

where ζ is the azimuthal orientation angle of the grid element normal with respect to the direction of dA.

$$\cos\beta_c' = \frac{R_c\cos\omega_c\cos\gamma - \sin\gamma}{r_c}$$

and

$$\cos\eta_c = \cos\theta\cos\alpha_s + \cos\varphi\sin\theta\sin\alpha_s$$

These equations give for the inclined element

$$f_{dA_{inc}} = G_s(\cos\theta\cos\alpha_s + \cos\varphi\sin\theta\sin\alpha_s) \times \frac{(R_c\cos\omega_c\cos\gamma - \sin\gamma)(R_c\sin\theta\cos\zeta + \cos\theta)\alpha^2}{(R_c^2 + 1)^2} \quad \text{(D-2)}$$

and so

$$\mathcal{F}_{NN} = \frac{f_{dA_{inc}}}{f_{dA_{flat}}} = (\cos\theta + \cos\varphi\sin\theta\tan\alpha_s)(R_c\cos\zeta\sin\theta + \cos\theta) \quad \text{(D-3)}$$

Now rearranging this equation to give $\mathcal{F}_{NN}$ in the standard form of an equation for a straight line in R_c

$$\mathcal{F}_{NN} = \left[\cos\zeta\sin\theta(\cos\theta + \cos\varphi\sin\theta\tan\alpha_s)\right] R_c + \cos^2\theta + \cos\varphi\cos\theta\sin\theta\tan\alpha_s \quad \text{(D-4)}$$

If $\alpha_s = 0$ this simplifies to

$$\mathcal{F}_{NN} = (\cos\zeta\cos\theta\sin\theta)\ R_c + \cos^2\theta \quad \text{(D-5)}$$

Now if a test area is considered (i.e., a collection of grid elements of sufficient number to give a good sample for the height distribution), and average values for the distribution for the terms in equation (D-4) are used then an approximate value of the flux ratio for the test area can be written

$$\mathcal{F}_{NN_{c_t}} \cong \left[(\cos\zeta)_{av}(\sin\theta\cos\theta)_{av} + (\cos\zeta\cos\varphi)_{av}(\sin^2\theta)_{av}\tan\alpha_s\right]R_{c_t}$$

$$+ \quad (\cos^2\theta)_{av} + (\cos\varphi)_{av}(\sin\theta\cos\theta)_{av}\ \tan\alpha_s \qquad \text{(D-6)}$$

where R_{c_t} = distance to center of test area. It should be noted that terms of the same or related distributions are grouped together since, in general, the average value of the product of two functions is not equal to the product of the average values of the two functions [e.g., $(\cos^2\theta)_{av} \neq (\cos\ \theta)_{av}(\cos\ \theta)_{av}$]. The angles ζ and θ are related by the equation

$$\zeta = \pi - (\varphi + \omega)$$

so that the product of functions of ζ and φ must be taken before averaging. To obtain the average values the ranges of interest were divided into 500 segments and the average values for the height and azimuthal distributions were calculated. The results are as follows:

Random Height Distribution

$$(\sin\theta)_{av} = .50000$$

$$(\cos\theta)_{av} = .78541$$

$$(\sin\theta\ \cos\theta)_{av} = .33334$$

$$(\sin^2\theta)_{av} = .33333$$

$$(\cos^2\theta)_{av} = .66667$$

Normal Height Distribution

$$(\sin\theta)_{av} = .30159$$

$$(\cos\theta)_{av} = .92031$$

$$(\cos^2\theta)_{av} = .86059$$

$$(\sin^2\theta)_{av} = .13941$$

$$(\sin\theta\ \cos\theta)_{av} = .25427$$

Random Azimuthal Direction Distribution

$$(\cos\zeta)_{av} = (\sin\zeta)_{av} = .63662$$

$$(\cos^2\zeta)_{av} = .50000$$

Using these values in equation (D-6) gives for a normal distribution

$$\mathcal{F}_{NN_{c_t}} = \left[.16258 + .13941(\cos\zeta\cos\varphi)_{av}\tan\alpha_s\right] R_{c_t} + .86097 + .25493(\cos\varphi)_{av}\tan\alpha_s \qquad \text{(D-7)}$$

and for random distribution

$$\mathcal{F}_{NN_{c_t}} = \left[.21221 + .33333(\cos\zeta\cos\varphi)_{av}\tan\alpha_s\right] R_{c_t}$$

$$+ .66667 + .33334(\cos\varphi)_{av}\tan\alpha_s \qquad \text{(D-8)}$$

For negative sun angles and $\omega_{av} = 0$ the sun and dA have the same azimuthal direction so that the distribution of ζ is the same as the distribution at φ except the values differ by π . This gives

$$(\cos\zeta\cos\varphi)_{av} = -(\cos^2\zeta)_{av} = -.50000$$

and

$$(\cos\varphi)_{av} = -(\cos\zeta)_{av} = -.63662$$

Now equations (D-7) and (D-8) can be written

Normal:

$$\mathcal{F}_{NN_{c_t}} = \left[.16258 - .06971\ \tan\alpha_s\right]R_{c_t} + .86097 - .16229\ \tan\alpha_s$$

Random:

$$\mathcal{F}_{NN_{c_t}} = \left[.21221 - .16667\ \tan\alpha_s\right]R_{c_t} + .66667 - .21221\ \tan\alpha_s$$

where $\tan\alpha_s$ will be negative for negative sun angles. Plots of these average value flux ratios agree very closely with the computer results of test area analysis. Due to the close

agreement a better comparison can be made by tabulating the measured slopes and intercepts from computer analysis (as plotted in Figures 9 through 12) and the slopes and intercepts from the average value distribution results. These results are listed in Table D-1.

Derivation of Approximation for $\mathcal{F}$ as R Becomes Large

Indicated in Figure D-2 is a single element in an infinite flat plane. The element is assumed to be oriented such that the normal is in the plane formed by the line connecting dA and the center of the element and the line from dA perpendicular to the mean surface level. From geometry

$$R_c = \frac{1}{\tan\lambda_c} = \cot\lambda_c$$

$$d_{i_v} = \frac{h_s}{\sin\lambda_c} = \frac{\alpha}{2}(\sin\theta\cot\lambda_{ct} + \cos\theta)$$

$$= \frac{\alpha}{2}(R_c\sin\theta + \cos\theta)$$

and

$$d_{vB} = \frac{\alpha}{2}(R_c\sin\theta + \cos\theta + 1)$$

So the area in the mean surface level which is missing or blocked from view is

$$A_{vB} = d_{vB} \times \alpha = \frac{\alpha^2}{2} (R_c \sin\theta + \cos\theta + 1)$$

Now to calculate the area of the element from Figure D-2 and the law of sines with the restriction $R > 1 (\lambda < 45°)$

$$\frac{\alpha/2 - h_{av}}{\sin\lambda} = \frac{\alpha/2}{\sin[\pi - (\theta + \lambda)]}$$

$$= \frac{\alpha}{2[\sin(\theta + \lambda)]}$$

$$\frac{\alpha}{2} - h_{av} = \frac{\alpha \sin\lambda}{2(\sin\theta\sin\lambda + \cos\theta\sin\lambda)}$$

$$\frac{\alpha}{2} - h_{av} = \frac{\alpha}{2(R_c \sin\theta + \cos\theta)}$$

So the visible area of the element is

$$A_e = \alpha \left(\frac{\alpha}{2} + \frac{\alpha}{2} - h_{av}\right)$$

$$= \frac{\alpha^2}{2} \left[\frac{R_c \sin\theta + \cos\theta + 1}{R_c \sin\theta + \cos\theta}\right]$$

As in the first part of this Appendix G for the mean surface level is

$$G = G_s \cos\alpha_s$$

and for the inclined element

$$G = G_s (\cos\theta\cos\alpha_s - \cos\omega\sin\theta\sin\alpha_s)$$

For the inclined element

$$\frac{\cos\beta_c \cos\beta_c'}{r_c^2} = \frac{R_c \cos\omega_c (R_c \cos\theta + \sin\theta)}{(R_c^2 + 1)^2}$$

and for the flat region

$$r_c = R_c - \frac{\alpha}{2} + \frac{d_{vB}}{2}$$

$$= R_c + \frac{\alpha}{2} (R_c \sin\theta + \cos\theta + 1)$$

and

$$\frac{\cos\beta_c \cos\beta_c'}{r_c^2} = \frac{R_c \cos\omega_c}{\left\{\left[R_c\left(1 + \frac{\alpha}{4}\sin\theta\right) + \frac{\alpha}{4}\left(\cos\theta - 1\right)\right]^2 + 1\right\}^2}$$

The ratio of the fluxes with view blockage included gives

$$\mathcal{F} = \frac{\left(\cos\theta - \cos\omega_c \sin\theta \tan\alpha_s\right)\left\{\left[R_c\left(1 + \frac{\alpha}{2}\sin\theta\right) + \frac{\alpha}{4}\left(\cos\theta - 1\right)\right]^2 + 1\right\}^2}{\left[R_c^2 + 1\right]^2}$$

and for large values of R_c ($>> 1$)

$$\mathcal{F} \cong \left[\cos\theta - \sin\theta\cos\omega_c \tan\alpha_s\right]\left[1 + \frac{\alpha}{2}\sin\theta + \frac{\alpha^2 \sin^2\theta}{16}\right]$$

and for small α with respect to 1

$$\mathcal{F} \cong \cos\theta - \cos\omega_c \sin\theta \tan\alpha_s$$

So with the above approximations and using average values of the distribution the ratio of the rough surface flux to the flat surface flux can be approximated as

$$\mathcal{F} = (\cos\theta)_{av} - (\sin\theta)_{av} \cos\omega \tan\alpha_s \qquad \text{(D-7)}$$

From experimental data with earth-bound measurements of the lunar surface made by Saari and Shorthill (Reference 8) a comparison of experimental results for this quantity can be made with the approximation for $\mathcal{F}$. This comparison is plotted in Figure 18. To give a more valid comparison the curves are for $(\mathcal{F})_{av}$ and not for $\mathcal{F}$ using the average values for the distribution. This means that $\mathcal{F}$ was obtained by taking values of $\cos\theta$ and $\sin\theta$ from the distribution and calculating $\mathcal{F}$, and these values of $\mathcal{F}$ were averaged with the modification that negative values of $\mathcal{F}$ were set equal to zero. This makes no change in the portion of the curve for negative sun angle. The only difference is that for large positive sun angles (greater than 50°) these results are higher than the case of using the average values of the distribution.

TABLE D-1

α_s (deg)	SLOPE		INTERCEPT	
	Computer Results	Average Value Results	Computer Results	Average Value Results
$\omega_{ct} = 0°$				
Normal Distribution:				
0	.166	.1626	.860	.8610
-30	.207	.2028	.955	.9547
-45	.238	.2323	1.022	1.0233
-60	.290	.2833	1.145	1.1421
Random Distribution:				
0	.218	.2122	.660	.6667
-30	.316	.3084	.792	.7892
-45	.387	.3789	.884	.8788
-60	.510	.5009	1.050	1.0342
$\omega_{ct} = 45°$				
Normal Distribution:				
-30	.196	.190	.915	.939
-60	.260	.2622	1.075	1.106
Random Distribution:				
-30	.293	.279	.760	.770
-60	.391	.413	.930	.978

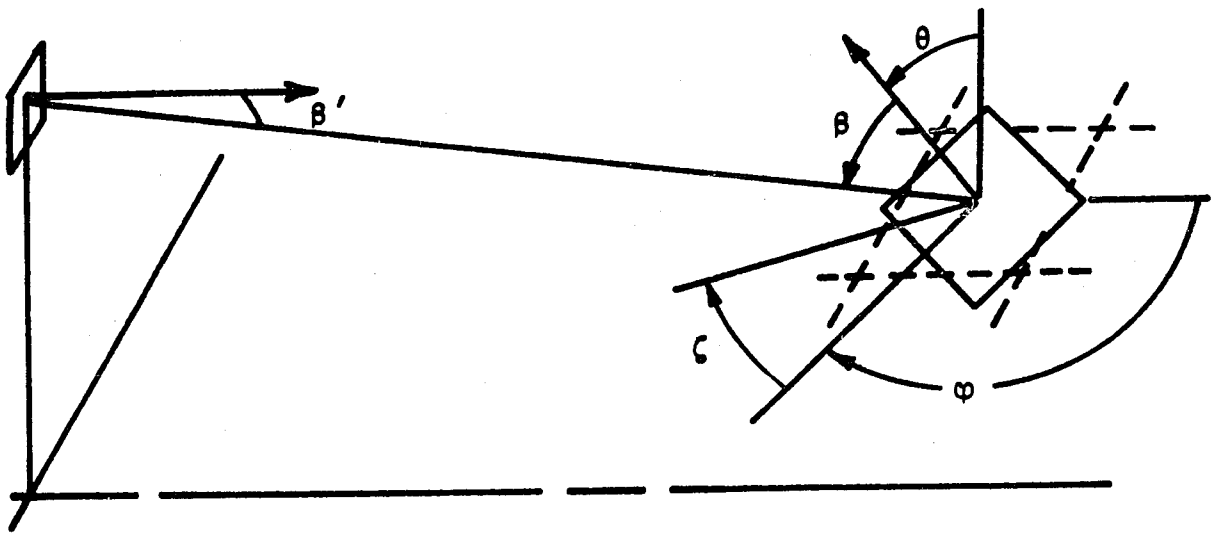

Figure D-1: Grid element in mean surface level

Figure D-2: Geometry for approximation to the limiting case evaluation of flux

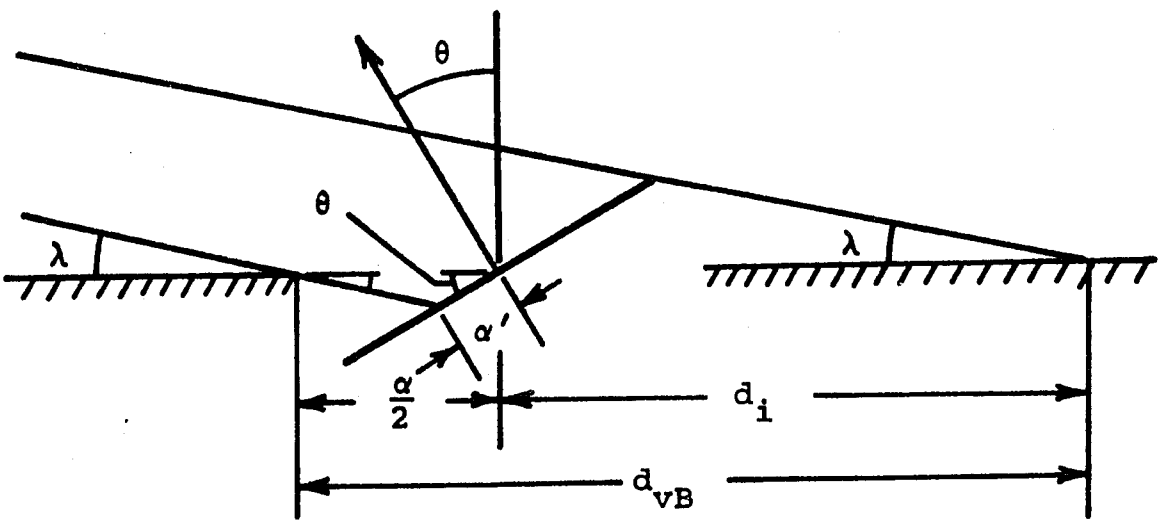

APPENDIX E

Description of Random and Normal Distributions

As mentioned in Chapter III random and normal distributions were used to determine grid element heights, and a random distribution was used to determine azimuthal orientation of the elements for both height distributions. Although several ranges were used for random functions, the problem of generating a random distribution can be reduced to generating a set of random values between 0 and 1. Since a random distribution can only be approximated, the values used in this analysis should technically be called pseudorandom numbers. The method used is a standard congruential method and the algorithm was taken from Reference (12). The algorithm is listed with pertinent data at the end of this Appendix. Now to consider the method of constructing the normal height distribution. Following the derivation of Chapter 6 of Reference (13),the frequency function of interest is a normal distribution. Due to the uniform grid size there is a maximum value for the deviation from the mean surface level by an element

for any fixed grid size. The frequency distribution is used to determine these deviations and since the normal frequency distribution would have a finite probability for any height deviation up to infinity, a trunkated normal distribution was used for the frequency distribution. The normal distribution was trunkated at 99% (i.e., 99% of the values in a normal distribution are contained within the frequency distribution used). The distribution is shown schematically in Figure E-1. Now to determine the method of generating values with the 99% normal frequency distribution. By definition the probability function for a frequency distribution curve f(x) is

$$P(h) = \frac{f(x)}{\int_0^{\infty} f(x)\ dx} = \frac{f(x)}{\int_0^{h_{max}} f(x)\ dx}$$

where

h_{max} = the maximum height deviation from the mean surface level (1/2 the grid dimension)

$P(h)$ = probability function

And by definition the cumulative distribution function is

$$N_R = \int_{-\infty}^{h} P(x)\ dx$$

and for this distribution

$$N_R = \int_o^x P(x)\ dx$$

For the 99% normal distribution

$$f(x) = \begin{cases} \frac{2}{\sqrt{\pi}}\ e^{-x^2} & 0 \le x \le x_{max} \\ 0 & \text{all other } x \end{cases}$$

so

$$P(x) = \frac{f(x)}{\int_o^{\infty} f(x)\ dx} = \frac{2\ e^{-x^2}}{(.99)\sqrt{\pi}}$$

and the cumulative distribution function becomes

$$N_R(h) = \int_{-\infty}^{h} P(x)\ dx = \frac{2}{.99\sqrt{\pi}} \int_o^h e^{-x^2} dx \qquad \text{(E-1)}$$

To assign heights to the grid location with the desired frequency distribution, random numbers are substituted for $N_R(h)$ in equation (E-1). The corresponding value of h is calculated and assigned to the grid location. Noting that the right side of equation (E-1) is the error function [normally written as erf(h)] the equation (E-1)

becomes

$$\text{erf}(h) = .99\ N_R \ .$$

To solve for h given a value of N_R , tabulated values of erf(h) (from Reference 14) were used to construct interpolating polynomials giving h as a function of N_R . To accomplish this the interval from 0 to .99 of the function erf(h) was divided into 6 segments and a 6th order polynomial was constructed for each interval to give

$$h = \text{erf}^{-1}(.99\ N_R) \ .$$

An algorithm for a congruential method for generating pseudorandom numbers in the open interval (0,1):

```
IC    =  starting number (or previous random number)
IB    =  3125 * IC
IA    =  MOD (IB, 67108864)
IC    =  IA
RANDO =  IA/67108864.0
```

where RANDO is a pseudorandom number between 0 and 1. The starting number used was

```
IC    =  20555724
```

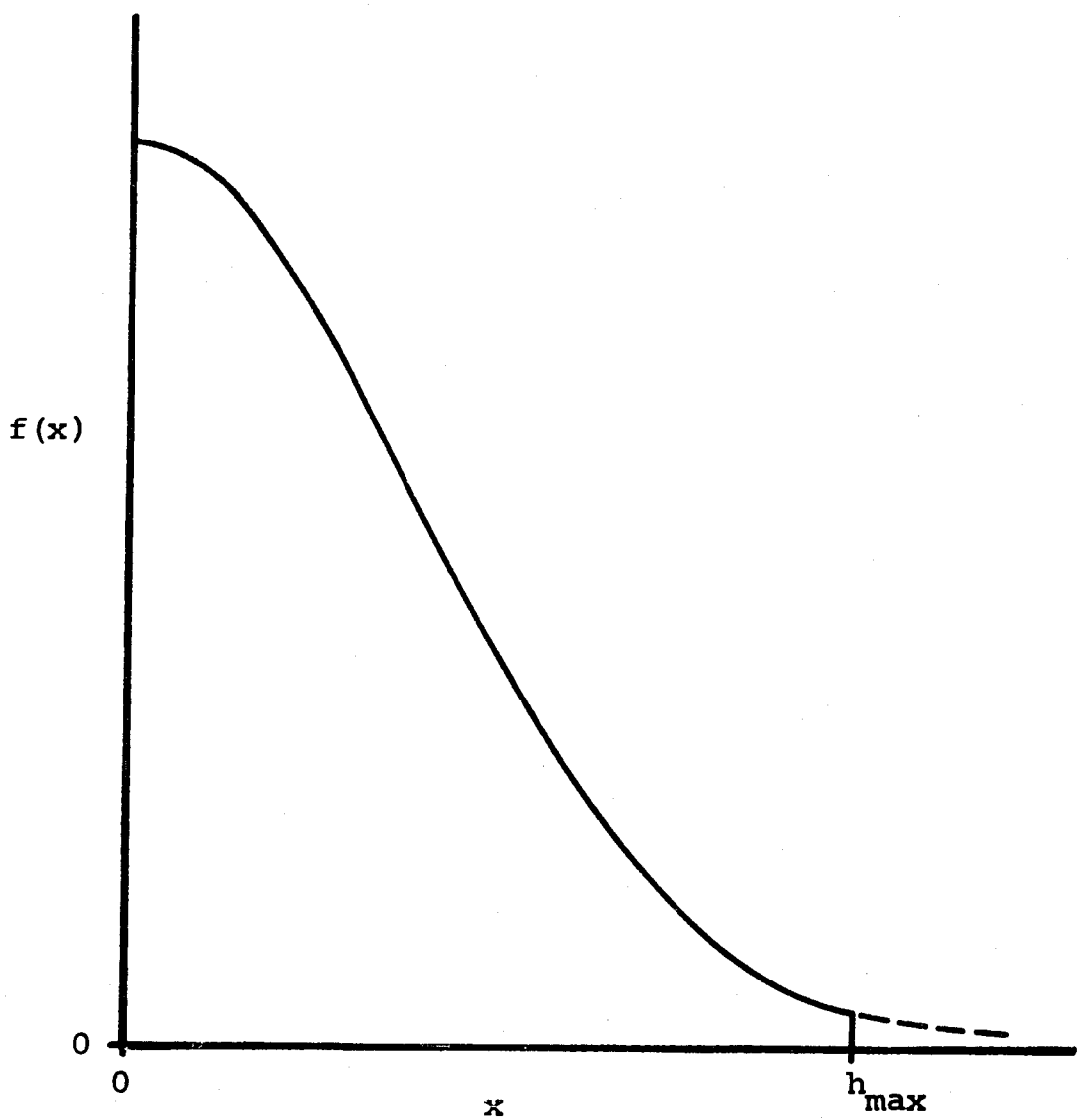

Figure E-1: Schematic of the frequency function for a 99% normal distribution

APPENDIX F

Determination of F_{dA_ℓ} Using the Approximation for $\mathcal{F}$ Derived in Appendix D

From equation (D-7) of Appendix D the ratio of the rough surface energy flux to the flat surface energy flux is a function of the angle ω . To solve for the rough surface energy flux the flat surface flux is calculated, then multiplied by the ratio to give the rough surface energy flux. Since the ratio is a function of angle ω , the region of interest was divided into segments of small angular increments with lines of constant value for ω as boundaries. This is indicated schematically in Figure F-1 for the possible values of γ . There are four possible cases to consider depending on the value of γ . The value of the angle subtended by the region included in the four cases is determined as follows:

$$\omega_{(1)} = \tan^{-1}\left(\frac{b_o}{a_o}\right)$$

$$\omega_{(2)} = \begin{cases} \tan^{-1}\left(\frac{b_o}{c_o}\right) - \omega_{(1)} & c_o > 0 \\ \frac{\pi}{2} - \omega_{(1)} & c_o \leq 0 \end{cases}$$

$$\omega_{(3)} = \frac{\pi}{2} - \omega_{(2)} \qquad (c_o > 0)$$

$$\omega_{(4)} = \tan^{-1}\left(\frac{c_o}{b_o}\right) - \frac{\pi}{2} \qquad (c_o < 0)$$

where

$c_o = \tan\gamma$,

a_o and b_o are the maximum χ intercept, and the ξ intercept of A_g , respectively.

The angular increments for each case [(1) → (4)] are determined by

$$\Delta\omega_k = \frac{\omega_{(i)}}{n}$$

where the value of n used was 25. To calculate the flux from the entire region not treated by the grid system the rough surface flux is calculated for each segment and summed to give the rough surface flux for the entire region. So to use this procedure the flat surface energy

flux for the angular segments indicated in Figure F-1 is needed. Figure F-2 shows the four possible segment configurations that are necessary to solve the problem for all values of γ (orientation of dA). The solution of the flux for case (1) will be worked out and the solutions for the other three cases will be listed. Figure F-3 shows the geometry involved in case (1). From Appendix A converting to coordinates ω and R equation (A-5) becomes

$$\frac{\cos\beta\cos\beta'}{r^2} = \frac{R\cos\omega\cos\gamma - \sin\gamma}{(R^2 + 1)^2}$$

and from equation (A-4) for the k^{th} segment

$$f_{dA_k} = \frac{G_s\cos\alpha_s}{\pi} \int_{A_k} \frac{(R\cos\omega\cos\gamma - \sin\gamma)}{(R^2 + 1)^2} dA_k$$

and $dA_k = Rd\omega\, dR$

$$f_{dA_k} = \frac{G_s\cos\alpha_s\cos\gamma}{\pi} \int_{A_k} \frac{R^2\cos\omega d\omega dR}{(R^2+1)^2} - \frac{G_s\cos\alpha_s\sin\gamma}{\pi} \int_{A_k} \frac{Rd\omega dR}{(R^2+1)^2}$$

or in abbreviated form

$$f_{dA_k} = \frac{G_s\cos\alpha_s}{\pi} \left[\cos\gamma S_3 - \sin\gamma S_4\right]$$

To solve S_3 in part I indicated in Figure F-3 the limits of integration are

$$\omega = \omega_\ell \qquad \text{or} \qquad \omega = \omega_\ell$$

$$\omega = \omega_u = \cos^{-1}\left(\frac{a_o}{R}\right) \qquad \omega = \omega_u$$

$$R = R_\ell = a_o \sec\omega_\ell \qquad R = R_\ell = a_o \sec\omega$$

$$R = R_u = a_o \sec\omega_u \qquad R = R_u = a_o \sec\omega_u$$

So

$$S_{3_I} = \int_{R_\ell = a_o \sec\omega_\ell}^{R_u = a_o \sec\omega_u} \frac{R^2}{(R^2+1)^2} \int_{\omega_\ell}^{\omega_u = \cos^{-1}\left(\frac{a_o}{R}\right)} \cos\omega \, d\omega \, dR$$

and

$$S_{4_I} = \int_{\omega_\ell}^{\omega_u} \int_{R_\ell = a_o \sec\omega}^{R_u = a_o \sec\omega_u} \frac{R}{(R^2+1)^2} \, dR \, d\omega$$

Performing the first integration gives

$$S_{3_I} = \int_{R_\ell}^{R_u} \frac{R\sqrt{R^2 - a_o^2}}{(R^2+1)^2}\,dR - \sin\omega_\ell \int_{R_\ell}^{R_u} \frac{R^2}{(R^2+1)^2}\,dR$$

Rewriting the first integral with $u = R^2$ and using equations (14.119), (14.114) and (14.134) from Reference (10) gives

$$2S_{3_I} = \frac{a_o\tan\omega_u}{a_o^2\sec^2\omega_u + 1} + \frac{a_o\tan\omega_\ell}{a_o^2\sec^2\omega_\ell + 1}$$

$$+ \frac{1}{\sqrt{a_o^2+1}}\left[\tan^{-1}\left(\frac{a_o\tan\omega_\ell}{\sqrt{a_o^2+1}}\right) - \tan^{-1}\left(\frac{a_o\tan\omega_\ell}{\sqrt{a_o^2+1}}\right)\right]$$

$$- \sin\omega_\ell\left[\frac{a_o\sec\omega_u}{a_o^2\sec^2\omega_u + 1} + \frac{a_o\sec\omega_\ell}{a_o^2\sec^2\omega_\ell + 1}\right.$$

$$\left. + \tan^{-1}(a_o\sec\omega_u) - \tan^{-1}(a_o\sec\omega_\ell)\right]$$

Now for S_{4_I} after one integration gives

$$2S_{4_I} = \int_{\omega_\ell}^{\omega_u} \frac{-1}{a_o^2 \sec^2 \omega_u + 1}\, d\omega - \int_{\omega_\ell}^{\omega_u} \frac{-1}{(a_o^2 \sec^2 \omega + 1)}\, d\omega$$

$$= \frac{(\omega_u - \omega_\ell)}{(a_o^2 \sec^2 \omega_u + 1)} + \int_{\omega_\ell}^{\omega_u} \frac{d\omega}{(a_o^2 \sec^2 \omega + 1)}$$

Using $\sec = \dfrac{1}{\cos\omega}$

and

$$\cos^2\omega = \frac{1}{2}(1 + \cos 2\omega)$$

reduces the remaining integral into a form which from equation (14.459) and (14.390) of Reference (10) gives

$$2S_{4_I} = (\omega_u - \omega_\ell) - \frac{a_o}{\sqrt{a_o^2 + 1}} \left[\tan^{-1}\left(\frac{a_o \tan\omega_u}{\sqrt{a_o^2 + 1}}\right) - \tan^{-1}\left(\frac{a_o \tan\omega_\ell}{\sqrt{a_o^2 + 1}}\right)\right] - \frac{(\omega_u - \omega_\ell)}{(a_o^2 \sec^2 \omega_u + 1)}$$

Now consideration is given to part II as pictured in Figure F-3. The limits of integration are

$$\omega = \omega_\ell$$

$$\omega = \omega_u$$

$$R = R_u \to \infty$$

$$R = R_\ell = a_o \sec\omega_u$$

This gives

$$S_{3_{II}} = \int_{R_\ell}^{R_u} \frac{R^2}{(R^2+1)^2} \int_{\omega_\ell}^{\omega_u} \cos\omega d\omega dR$$

and after one integration

$$S_{3_{II}} = (\sin\omega_u - \sin\omega_\ell) \int_{R_\ell}^{R_u} \frac{R^2}{(R^2+1)^2} dR$$

and from equation (14.134) Reference (10)

$$2S_{4_{II}} = \frac{(\omega_u - \omega_\ell)}{(a_o^2 \sec^2\omega_u + 1)}$$

So for the area segment A_k

$$f_{dA_k} = \frac{G_s \cos\alpha_s}{\pi} \left[\cos\gamma \left(S_{3_I} + S_{3_{II}} \right) - \sin\gamma \left(S_{4_I} + S_{4_{II}} \right) \right]$$

and after cancellation this becomes

$$f_{dA_k} = \frac{G_s \cos\alpha_s}{2\pi} \left\{ \cos\gamma \left[(\sin\omega_u - \sin\omega_\ell) \frac{\pi}{2} \right. \right.$$

$$+ \sin\omega_\ell \tan^{-1}(a_o \sec\omega_\ell) - \sin\omega_u \tan^{-1}(a_o \sec\omega_u)$$

$$\left. + \frac{1}{\sqrt{a_o^2 + 1}} \left[\tan^{-1}\left(\frac{a_o \tan\omega_u}{\sqrt{a_o^2 + 1}} \right) - \tan^{-1}\left(\frac{a_o \tan\omega_\ell}{\sqrt{a_o^2 + 1}} \right) \right] \right]$$

$$- \sin\gamma \left[(\omega_u - \omega_\ell) - \frac{a_o}{\sqrt{a_o^2 + 1}} \left[\tan^{-1}\left(\frac{a_o \tan\omega_u}{\sqrt{a_o^2 + 1}} \right) \right. \right.$$

$$\left. \left. \left. - \tan^{-1}\left(\frac{a_o \tan\omega_\ell}{\sqrt{a_o^2 + 1}} \right) \right] \right] \right\}$$

This gives the solution of the flat surface energy flux for a segment of case (1). The solutions of the other three cases are as follows:

Case (2):

$$f_{dA_k} = \frac{G_s \cos\alpha_s}{2\pi} \left\{ \cos\gamma \left[- \sin\omega_u \tan^{-1}\left(\frac{b_o}{\sin\omega_u}\right) + \sin\omega_\ell \tan^{-1}\left(\frac{b_o}{\sin\omega_\ell}\right) + \frac{\pi}{2} (\sin\omega_u - \sin\omega_\ell) \right] - \sin\gamma \left[(\omega_u - \omega_\ell) + \frac{b_o}{\sqrt{b_o^2 + 1}} \cdot \left[\tan^{-1}\left(\frac{\sqrt{b_o^2 + 1}\,\tan\omega_u}{b_o}\right) - \tan^{-1}\left(\frac{\sqrt{b_o^2 + 1}\,\tan\omega_\ell}{b_o}\right) \right] \right] \right\}$$

Case (3):

$$f_{dA_k} = \frac{G_s \cos\alpha_s}{2\pi} \left\{ \cos\gamma \left[(\sin\omega_u - \sin\omega_\ell) \frac{\pi}{2} \right.\right.$$

$$+ \sin\omega_\ell \tan^{-1}(c_o \sec\omega_\ell) - \sin\omega_u \tan^{-1}(c_o \sec\omega_u)$$

$$\left.\left. + \frac{1}{\sqrt{c_o^2 + 1}} \left[\tan^{-1}\left(\frac{c_o \tan\omega_u}{\sqrt{c_o^2 + 1}} \right) - \tan^{-1}\left(\frac{c_o \tan\omega_\ell}{\sqrt{c_o^2 + 1}} \right) \right] \right] \right.$$

$$- \sin\gamma \left[(\omega_u - \omega_\ell) - \frac{c_o}{\sqrt{c_o^2 + 1}} \left[\tan^{-1}\left(\frac{c_o \tan\omega_u}{\sqrt{c_o^2 + 1}} \right) \right.\right.$$

$$\left.\left.\left. - \tan^{-1}\left(\frac{c_o \tan\omega_\ell}{\sqrt{c_o^2 + 1}} \right) \right] \right] \right\}$$

Case (4):

$$f_{dA_k} = \frac{G_s \cos\alpha_s}{2\pi} \left\{ \cos\gamma \left[\sin\omega_\ell \tan^{-1}(b_o \csc\omega_\ell) \right.\right.$$

$$+ \sin\omega_u \tan^{-1}\left(\frac{c_o}{-\cos\omega_u}\right) - \sin\omega_u \tan^{-1}(b_o \csc\omega_u)$$

$$- \sin\omega_\ell \tan^{-1}\left(\frac{c_o}{-\cos\omega_u}\right) - \frac{1}{\sqrt{c_o^2 + 1}} \left[\tan^{-1}\left(\frac{c_o \tan\omega_\ell}{\sqrt{c_o^2 + 1}}\right) \right.$$

$$\left.\left. - \tan^{-1}\left(\frac{c_o \tan\omega_u}{\sqrt{c_o^2 + 1}}\right)\right]\right] - \sin\gamma \left[\frac{-b_o}{\sqrt{b_o^2 + 1}} \right.$$

$$\cdot \left[\tan^{-1}\left(\frac{\sqrt{b_o^2 + 1}\, \tan\omega_u}{b_o}\right) - \tan^{-1}\left(\frac{\sqrt{b_o^2 + 1}\, \tan\omega_\ell}{b_o}\right)\right]$$

$$\left. + \frac{c_o}{\sqrt{c_o^2 + 1}} \left[\tan^{-1}\left(\frac{c_o \tan\omega_u}{\sqrt{c_o^2 + 1}}\right) - \tan^{-1}\left(\frac{c_o \tan\omega_\ell}{\sqrt{c_o^2 + 1}}\right)\right]\right]\right\}$$

In the computer program the equations of cases 3 and 4 were modified to allow ω_u and ω_ℓ to be equal to $\pi/2$. This gives the flux for all the possible flat surface configurations that can be encountered in this analysis. Now the rough surface energy flux of a segment k for small angular increments can be written

$$F_{dA_k} \cong \left[\mathcal{F} \right]_{\omega=\omega_{k_{av}}} f_{dA_k}$$

and to get the total energy flux from the region outside of A_g

$$F_{dA_\ell} = \sum F_{dA_k}$$

Figure F-1: Geometry of the regions of the infinite surface treated by approximation of Appendix D for the three possible cases of γ

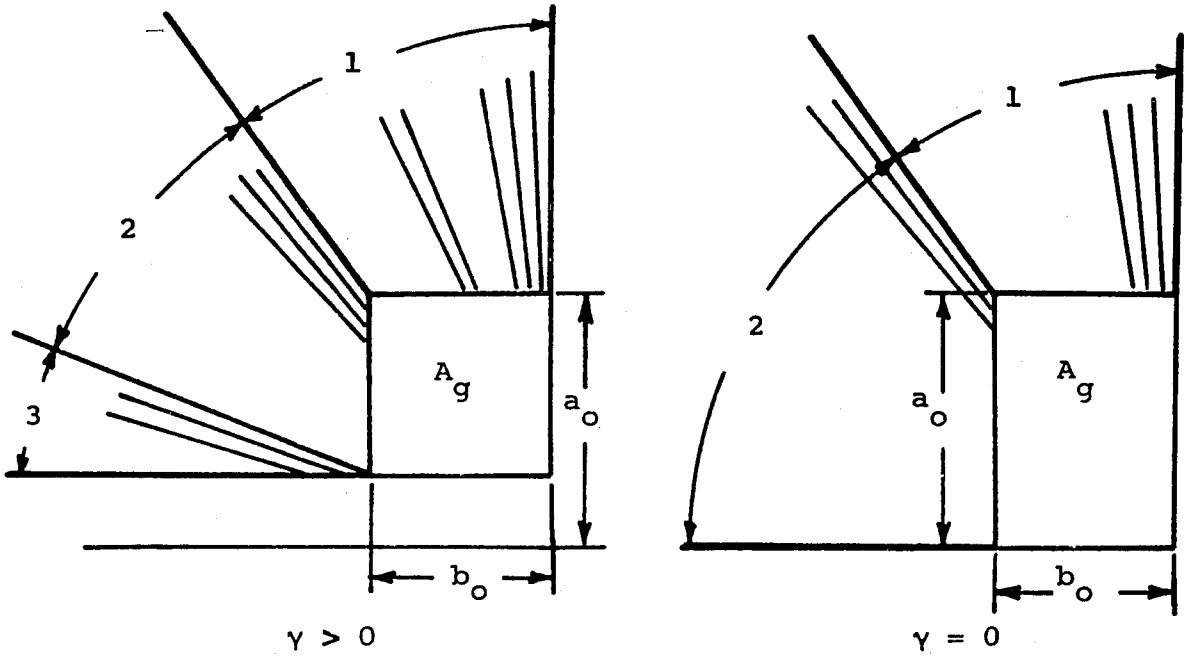

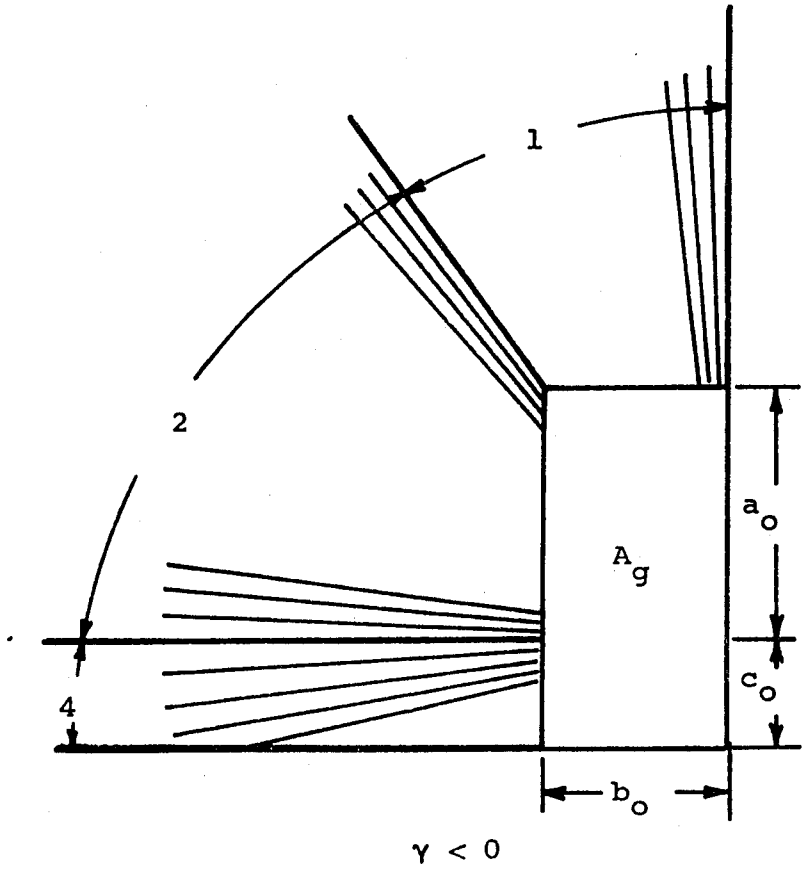

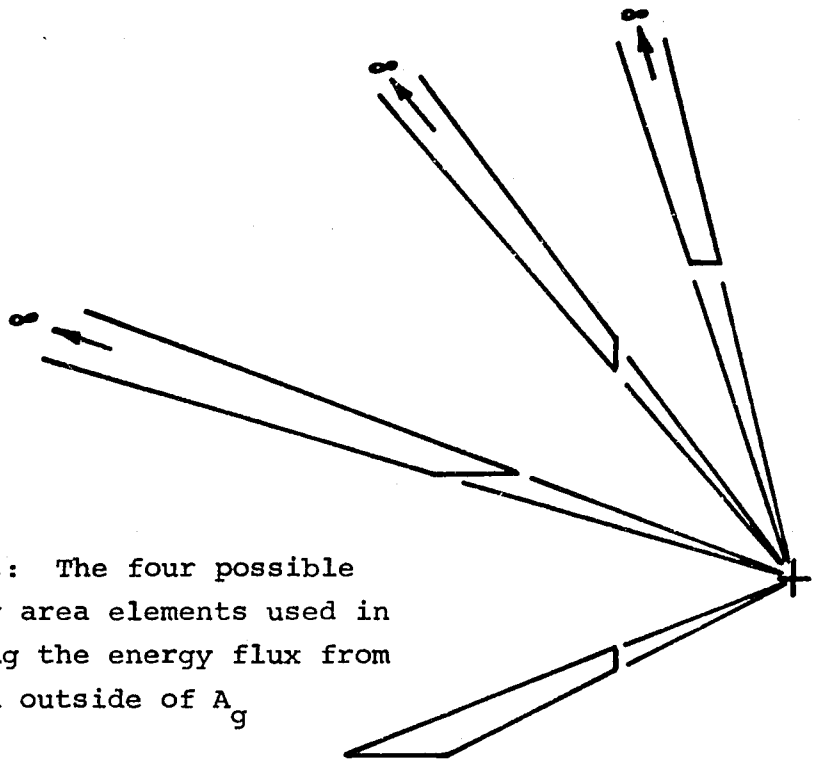

Figure F-2: The four possible shapes for area elements used in calculating the energy flux from the region outside of A_g

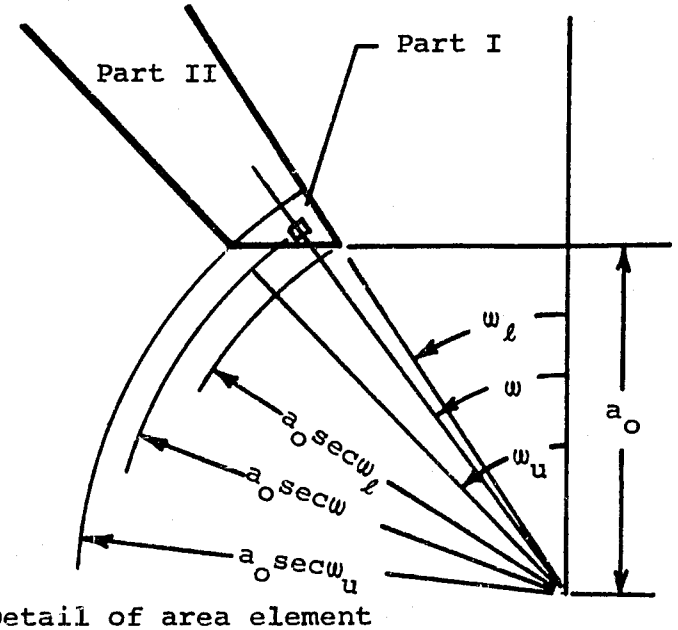

Figure F-3: Detail of area element with geometry required for integration